UCLouvain

epl

École polytechnique de Louvain

EPL23-134

Diffusion MRI studies in abstinent alcoholic patients to identify relationships between behavioural and microstructural evolution in the corpus callosum and the uncinate fasciculus.

Author: **Pauline Hermans**
Supervisors: **Benoit Macq, Laurence Dricot**
Readers: **Manon Dausort, Cyril Debodt, Mélissa Salavrakos**
Academic year 2022–2023
Master [120] in Biomedical Engineering

Acknowledgements

I would like to express my sincere gratitude to my academic supervisors, Pr Benoît Macq and Pr Laurence Dricot, for their guidance and help throughout this work.

I would like to address a special thanks to Nicolas Delinte and Manon Dausort for their expert support, their insightful advice and their invaluable knowledge transfer. They enabled me to deepen and improve my research and thereby to complete my master's thesis.

I am also grateful to Philippe de Timary and Mélissa Salavrakos for their valuable data and assistance.

Finally, I would like to extend my appreciation to my family and friends for their support and encouragement having been a constant source of motivation over the entire course of my studies.

Abstract

Many ongoing research studies focus on elucidating the short-term effects of abstinence on the brain's microstructure in patients with alcohol use disorder (AUD). Diffusion MRI (dMRI) is recognised as a powerful tool for non-invasive analysis of the brain microstructures. It has also been observed that AUD is frequently accompanied by behavioural disorders, although the causal relationships between the two remain unclear. This study aimed at investigating the relationships between behavioural alterations and microstructural changes in the corpus callosum (CC) and the uncinate fasciculus (UF) among alcoholic patients following an 18-day abstinence period. A total of 53 patients were studied on the basis of data collected on the first and 18th day of abstinence and equivalent data were collected from 20 control subjects. Fibre tracts belonging to both structures were isolated from the complete brain tractography and 4 models (DTI, NODDI, DIAMOND and MF) were used to compute metrics, providing an insight into the microstructure of the white matter. At the same time, self-reported questionnaires were used to assess 5 behaviours: depression, obsession, compulsion, anxiety and fatigue. Comparisons between patients and controls at 1 and 18 days of abstinence confirmed the non-negligible impact of AUD on the microstructure of the CC and UF as well as on the behaviours of alcoholics. Although the changes in UFs remain largely non-significant in patients as compared to controls to be able to draw correlations with altered behaviour, noteworthy results were observed in the CC. Most of the behaviours studied were significantly correlated with changes within the posterior regions of the CC (including the isthmus and splenium). Obsession, on the other hand, was correlated with the most anterior region of the CC, the genu. Interpretation of the correlations with compulsion and obsession could indicate a reduction in inflammation in the splenium and the genu respectively, occurring in early stages of abstinence and suggesting a recovery process consistent with the behavioural improvements. Moreover, anxiety appears to be significantly correlated to an increase in volume and a reorganisation of fibres in the splenium. Further research on these results could be promising for a better understanding of the numerous mechanisms involved in AUD.

Keywords : Alcoholism, AUD, Abstinence, dMRI, Corpus Callosum, Uncinate Fasciculus, Behaviours

Contents

Acknowledgements i

Abstract ii

List of Figures vii

List of Tables viii

Abbreviations ix

Introduction 1

I State of the art 3

1 MRI 4
1.1 Basic principle of MRI . . . 4
1.1.1 Magnetism of matter . . . 4
1.1.2 Nuclear magnetic resonance (NMR) . . . 5
1.1.3 Relaxation . . . 6
1.1.4 Spin Echo sequence . . . 8
1.1.5 Contrast . . . 9
1.2 Acquisition process . . . 11
1.3 Diffusion imaging . . . 12
1.3.1 Diffusion-weighted imaging (DW-MRI) . . . 12
1.3.2 Diffusion tensor imaging (DTI) . . . 14
1.3.3 Limitations of DTI . . . 15
1.4 Advanced diffusion models . . . 16
1.4.1 NODDI . . . 16
1.4.2 DIAMOND . . . 18
1.4.3 Microstructure Fingerprinting . . . 19
1.5 Tractography of the WM . . . 19
1.6 ElikoPy pipeline . . . 21

2 Alcohol Use Disorders 24
2.1 Definition of AUD . . . 24
2.2 Biological impacts of AUD . . . 25
2.2.1 Anatomical content . . . 26

2.2.2 Microstructural modifications due to alcohol . . . 29
2.2.3 Benefits of abstinence . . . 31
2.3 Psychological impacts of AUD . . . 32
2.3.1 Objective psychological state assessment . . . 32
2.3.2 Behavioural modifications due to alcohol and abstinence . . . 34
2.4 Neurocognitive and functional impacts of AUD . . . 36

II Analysis 38

3 Objectives and Methods 39
3.1 Objectives . . . 39
3.2 Data . . . 39
3.2.1 Data acquisition . . . 39
3.2.2 Data conversion . . . 40
3.2.3 Data preprocessing . . . 41
3.3 Regions of interest . . . 41
3.3.1 Tractography . . . 41
3.3.2 Brain parcelation . . . 42
3.3.3 Tracts isolation . . . 43
3.3.4 ROI and fibre density . . . 44
3.4 Metrics . . . 45
3.4.1 Microstructural metrics . . . 45
3.4.2 Behavioural metrics . . . 49
3.4.3 Evolution over time . . . 50
3.5 Outliers . . . 50
3.5.1 Behavioural outliers . . . 50
3.5.2 Microstructural outliers . . . 52
3.6 Statistical analysis . . . 52
3.7 Technical resources . . . 54

4 Results 55
4.1 Patients and controls comparison . . . 55
4.1.1 Behavioural comparison . . . 55
4.1.2 Microstructural comparison . . . 55
4.2 Evolution comparison . . . 59
4.2.1 Microstructural metrics evolution . . . 59
4.2.2 Behavioural metrics evolution . . . 62
4.3 Correlations between behavioural and microstructural metrics . . . 63

5 Discussion 67
5.1 Coherence of the metrics . . . 67
5.2 Behavioural comparison . . . 68
5.2.1 Patients-Controls comparison . . . 68
5.2.2 T1-T2 comparison . . . 68
5.3 Microstructural comparison . . . 68
5.3.1 Patients-Controls comparison . . . 68

5.3.2 T1-T2 evolution comparison 69
5.4 Correlation between microstructural and behavioural evolution 72
5.4.1 Correlations with BDI, STAI and MFI 72
5.4.2 Correlation with OCDS (obsession and compulsion) 74
5.4.3 General remarks 75
5.5 Limitations 76
5.6 Further perspectives 78

Conclusion **81**

Appendix **90**

A Additional details about the gradients used in the signal acquisition process in MRI **90**

B Example of a `.json` file containing all the acquisition parameters **93**

C WMQL file for the CC and the UF **95**

D Outliers justifications **100**

E Additional tables for the patients-controls comparison analysis **104**

F Additional tables for the evolution comparison analysis **107**

G Additional tables and graphs for the correlation analysis **110**

H UFs asymmetry comparison **117**

List of Figures

1.1 Magnetism of a charged particle . . . 4
1.2 Precession of a charged particle . . . 5
1.3 Magnetisation of the matter in a magnetic field . . . 6
1.4 Flip of the magnetisation vector induced by RF pulses . . . 7
1.5 T1 and T2 relaxation curves . . . 7
1.6 FID acquisition . . . 8
1.7 Visualisation of the spin echo phenomenon . . . 9
1.8 SE sequence . . . 9
1.9 T1 weighted signals . . . 10
1.10 T2 weighted signals . . . 10
1.11 Proton density weighted signals . . . 11
1.12 Complete SE sequence acquisition chronology . . . 12
1.13 Diffusion-weighted imaging principle . . . 13
1.14 Geometric visualisation of the diffusion tensor . . . 14
1.15 NODDI model . . . 17
1.16 DIAMOND model . . . 18
1.17 WM tractography principle . . . 20
1.18 Illustration of the probabilistic tractography approach . . . 20
1.19 ElikoPy pipeline . . . 22

2.1 Views of the CC . . . 27
2.2 CC division scheme . . . 27
2.3 3D reconstruction of the left uncinate fasciculus using diffusion tensor tractography. . . . 29
2.4 Volume differences in the CC regions due to AUD . . . 30
2.5 Correlation between OCDS score and relapse . . . 35

3.1 Whole brain tractography . . . 42
3.2 FreeSurfer parcelation output file . . . 42
3.3 Adapted parcelation of the CC . . . 43
3.4 Tracts of the CC . . . 44
3.5 Tracts of the UF . . . 44
3.6 Example of a CC density weighted ROI . . . 45
3.7 DTI metrics example maps . . . 46
3.8 NODDI metrics example maps . . . 47
3.9 DIAMOND metrics example maps . . . 48
3.10 Difference between `fvf_tot` and `wfvf` . . . 49
3.11 MF metrics example maps . . . 50

3.12 Boxplots illustrating the identification of outliers for the behavioural metrics in AUD patients at T2 . . . 51
3.13 Boxplots illustrating the identification of outliers for the behavioural metrics in controls . . . 51

4.1 Patients-Controls behavioural boxplot comparison . . . 56
4.2 Comparison of FA (DTI) between patients and controls at T1 and T2 . . . 59
4.3 Comparison of `frac_ftot` (DIAMOND) between patients and controls at T1 and T2 . . . 59
4.4 Comparison of `fvf_tot` evolutions between patients and controls . . . 61
4.5 Comparison of `fvf_tot` evolutions (from both DIAMOND and MF) between patients and controls . . . 62
4.6 Behavioural metrics evolution in AUDs . . . 63
4.7 Significant correlations of microstructural metrics with BDI . . . 64
4.8 Significant correlations of microstructural metrics with OCDS (obsessions) 65
4.9 Significant correlations of microstructural metrics with OCDS (compulsion) 65
4.10 Significant correlations of microstructural metrics with STAI . . . 66
4.11 Significant correlations of microstructural metrics with MFI . . . 66

5.1 Schematic overview of the main hypotheses . . . 75

A.1 Complete SE sequence acquisition chronology . . . 90
A.2 Spatial coding with the slice plane gradient Gss . . . 91

E.1 Tables of p-values for the comparison of behavioural metrics between AUDs patients and controls . . . 104
E.2 Tables of p-values for the comparison of microstructural metrics between AUDs patients and controls . . . 105
E.3 Tables of differences of means between patients and controls for each metric-region pairs . . . 106

F.1 Tables of p-values for the comparison of behavioural metrics between AUDs patients at T1 and T2 . . . 107
F.2 Tables of absolute percentage changes for each metric-region pairs in controls and patients . . . 108
F.3 Tables of means percentage changes for each metric-region pairs in controls and patients . . . 109

G.1 Pearson's coefficients and p-values for the correlation with BDI . . . 111
G.2 Pearson's coefficients and p-values for the correlation with OCDS (obsession) 112
G.3 Pearson's coefficients and p-values for the correlation with OCDS (compulsion) 113
G.4 Pearson's coefficients and p-values for the correlation with STAI . . . 114
G.5 Pearson's coefficients and p-values for the correlation with MFI . . . 115
G.6 Significant correlations of microstructural metrics with OCDS (obsessions) 116
G.7 Significant correlations of microstructural metrics with OCDS (compulsion) 116

H.1 Boxplot for the UF asymmetry comparison . . . 118
H.2 Metrics comparison between UFs left and right . . . 119

List of Tables

4.1 Comparison of the microstructural metrics between AUD patients and controls at T1 . . . 57
4.2 Comparison of the microstructural metrics between AUD patients and controls at T2 . . . 57
4.3 Comparison of the percentage of changes between T1 and T2 in patients and controls . . . 60
4.4 Significant correlation between the evolution of microstructural metrics and behavioural scores. . . . 63

5.1 Example of the consequences of using the difference or the percentage of changes to measure metric evolution . . . 78

D.1 Tables of the excluded data and justifications . . . 100

H.1 UF asymmetry : p-values of number and density of fibres . . . 117

Abbreviations

BDI Beck Depression Inventory

CC Corpus Callosum

CNS Central Nervous ssystem

CSF Cerebrospinal Fluid

CS Controls Subjects

ES Echo Spin

DIAMOND DIstribution of 3D Anisotropic MicrOstructural eNvironments in Diffusion-compartment imaging

DW-MRI Diffusion Weighted Magnetic Resonance Imaging

DTI Diffusion Tensor Imaging

GM Gray Matter

IQR InterQuartile Range

MF Microstructure Fingerprinting

MFI Multidimensional Fatigue Inventory

MRI Magnetic Resonance Imaging

NODDI Neurite Orientation Dispersion and Density Imaging

OCDS Obsessive Compulsive Drinking Scale

ODF Fibre Orientation Distribution

PNS Peripheral Nervous Sysytem

RF Radio Frequency

SNR Signa-to-Noise Ratio

STAI State-Trait Anxiety Inventory

TE Echo Time

TR Repetition Time

UF Uncinate Fasciculus

WM White Matter

Introduction

Alcohol use disorder (AUD) is a complex neuropsychiatric condition characterised by excessive and uncontrolled consumption of alcohol, leading to severe physical, psychological, and social consequences. It is estimated that AUD affects about 6% of the American population, mainly in the 18-26 age group [1]. This is even one of the targets included in goal number 3 of the Sustainable Development Goals from the United Nations. "*Strengthen the prevention and treatment of substance abuse, including [...] harmful use of alcohol*" constitutes therefore a significant public health concern [2].

Despite the well-known detrimental effects of chronic alcohol abuse on various brain regions, the underlying neural mechanisms contributing to these alterations remain incompletely understood. One of the brain areas particularly susceptible to the damaging effects of alcohol is the white matter (WM), which serve as structural connector between different brain structures. This study will focus on the corpus callosum and the uncinate fasciculus. The corpus callosum plays a crucial role in interhemispheric communication, while the uncinate fasciculus is involved in the limbic system and is implicated in the control of emotional, behavioural and cognitive functions.

Diffusion Magnetic Resonance Imaging (dMRI) is a specialised imaging technique that utilises Magnetic Resonance Imaging (MRI) to examine the diffusion of water molecules within biological tissues, particularly in the brain. This diffusion being influenced by barriers such as cell membranes and fibre tracts, dMRI can provide valuable insights into the microstructural organisation and integrity of the WM. Diffusion Tensor Imaging (DTI) relies on dMRI images to compute a variety of metrics quantifying the properties of these WM tracts [3]. Other models have also been developed, such as Neurite Orientation Dispersion and Density Imaging (NODDI), DIstribution of 3D Anisotropic MicrOstructural eNvironments in Diffusion-compartment imaging (DIAMOND) and Microstructure Fingerprinting (MF), to obtain even more precise and informative metrics.

AUD can have profound psychological consequences on individuals who struggle with this condition. These consequences can manifest in various ways, impacting emotional well-being, cognitive functioning, and overall mental health. This study analyses five behaviours in particular, including depression, obsession, compulsion, anxiety and fatigue. The significant deterioration of these behaviours with alcoholism further worsens AUD and makes recovery a slow and difficult process.

Abstinence takes an important place in the treatment and recovery process for AUD patients. The aim of this study is to investigate the relationships between changes in behavioural scores and microstructural metrics in alcohol-dependent patients following an 18-day period of abstinence. The acquisition of data from control subjects also enable us to compare the behavioural state and microstructural properties of WM tracts between the two populations.

First, a state of the art will explain the theoretical concepts relating to dMRI and the neuroanatomy of the studied structures. A review of the literature will also summarise all the current knowledge on the impact of alcoholism on brain microstructure and behaviour. Next, the methods used for the data analyses will be detailed, and the results obtained will be presented. These will be interpreted and discussed in order to conclude on the putative relationships between changes in microstructures and alteration in behaviour. Finally, the limitations encountered will be discussed, and future perspectives will be proposed.

Part I

State of the art

Chapter 1

MRI

1.1 Basic principle of MRI

1.1.1 Magnetism of matter

Magnetic resonance imaging (MRI) uses the magnetic properties of matter to image parts of the human body in a non-invasive way. From an atomic point of view, the nucleus rotates on itself around an axis passing through its centre which induces a kinetic moment also called "spin" and represented by the vector $\vec{S}$. Moreover, the nucleus of atoms is composed of charged particles called nucleons: neutrons (neutral charge) and protons (positive charge). Their collective movement creates a magnetic field, called magnetic moment, which is represented by a magnetisation vector noted $\vec{\mu}$. It can be seen as a small magnet with a North and a South pole (see Figure 1.1) [3].

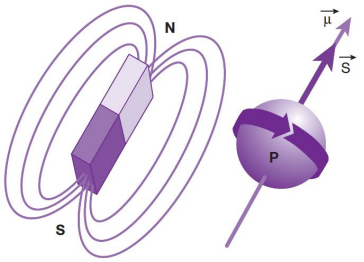


Figure 1.1: Magnetism of a charged particle. The nucleus rotating on itself induces a kinetic moment ($\vec{S}$) and the movement of charged nucleons creates a magnetic moment ($\vec{\mu}$) [3].

In the nucleus, neutrons and protons pair up, cancelling their magnetic moment. This allows a more stable energy level to be maintained. However, some atoms have an odd number of nucleons, which prevents all magnetic moments from pairing up and cancelling each other out. What remains is an intrinsic or elementary magnetic moment, which therefore provides the magnetic properties of the material. In MRI, the essential atom is the hydrogen, as it represents more than half of the atoms in the body and is composed of only one proton. Its intrinsic magnetic moment is therefore very high, which makes it possible to induce a resonance phenomenon [3].

1.1.2 Nuclear magnetic resonance (NMR)

Most of the time, these magnetic vectors orient themselves randomly in space. When exposed to an external magnetic field $\overrightarrow{B_0}$ oriented along Oz, their kinetic moments (spin) align themselves in the direction of this field. It should be noted that their alignment is not perfect but is a precessional motion around the axis of $\overrightarrow{B_0}$ (see Figure 1.2) with a given angle and a precise angular frequency ω_0 predicted by the Larmor equation:

$$\omega_0 = \gamma B_0 \tag{1.1}$$

where γ is the gyromagnetic ratio which is specific to each atomic nucleus [3].

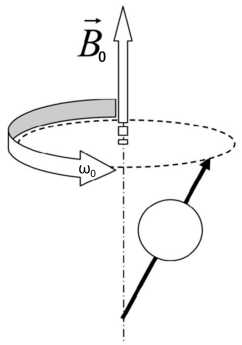


Figure 1.2: Precession of a charged particle in a magnetic field $\overrightarrow{B_0}$ at an angular frequency ω_0. Adapted from [4].

When a set of protons is subjected to an external field $\overrightarrow{B_0}$, the appearance of a macroscopic magnetisation vector is observed, resulting from the sum of the magnetisation vectors of each proton (see Longitudinal component in Figure 1.3). The amplitude of this vector increases with the proton density as well as with the strength of the field $\overrightarrow{B_0}$ [3].

This proton population is divided into two populations, one composed of protons oriented in the same direction as $\overrightarrow{B_0}$ (parallel) called "spin up" and another composed of protons oriented in the opposite direction to $\overrightarrow{B_0}$ (antiparallel) called "spin down". Each population is therefore characterised by a defined precession angle corresponding to precise energy levels: parallel, low energy and antiparallel, high energy. The difference between the two populations is only about 2 more in the parallel direction than in the antiparallel direction for every 1 million protons. This low difference is still sufficient to obtain an NMR signal. In the case where there is only one magnetic field $\overrightarrow{B_0}$, there is no transverse component $\overrightarrow{M}_{xy}$ in the xOy plane, since the protons are out of phase, which means that the sum of the transverse components of the elementary magnetisation vectors of each atom cancels out (see Figure 1.3) [3].

To measure the longitudinal component $\overrightarrow{M}_z$, it must be flipped in the xOy plane because it is too small compared to the external field $\overrightarrow{B_0}$ in the Oz direction. For this purpose, a second external magnetic field or an electromagnetic radiofrequency (RF) wave is used: $\overrightarrow{B_1}$ oriented along Ox. To ensure the transfer of energy in order to properly flip the magnetisation vector, resonance conditions must be respected: the rotation frequency ω_r of the field $\overrightarrow{B_1}$ must be equal to the Larmor frequency ω_0 which is specific to protons that have already been excited by the field $\overrightarrow{B_0}$. The protons after an RF pulse will then precess twice (around $\overrightarrow{B_0}$ and around $\overrightarrow{B_1}$). During this flipping movement, the longitudinal component $\overrightarrow{M}_z$ will decrease, while the transverse component $\overrightarrow{M}_{xy}$ will increase. Indeed, the RF pulse allows two things. Firstly, the distribution of the two populations (parallel

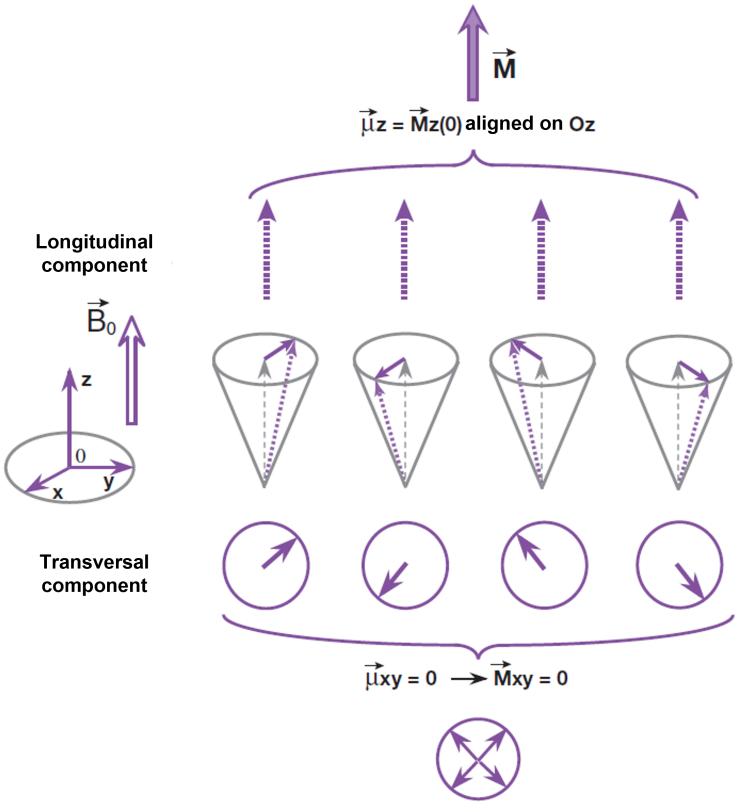


Figure 1.3: Magnetisation of the matter in a magnetic field. The macroscopic magnetisation vector results from the sum of the magnetisation vectors of each proton. The longitudinal components add up to create a positive longitudinal magnetisation while the transversal components cancel each other and the resulting transversal magnetisation is null. Adapted from [3].

and antiparallel) is modified as some protons acquire sufficient energy to move from the low energy (parallel) to the high energy (antiparallel) state. The number of protons which can change state depend on the time during which the RF pulse is applied or on the field strength of $\overrightarrow{B_1}$. The longitudinal component cancelled out as both populations become equal (this is called a 90° pulse, see Figure 1.4 A) or the antiparallel population can become larger than the parallel population and the longitudinal component (this is called a 180° pulse, see Figure 1.4 B). Secondly, the protons will precess in phase around $\overrightarrow{B_0}$ which will allow the transverse component $\overrightarrow{M}_{xy}$ to appear [3].

1.1.3 Relaxation

As soon as the RF wave stops, the magnetisation vector returns to its unexcited state. The longitudinal component $\overrightarrow{M}_z$ grows back to its initial position along Oz (longitudinal or T1 relaxation) and the transverse component $\overrightarrow{M}_{xy}$ disappears due to the rapid phase shift of the protons (transverse or T2 relaxation) [3].

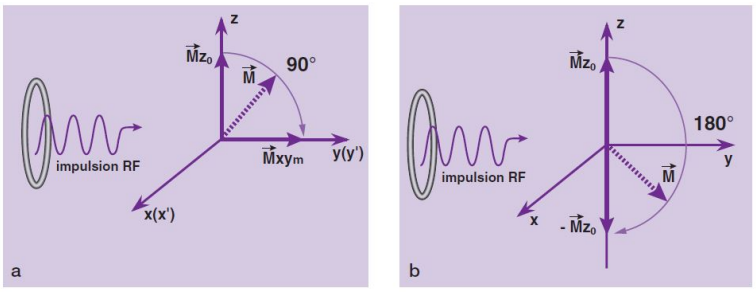
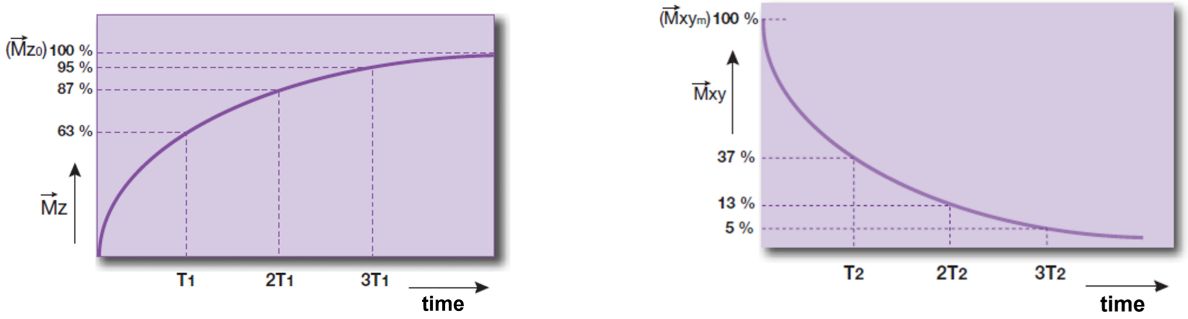


Figure 1.4: Flip of the magnetisation vector induced by **(A)** a 90° pulse and **(B)** a 180° pulse [3].

On the one hand, the spin-lattice interactions release energy by moving protons from the high-energy state (antiparallel population) to the low-energy state (parallel population). The longitudinal component thus grows back following an increasing exponential (see Figure 1.5a), characterised by the time constant T1 (around $500ms$ - $1000ms$).

$$\overrightarrow{M}_z(t) = 1 - e^{-t/T1} \tag{1.2}$$

After T1 milliseconds, $\overrightarrow{M}_z$ has recovered 63% of its maximum amplitude. This time constant depends on the molecular structure and the state of the material. For example, T1 is long for solid environments or in the presence of pure water, whereas T1 is shorter for fatty tissue or for environments with water in the presence of large molecules [3].



(a) T1 relaxation **(b)** T2 relaxation

Figure 1.5: T1 **(a)** and T2 **(b)** relaxation exponential functions. Adapted from [3].

On the other hand, as protons evolve in slightly different environments with the presence of small magnetic fields that add to the $\overrightarrow{B_0}$ field, spin-spin interactions result in a phase shift of the protons, without energy exchange. The decrease in the transverse component $\overrightarrow{M}_{xy}$ follows a decreasing exponential (see Figure 1.5b), characterised by a time constant T2 (around $50ms$ - $100ms$).

$$\overrightarrow{M}_{xy}(t) = e^{-t/T2} \tag{1.3}$$

T2 corresponds to a decrease of 63% of its maximum amplitude. This time constant also varies according to the molecular structure or the solid or liquid state of the tissue. T2 is for example shorter in tissues composed of large molecules and in solids [3].

It should be noted however, that the $\overrightarrow{B_0}$ field is not perfectly homogeneous at the microscopic scale. These inhomogeneities lead to an even faster phase shift of the protons. The time constant T2* is therefore a modification of the T2 constant to take account of this phenomenon. T2* is always lower than T2 since $\overrightarrow{M}_{xy}$ decreases faster than expected [3].

The MRI signal measured is called Free Induction Decay (FID). It measures the decay of $\overrightarrow{M}_{xy}$ as it continues to precess around Oz, using a coil placed in the xOz plane. This is shown in Figure 1.6 [3].

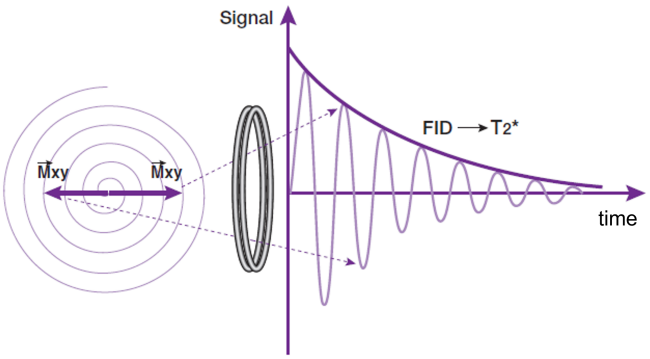


Figure 1.6: Free Induction Decay (FID) acquisition process using a coil. Adapted from [3].

1.1.4 Spin Echo sequence

To measure the true T2 constant and not T2*, a particular acquisition sequence called spin echo (SE) sequence must be used in order to preserve the inhomogeneities due to the type of tissue and eliminate the inhomogeneities of the $\overrightarrow{B_0}$ field which are constant over time. As a reminder, the sequence starts with a 90° RF impulse which aligns the magnetisation vector along Ox (see Figure 1.7 A). The relaxation begins immediately at the end of this first pulse (see Figure 1.7 B). Then, after a TE/2 time (TE = echo time), a 180° RF pulse is applied. This reverses the orientation of the longitudinal component by inverting the phase shifts (see Figure 1.7 C). However, the direction of rotation of the spins will not have changed. After a second interval of time TE/2, the signal is measured. As all spins will have returned to the starting point, the decrease in the measured transverse component will only be due to the true time constant T2 (see Figure 1.7 D) [3].

A SE sequence is used to acquire one line of the Fourier plane in the K-space (frequency space), used to recreate the entire image. A repetition time (TR) is waited between the acquisition of each line ensuring the protons have completely relaxed, i.e. that the transverse component $\overrightarrow{M}_{xy}$ has completely disappeared and that the longitudinal component $\overrightarrow{M}_z$ has regained its maximum amplitude [3]. This mechanism is schematically resumed on the Figure 1.8.

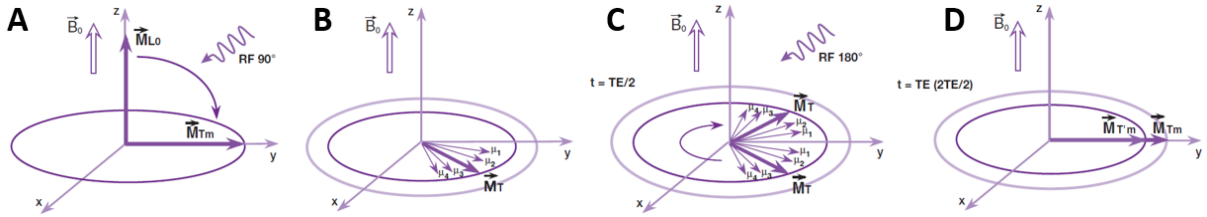


Figure 1.7: Visualisation of the SE phenomenon. **(A)** A 90° RF impulse aligns the magnetisation vector along Ox. **(B)** The relaxation begins. **(C)** After a TE/2 time, a 180° RF pulse reverses the orientation of the longitudinal component by inverting the phase shifts without changing the direction of rotation. **(D)** After another TE/2 time, the signal is measured. Adapted from [3].

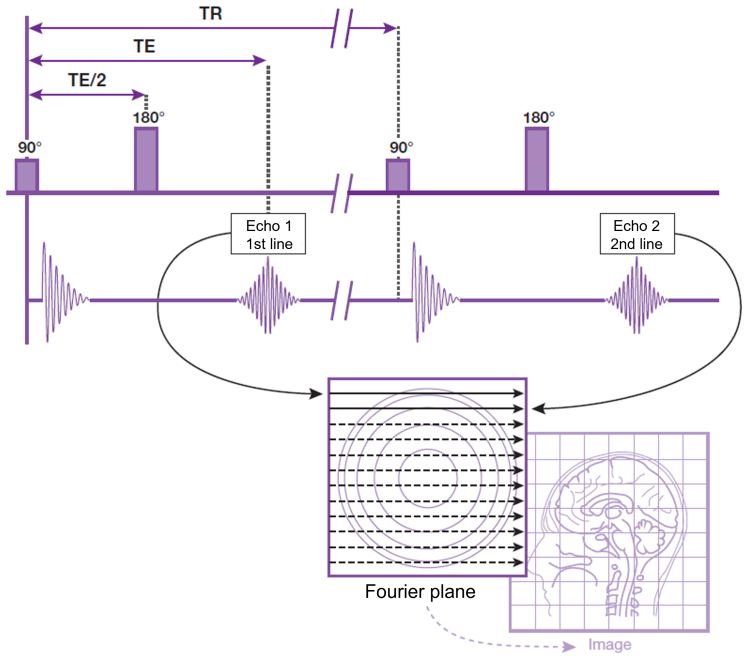


Figure 1.8: SE sequences and the complete Fourier plane acquisition process. Each SE sequence allows the acquisition of one line of the Fourier plane used to reconstruct the final image. Adapted from [3].

.

1.1.5 Contrast

Each type of tissue is characterised by its own T1 and T2 time constants and proton density. Depending on what you want to study, one or the other of these characteristics may be more interesting to highlight. The process of weighting an image in T1, T2, or proton density to achieve contrast between various tissues is accomplished by selecting appropriate sequence parameters (TE, TR) [3].

T1-weighted image

TR is the main parameter to weight the image in T1. Indeed, the longer TR is, the greater the longitudinal component whose regrowth is characterised by the T1 time. If TR

is decreased, the longitudinal component of tissues with a short T1 will still have managed to approach their maximum amplitude. In the contrary, the longitudinal component of tissues with a long T1 will not have been able to regrow fully. The difference between the two will therefore be quite marked. TE must also be short in order to measure the signal before relaxation, allowing the two tissues to be distinguished. A long TE also minimises T2 contrast (see Figure 1.9) [3, 5].

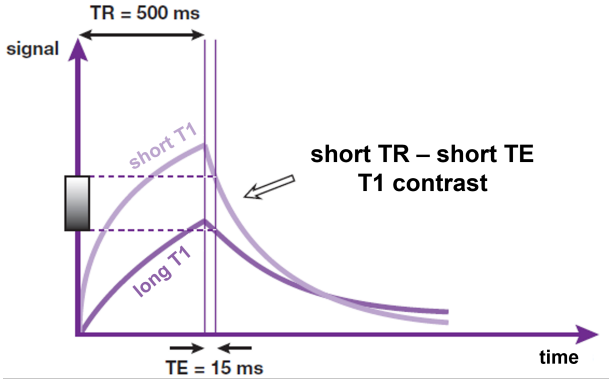


Figure 1.9: Evolution of the signal of two tissues either with a long T1 or a short one, leading respectively to low and high signal amplitude at TE. Adapted from [3].

Tissues with a shorter T1 will show a higher signal (they will appear white). In the brain, white matter (WM) will be white on the images, grey matter (GM) will be grey and cerebrospinal fluid (CSF) will be black because it has the longest T1. Cavities and bones or calcified parts will also appear black [3, 5].

T2-weighted image

To weight an image according to T2, you have to play mostly on TE. First, a long TR leads to a maximal longitudinal component. TE is then used to vary the proportion of signal fading. If TE is too short, the two signals will be close and will therefore be difficult to distinguish. If TE is longer, the signal of a tissue with a short T2 will have already almost completely disappeared. In contrary, the signal of a tissue with a long T2 will not finish decaying (see Figure 1.10) [3, 5].

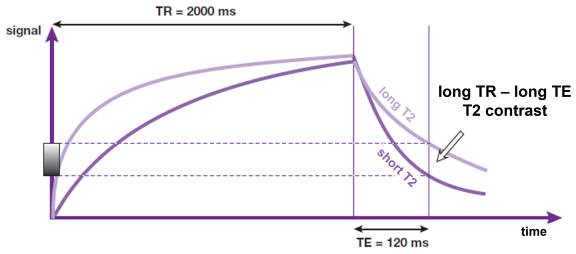


Figure 1.10: Evolution of the signal of two tissues either with a long T2 or a short one, leading respectively to high and low signal amplitude at TE. Adapted from [3].

Tissues with long T2 will therefore appear bright (white) while tissues with short T2

will be dark (black). In the brain, the WM will appear black because it has a short T2, the GM will appear grey and the CSF will appear white. In this case, cavities appear white and bones appear black [3, 5].

Proton density weighted

Finally, it is possible to weight the image in proton density by lengthened TR (to minimise T1 contrast) and shortened TE (to minimise T2 contrast). By examining the difference in amplitude of the longitudinal components $\overrightarrow{M_z}$ at equilibrium, the variations proportional to the proton density within the tissue is observable (see Figure 1.11). The denser in proton a tissue is, the stronger its signal will be (white) and conversely, a tissue with a low proton density will appear black [3, 5].

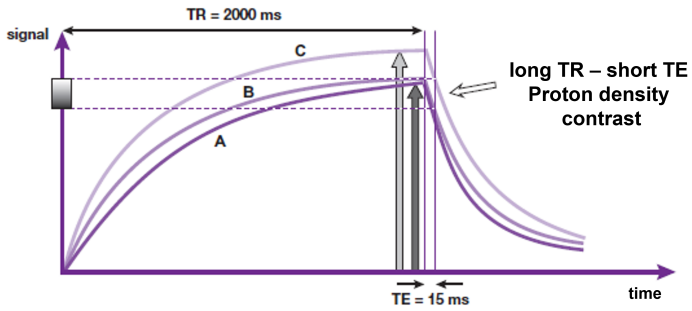


Figure 1.11: Evolution of the signal of three tissues with tissues A and B with the same proton density and tissue C with a different one. The amplitude of the signal after a TR time is higher for tissue C since it has a higher proton density than tissues A and B. Adapted from. Adapted from [3].

1.2 Acquisition process

Having understood the interpretation of the obtained signal, the next step is to determine its spatial location. This involves selecting a slice plane and traversing the K-space (frequency space) in order to obtain the final image through the Fourier transform. This is achieved by using different gradients created by coils placed around the patient. As shown on Figure 1.12, the chronology and the elements that make up a complete SE sequence [3].

In a nutshell, a first magnetic field gradient (the slice plane gradient Gss) is added to the $\overrightarrow{B_0}$ field. This allows the selection of a slice plane oriented perpendicular to the direction of the gradient by only exciting the protons that meet the resonance condition (i.e. only protons with a specific angular frequency) when a precise RF pulse is applied. Secondly, during the signal acquisition, a frequency encoding gradient, G_ω, is applied perpendicular to the slice plane gradient, Gss, and allows the encoding of the different frequencies on one line of the K-space. Finally, a phase encoding gradient, G_ϕ, is applied perpendicular to the other two gradients with a different amplitude at each repetition allowing the acquisition of each line of the K-space [5]. Additional details on these 3 gradients are available in Appendix A.

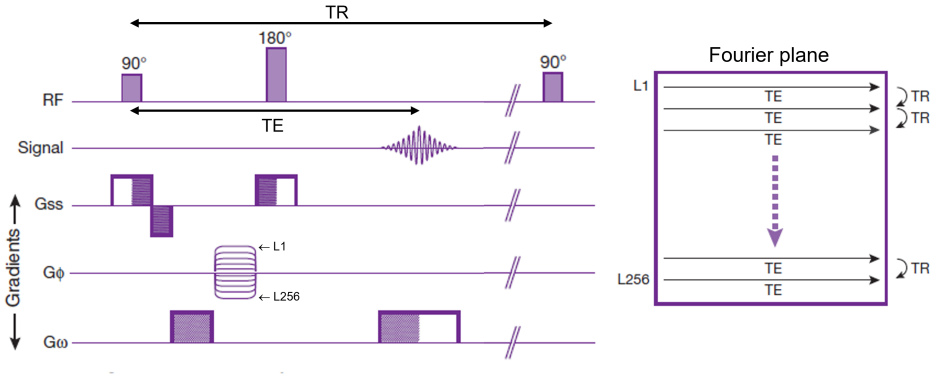


Figure 1.12: Complete acquisition chronology with all gradients of the SE sequence. Adapted from [3].

The SE sequence is what could be considered as the basic sequence, at least the first sequence used. A major disadvantage of this sequence is that it requires a long TR for the magnetisation vector to fully cancel and therefore a long total duration. This is particularly the case for T2-weighted and proton density sequences, which reach TR times of 2000ms, as opposed to T1-weighted sequences, which only reach 500ms. A large part of this time is actually a waiting time not really used. Technological developments allowed to develop other types of frequencies to reduce this "lost" time and therefore the total duration of the acquisition or even increase the quality of the image (without modifying the acquisition time). This is done by playing with the application of gradients and pulses to obtain, for example, several K-plane lines or several images in the same TR time.

1.3 Diffusion imaging

1.3.1 Diffusion-weighted imaging (DW-MRI)

Another type of contrast can be used in MRI. This is a diffusion contrast which allows the movement of water molecules to be highlighted. At the microscopic level, water is constantly in motion. Depending on the environment and the obstacles encountered by these molecules, their diffusion will be more or less restricted [3, 6].

This type of contrast is done using a new sequence in which new gradients are applied on either side of the 180° pulse. A first gradient is applied to dephase the protons. The amplitude of the phase shift is proportional to the amplitude of the applied field and therefore depends on the position of the proton in the slice. A second gradient, identical to the first in amplitude and duration but of opposite sign, is then applied and results in the protons being re-phased. If the protons do not moved, do not diffuse between the application of the two gradients, the measured signal is maximum. Conversely, if the protons are no longer at the same position, the perceived field strength will be different and they will not re-phase correctly. The measured signal will therefore be reduced. This principle is schematically explained on Figure 1.13 [3, 6].

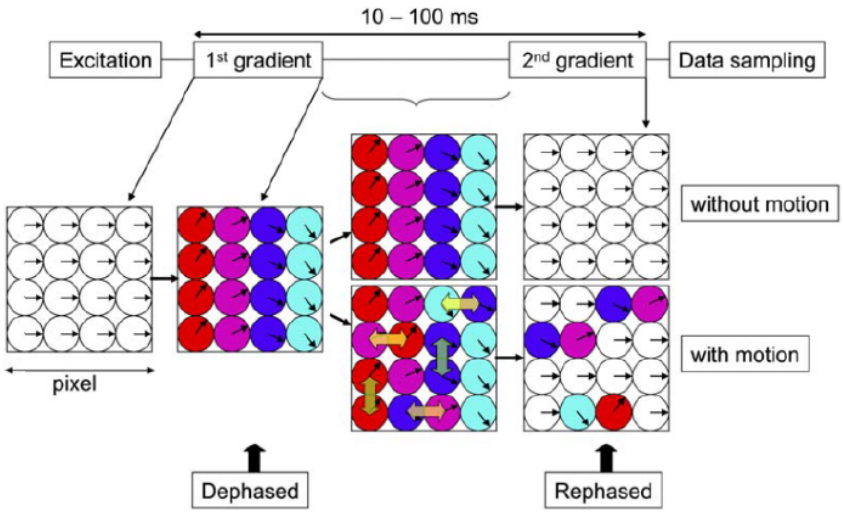


Figure 1.13: Schematic explanation of diffusion-weighted imaging principle. Protons that have not diffused perceive two magnetic fields of identical amplitude and duration but opposite direction and are therefore perfectly re-phased. Conversely, protons that have diffused do not perceive fields of the same amplitude and the resulting phase shift induced a reduction of the measured signal [7].

In a three-dimensional volume, water molecules can diffuse along all directions. However, the application of a gradient is done along one of the three directions and can only measure diffusion along this axis. In order to have a global view, the process must be repeated by successively applying gradients along the three directions [3, 6].

The image can be more or less contrasted by the diffusion according to a gradient factor, b, which takes into account the amplitude of the gradient (G), the time of application of the gradient (τ) and finally the time between the two gradients (T) according to the following formula :

$$b = (\gamma G \tau)^2 (T - \tau/3) \tag{1.4}$$

where γ is the gyromagnetic ratio. It varies between 0 and 3000s/mm^2. The higher the value of b, the more sensitive the sequence will be to the diffusion of molecules [3].

A complete sequence is usually composed of one acquisition with a zero b followed by three acquisitions with a b greater than zero to measure the diffusion along the three axes of the slice. An averaged image of these last three acquisitions can then be created to obtain an image illustrating the differences in diffusivity regardless of the directions for each position in the observed area [3].

The apparent diffusion coefficient (ADC) can be calculated. It measures the diffusion of water in the tissues, which is reduced by biological barriers [6]. The ADC can be calculated from the following relationship:

$$log(S/S_0) = -b \cdot ADC \tag{1.5}$$

with S_0 the signal acquired with $b = 0$, and S the signal acquired with sensitivity corresponding to a gradient factor b [3].

1.3.2 Diffusion tensor imaging (DTI)

Water molecules do not diffuse freely in the same way in all parts of the brain. The presence of cell membranes, proteins, myelin, intracellular filaments, organelles and all the components of the nervous system restrains diffusion. In some areas, such as in the CSF and, to a lesser extent, in the GM, molecules diffuse in all directions and are equally constrained in all these directions. This is called isotropic diffusion. This is not the case in the WM, where the molecules are constrained by the axons to diffuse only along their axis. This is called anisotropic diffusion [6].

Combining all the data on diffusivity in the three directions by averaging them into a single image results in a significant loss of information. One solution is to gather them (without mixing them) in a 3D tensor called diffusion tensor :

$$\overline{\overline{D}} = \begin{pmatrix} D_{xx} & D_{xy} & D_{xz} \\ D_{yx} & D_{yy} & D_{yz} \\ D_{zx} & D_{zy} & D_{zz} \end{pmatrix} \tag{1.6}$$

This tensor is symmetric, meaning that $D_{xy} = D_{yx}$, $D_{yz} = D_{zy}$ and $D_{zx} = D_{xz}$ [8]. It can be visualised geometrically by an ellipsoid as shown in Figure 1.14.A. From this tensor, different quantitative information can be extracted such as the eigenvectors (shown in blue on the figure) indicating the main directions of the diffusion and the associated eigenvalues (shown in red on the figure). The left side of Figure 1.14 shows different shapes of this ellipsoid depending on the type of diffusion (anisotropic or isotropic) [6].

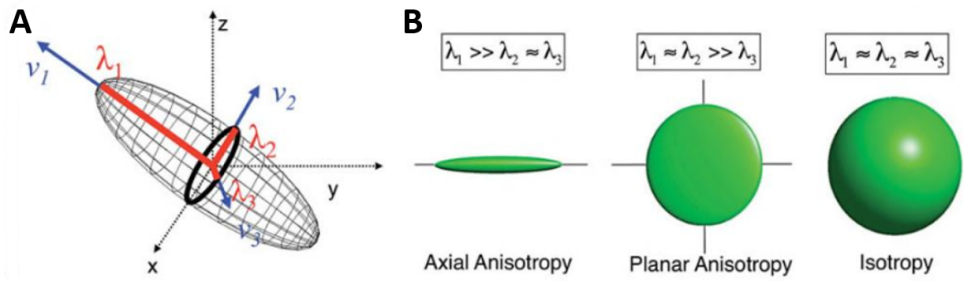


Figure 1.14: Geometric visualisation of the diffusion tensor. **A** The main axes of the ellipsoid correspond to the eigenvectors and represent the main directions of diffusion. **B** Depending on the type of diffusion, the ellipsoid can take different shapes. [6]

Not all eigenvalues are directly used as such but are combined to extract different quantitative metrics [9] :

The **Mean Diffusivity (MD)** measures the total diffusivity of a voxel regardless of direction. It is therefore an average of the diffusivity in all directions. It is calculated as follows:

$$MD = \frac{Tr(\overline{\overline{D}})}{3} = \frac{\lambda_1 + \lambda_2 + \lambda_3}{3} = \frac{D_{xx} + D_{yy} + D_{zz}}{3} \tag{1.7}$$

MD is low in regions where the movement of water molecules is strongly restricted, as is the case for example in the WM. In contrast, in the CSF where water molecules can move more freely, MD is much higher [9].

The **Axial Diffusivity (AD)** (also called longitudinal or parallel diffusivity) focuses on the diffusivity in the main direction of the ellipsoid. It is therefore simply the first (and therefore largest) eigenvalue [9].

$$AD = \lambda_1 \tag{1.8}$$

The **Radial Diffusivity (RD)** (also called transverse or perpendicular diffusivity) gathers the diffusivity along the other 2 axes (perpendicular to the main axis) [9].

$$RD = \frac{\lambda_2 + \lambda_3}{2} \tag{1.9}$$

Finally, **Fractional Anisotropy (FA)** is a measure of the anisotropy of diffusion.

$$FA = \sqrt{\frac{3}{2}} \frac{\sqrt{(\lambda_1 - \overline{\lambda})^2 + (\lambda_2 - \overline{\lambda})^2 + (\lambda_3 - \overline{\lambda})^2}}{\sqrt{(\lambda_1 + \lambda_2 + \lambda_3)}} \tag{1.10}$$

where $\overline{\lambda}$ equals the mean of the 3 eigenvalues (corresponding thus to MD). It is a value in the range [0,1], where 0 means that the diffusion is totally isotropic (the ellipsoid is a perfect sphere) and 1 means that the diffusion is very anisotropic and acts only in a specific direction (the ellipsoid is therefore very thin and elongated). FA gives an indication of the organisation and microarchitecture of the nervous tissue. In a healthy brain, the maximum FA is about 0.8, usually in the WM since diffusion is directed mainly along the axon axis, and the minimum FA is about 0.1, in the GM and CSF. Certain pathologies such as oedemas or demyelination result in a decrease in FA which is therefore often used to measure the integrity of nervous structures [6].

1.3.3 Limitations of DTI

DTI allows non-invasive observation and analysis of the brain structure. DTI is mainly used to study WM and, as it allows the extraction of quantitative values, is also widely used to study the evolution of microstructures and to detect many pathologies [6, 9].

However, it also has many disadvantages. The noise level is quite high resulting in a low signal-to-noise ratio (SNR) and therefore a decrease in the accuracy of the measurements. Lots of artefacts can also impact the estimation of the diffusion tensor and influence the values of the metrics obtained. The choice of the factor b is very important. If it is too low, the influence of diffusion is not sufficiently emphasised. But too high, it increases the sensitivity and therefore also the amount of noise and artefacts. In short, all the parameters and conditions of acquisition as well as the pre- and post-processing steps of the images can influence the metrics and the resulting analysis. When comparing patients or studying the evolution over time, one must be attentive to all these elements to have an accurate interpretation of the results [9].

In addition, DTI assumes that the motion of water molecules consistently follows a Gaussian distribution. This is true in extra-cellular regions, but not in intra-cellular regions where diffusion is restricted and follows a non-Gaussian distribution [9, 10, 11].

Moreover, the interpretation of the metrics is not unique and constant. Indeed, DTI is a powerful mathematical tool for reducing a complex and varied set of information into a small number of simple and sensitive metrics. However, it is an oversimplification that mixes biological, methodological and pathological contributions. For example, a decrease in FA can equally indicate a change in fibre density or a dispersion of these fibres. Despite the distinct interpretations, the impact on the metric remains the same. Blindly analysing the metric alone does not provide insight into the underlying cause of this evolution [10].

Finally, as the resolution of a voxel is much lower than a fibre, DTI cannot always identify the finest fibres and groups together all the fibres passing through a voxel without isolating different populations. The metrics obtained will be a combination of the values of the metrics for each of the populations, which no longer reflect the reality of the brain's complexity [6, 9].

To solve parts of these limitations, more advanced models have been developed.

1.4 Advanced diffusion models

1.4.1 NODDI

The acronym NODDI stands for Neurite Orientation Dispersion and Density Imaging. This model is used to estimate more accurately than DTI the complexity of the brain's microstructure, in particular the neurites constituted by axons or dendrites of neurons. The model is based on a combination of three compartments, each representing a type of tissue present in the brain: CSF, intra-cellular tissues and extra-cellular tissues. In each compartment, the water molecules are influenced differently by the tissue, resulting in variations in the signal measured by diffusion weighted MRI (DW-MRI). The signal obtained is therefore a combination of the signal from each compartment forming the complete voxel:

$$A = \nu_{iso}A_{iso} + (1 - \nu_{iso})(\nu_{ic}A_{ic} + (1 - \nu_{ic})A_{ec}) \tag{1.11}$$

with A_x the signal from the compartment x and ν_x, the volume fraction of the compartment x. iso stands for the compartment of CSF, ic for the intra-cellular compartment and ec for the extra-cellular compartment [10, 11]. Let's go through each compartment which are illustrated in Figure 1.15.

The **intra-cellular compartment** designates the interior of the neurites, i.e. delimited by the cell membranes of the neurons. This compartment is modelled by sticks, which means cylinders of radius zero. The diffusivity in this area follows a non-Gaussian distribution. The diffusion along the main axis is favoured, whereas the diffusion in the perpendicular directions is strongly reduced. An important parameter of this model is the orientation of the fibres varying from strongly parallel to strongly dispersed sticks [11].

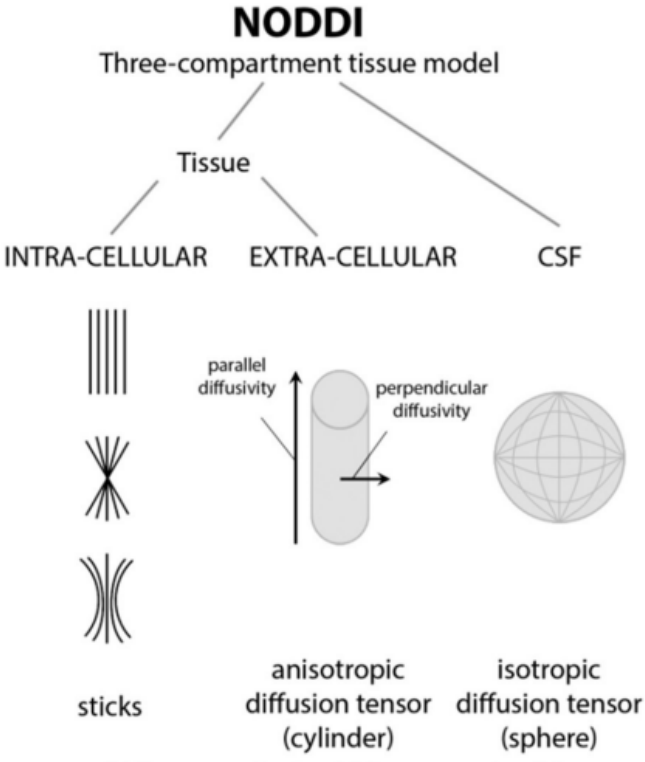


Figure 1.15: Representation of the three compartments used in the NODDI model (intra-, extracellular and CSF). The intracellular compartment is modelled by sticks (cylinders of zero radius). The constrained diffusion in the extracellular space is represented by a cylinder with a longitudinal and a radial diffusivity component. The isotropic (or free water) compartment, named CSF compartment, is represented by a sphere [10].

The **extra-cellular compartment** refers to the space between and around the neurites. It is mainly composed of glial cells to which cell bodies, the somata, are added. In this area, diffusion is restricted by the neurites, especially in directions perpendicular to the fibres, but not as much as in the neurites (i.e. in the intra-cellular compartment). Thus, in order to model this anisotropic diffusion following a Gaussian distribution, this compartment is represented by cylinders with non-zero radii [11].

Finally, the **CSF compartment** obviously corresponds to the space occupied by the CSF whose diffusion is isotropic and described by a Gaussian distribution. This compartment is therefore modelled by a sphere [11].

However, the NODDI model is not perfect. It models all types of WM fibres in a similar way (sticks). However, there are a variety of fibres in the brain with different properties such as radius and NODDI does not take into account this variable radial diffusivity inside fibres. Finally, NODDI considers only one fibre fascicle crossing each voxel, whereas the majority of voxels in the brain are crossed by several fascicles [12].

1.4.2 DIAMOND

DIAMOND is another DW-MRI model that attempts to go even further than DTI and NODDI. This model aims to characterise the DIstribution of 3D Anisotropic MicrOstructural eNvironments in Diffusion-compartment imaging, hence the name DIAMOND [12].

DIAMOND models in more detail the attenuation of the signal caused by the diffusion of water molecules. This signal does not undergo a simple monoexponential decrease due to a constant and heterogeneous apparent diffusion coefficient throughout the voxel. As in the NODDI model, the DIAMOND considers several types of tissue with different diffusion properties.Furthermore, it allows each tissue type to be modelled with different characteristics influencing diffusion properties. For example, WM fibres can be modelled differently depending on their radius [12].

Each voxel is composed of a series of spin packets characterised by an anisotropic diffusion following heterogeneous distribution. The signal of the measured voxel can thus be modelled by integrating the contributions of each spin packet whose diffusivity is D and whose voxel occupancy fraction is described by a probability distribution P(D). In the end, the measured signal S_k is expressed by the following formula :

$$S_k = S_0 \int P(D) exp(-b_k g_k^T D g_k) dD \tag{1.12}$$

where b_k is the gradient factor characterising the diffusion contrast, S_0 the signal without diffusion contrast and g_k the direction of the gradient. In order to get closer to reality, the diffusivity D is a 3D tensor to represent the anisotropy of the diffusion. Moreover, since each voxel is heterogeneous and is composed of different tissue types which are themselves also heterogeneous, the spin packets are characterised by P(D), a Gamma (not Gaussian) distribution. The parameters of this distribution vary between spin packets to best estimate the microstructure of the modelled tissue. In this way, a voxel can be composed of several compartments, some corresponding to the same type of tissue but with different diffusion and distribution properties [12]. This model is schematically illustrated on Figure 1.16.

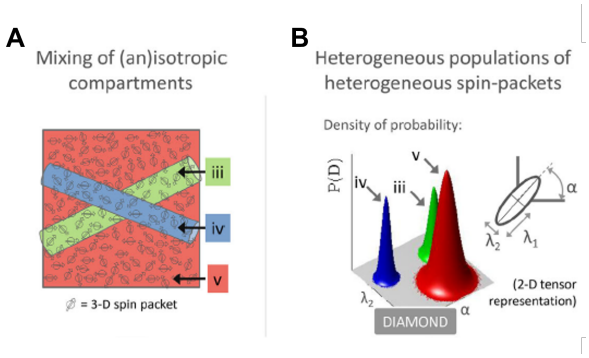


Figure 1.16: DIAMOND model : **A** Several compartments are represented inside a voxel by an isotropic compartment in red and two anisotropic compartments in blue and green. **B** Probability density function taking the diffusion heterogeneity of each compartment into account (adapted from [12]).

1.4.3 Microstructure Fingerprinting

The model Microstructure Fingerprinting (MF) tries to go one step further in modelling and thus interpreting DW-MRI signals. The models presented above are based on strong assumptions distancing the result from the biological reality of the brain microstructure. The MF model attempts to achieve a more accurate and robust estimate [13].

This model is based on Monte Carlo simulations, which are known to predict the random movement of water molecules quite reliably for a multitude of different gradient parameters, cell geometries and environments. DW-MRI signals are therefore predicted for a set of WM fascicle types and CSF compartment and stored them in a dictionary. The model then estimates the K number of fascicles in each voxel and the proportion of the CSF compartment and solves an optimisation problem to predict the most accurate independent combination of all these components producing the measured DW-MRI signal. Analytically, this can be summarised by the following equation:

$$S = M_0\left(\left[\sum_{k=1}^{K} \nu_k A_{fasc}(\Omega_k, T_k, u_k; g)\right] + \nu_{csf} A_{csf}(D_{csf}, T_{csf}; g)\right) \tag{1.13}$$

where M_0 is a scaling factor, ν_x are the occupation fraction of each WM fibres or CSF compartment, the A_x are the predicted DW-MRI signals founded in the dictionary that can be a function of the parameters characterising the microstructural environment Ω_k, the relaxation NMR parameters (such as T1, T2 and the proton density) T_k, the principal orientation of the WM fibres u_k, the magnetic field gradient profile g and the scalar diffusivity D (defining free and isotropic diffusion of water molecules in the CSF compartment) [13].

1.5 Tractography of the WM

Another common use of DTI is for tractography. This refers to the reconstruction of WM tracts in the brain. The first important thing to understand is that tractography does not represent each individual axon, but the macroscopic trajectory of an entire fascicle composed of a very large number of axons. Indeed, the diameter of an axon is generally around 1 to 10 µm whereas the voxels measure 2 x 2 x 2 mm^2. One of the most widespread applications is the segmentation of the different brain tracts individual to each subject. This allows the definition of a region of interest (ROI) in which the evolution of different parameters and metrics (such as those extracted from DTI) can be analysed. Sometimes called "tractometry", this will be used to delineate the ROI of this study [9].

The general principle of tractography is to create fibres propagating from voxel to voxel, each time following the main direction of diffusion, i.e. the direction of the largest eigenvector. More precisely, each fibre starts at a defined seed point r_0 in a certain voxel of interest. The fibre advances by a step of defined length in the direction of the largest eigenvector of this first voxel. A second point r_1 is then reached in a possible other voxel whose largest eigenvector will in turn define the direction of the next step to continue the propagation of the fibre. This consists of a first order integration method : only the direction of the voxel in which the point r_i is located is taken into account to extend the

fibre to the point r_{i+1}. It is possible to use higher order integration methods taking into account the main directions of several previous steps. For the second order integration method, the direction of propagation will depend for example on the points r_i and r_{i-1} [14]. This mechanism continues until a stop condition is reached. As illustrated on Figure 1.17, fibre tracking is not commutative since initiating a fibre by positioning a seed in the last voxel will not always recreate a fibre going to the initial seed [9].

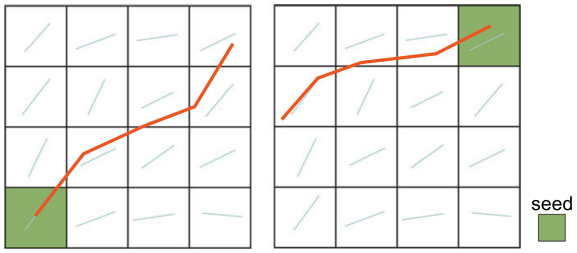


Figure 1.17: Illustration of the WM tractography principle. From a seed voxel, the propagation of the tract follows the direction of maximum diffusion corresponding to the direction of the largest eigenvector. The choice of seeds is very important because tractography is not bijective. Adapted from [9].

There are several ways to determine the main direction of diffusion at a certain point. The simplest method is to take the direction of the nearest voxel (nearest-neighbor interpolation). This method leads to more interpolation errors and may divert the fibres from their true path. Second or third order interpolation is then regularly applied to calculate the principal direction at a point, based on the neighbouring voxels [14].

The principle described above represents the general approach to tractography, called the deterministic approach. Unfortunately, it only considers one fibre population per voxel oriented along the principal direction of diffusion. Another approach, called probabilistic, calculates the distribution of all possible trajectories for a fibre starting from each seed point (see Figure 1.18). This approach represents the fibre orientations by continuous functions called fibre orientation distribution (ODF). This enables the execution of fibre tracking within regions characterised by intricate, for example in areas where fibres cross each other, such as in the corpus callosum [14].

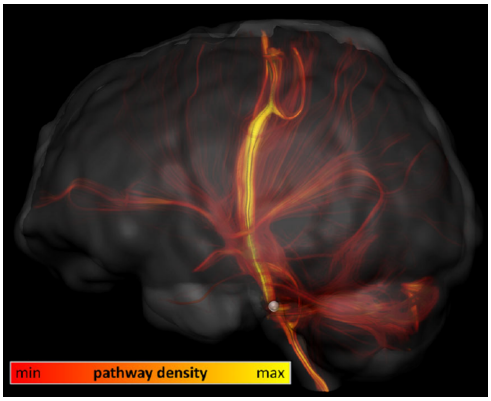


Figure 1.18: Distribution of all possible trajectories emanating from a single seeding point (white sphere) in a probabilistic tractography approach. The trajectories are coloured according to the local density of the trajectories. Locations with higher densities are considered to have a higher probability of "connection" to the starting point [14].

In addition, two types of strategy can be used. In a so-called local strategy, each step is taken independently of the others. Thus, the fibres are tracked step-by-step. On the other hand, in a global strategy, the algorithm tries to reconstruct the entire set of fibres by finding a configuration that best matches the dMRI data obtained as a whole [14].

Several conditions can be defined to stop the propagation of a fibre in order to prevent the creation of tracts with no anatomical feasibility. For example, the propagation of the fibre can be stopped when it reaches a region that the real bundle is too unlikely to reach. This can be done using anatomical priors on the type of tissue in the voxels (CSF, GM or WM). Also, a threshold can be set on the maximum angle of curvature of the fibres so that they do not acquire neurologically inaccurate shapes or rotate on themselves. Limits can also be applied to local fibre density or to the FA value to contain the fibres in regions of high fibre density or high FA. These criteria or parameters are usually chosen empirically to find the best balance between the number of false positives and false negatives. However, it is important to note that in a comparative analysis, identical parameters should be applied to avoid biasing the results. Finally, ROIs can be used to exclude fibres from certain regions and minimum and maximum values for tract lengths can be defined. For reliable tractography to be obtained, quality data must be used. This implies a sufficiently high spatial resolution, a high sensitivity to diffusion orientation and the highest possible SNR [9, 14].

The selection of seeds to initiate tractography can be done manually or on the basis of atlases and target specific areas to obtain only certain WM bundles. It is also possible to position a seed per voxel of WM or to make this operation automatic depending on anatomical prior (a seed in all WM voxels close to the GM for example), and to obtain a complete tractography of the whole brain. Then, logical operations (AND, OF, NOT) based on predefined ROIs can be used to isolate tracts by choosing areas where fibres should start, end and pass through or on the contrary exclusion regions. More details will be provided in the section 3.3.1 describing the methods used in this study [9].

1.6 ElikoPy pipeline

The ElikoPy pipeline is a python library for preprocessing diffusion images. It allows a series of corrections and enhancements to be made to images obtained by DW-MRI and to extract metrics for microstructure analysis (corresponding to the models introduced in the previous sections). This pipeline allows for effective, reliable and reproducible treatment of a large patient population [15].

An overview of the ElikoPy pipeline organisation is illustrated on Figure 1.19. The image treatment starts with a check of the data provided by the user, in particular the dimensions of the b-values and b-vectors files and their correspondence with the image files. If this check is successful, a subject-specific folder is created and the preprocessing suite can begin. If this is not the case, preprocessing cannot be performed for that subject. Then comes the preprocessing stage itself, with the aim of correcting the anatomical non-idealities and the errors and artefacts introduced during the acquisition. This can consist of several corrections and improvements that can be applied or not depending on

the user's choices. The only mandatory step is the removal of the voxels corresponding to the skull. The other steps proposed by ElikoPy are numerous, only those used to process the images in this study are described below [15].

- **Reslicing :** Clinical images are often rendered smoother and with an artificially higher resolution by an interpolation on the data. It is possible with this option to reslice the data and to remove this unwanted interpolation which can have negative consequences for further preprocessing and analysis.
- **Denoising :** The data is denoised using a Marcenko-Pastur PCA algorithm from the DiPy library [16]. This algorithm allows to obtain a noise reduction in a fast way without the addition of blur or artefact.
- **Gibbs Ringing Correction :** Diffusion images are regularly affected by ringing artefacts. These can be corrected using functions in the DiPy library.
- **Bias field correction :** As already explained above, the magnetic field used in scanners may contain inhomogeneities that will affect the measured signals. A correction can therefore be applied to avoid an impact on future metric extractions.
- **Eddy and motion correction :** The distortions created by movements and Eddy's currents have a relatively similar effect on the data. They can therefore be corrected simultaneously.

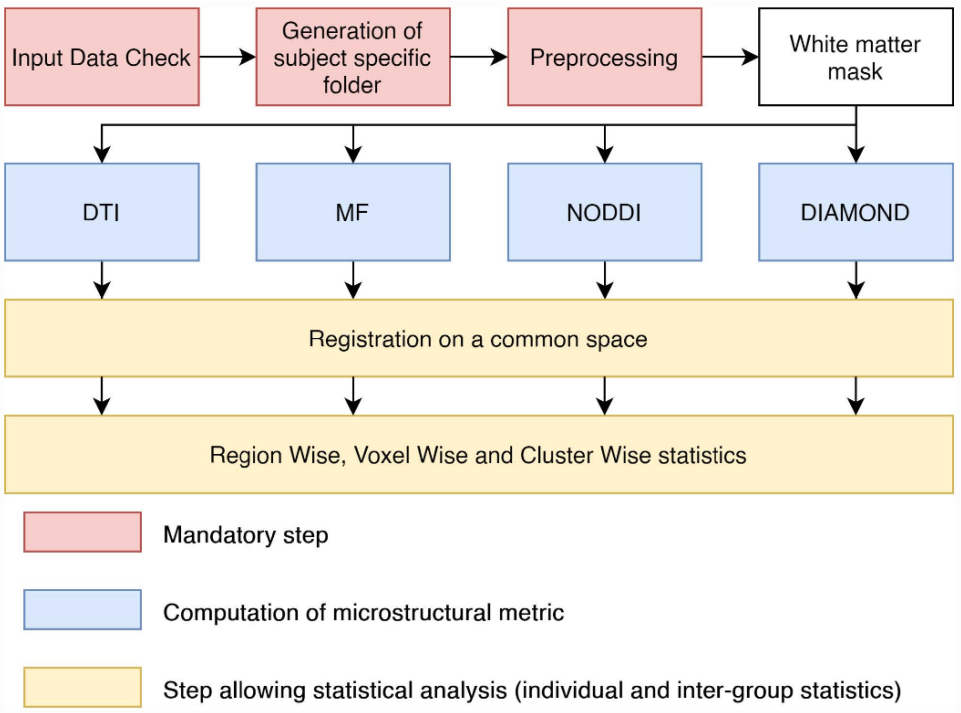


Figure 1.19: Schematic overview of the preprocessing steps provided by the ElikoPy pipeline [15].

The next step is the creation of a WM mask from the subject's T1 image if available. This allows to isolate certain structures of interest in the brain and to accelerate the next steps of the pipeline. In particular, the WM mask and preprocessing steps prevent error propagation and improve sensitivity for the computation of DTI metrics specific to each of the models (DTI, NODDI, DIAMOND and MF), which is the next step. Full brain tractography can also be performed using ElikoPy. An optional step to facilitate statistical analysis can be incorporated, although it will not be extensively discussed since it is not utilised in this study. Finally, each of the previously mentioned steps can be accompanied by a quality control report [15].

In summary, the ElikoPy pipeline provides a range of tools (sometimes from other existing libraries but providing corrections to each "sub-problem", each type of noise or artefact individually). Given the growth of DW-MRI in recent years and the desire to be able to process large numbers of subjects quickly, whether for individual patient clinical needs or for larger studies, a robust pre-processing framework provides a significant advantage and ensures consistency and artefact reduction for all subsequent analysis [15].

Chapter 2

Alcohol Use Disorders

2.1 Definition of AUD

Alcohol Use Disorder (AUD) is a medical condition that results in the inability for patients to control or stop drinking alcohol despite the negative consequences on health, social and professional relationships [17]. It is one of the most dominant disorders in the world and particularly in the more developed countries where incomes are higher. It is associated with a high mortality rate and many diseases due to the medical consequences of drinking on different parts of the body such as the liver [18]. In the United States in 2019, studies indicate that 5.1% of adults over the age of 26 suffer from AUD and this percentage reaches 9.3% for 18-25 year olds. Usually, men are more prone to this disorder, up to twice as much as women, but the risk of it reaching a level qualified as severe is higher for women. Women are also more likely to experience longer-term consequences [1].

Many factors can increase the risk of developing AUD and these are more or less dominant depending on the individual. Drinking alcohol frequently, rapidly or in large quantities increases the risk. The age of onset is also important : starting to drink before the age of 15 increases the risk by up to 5 times compared to those who wait until they are 21. Psychiatric conditions or mental illnesses including depression, trauma, attention deficit hyperactivity disorder, stress-related disorder, etc. are other elements that can lead to AUD. Genetics and family history are also part of these factors. Heredity can play a major role, as can the interaction between a person's genes and their environment or the environment alone. A child who lives with parents drinking a lot of alcohol, for example, is more likely to develop AUD later in life. Society itself can have a huge influence. Depending on the culture, drinking alcohol can be something totally forbidden or conversely, considered as normal and sometimes even encouraged [17, 18].

The diagnosis of AUD is based on a precise list of criteria defined by the Diagnostic and Statistical Manual of Mental Disorders 5th edition (DSM-5). These are the following [19] :

- Developing tolerance to alcohol i.e. needing more alcohol to feel the same effects as before.
- Experiencing withdrawal symptoms when stopping drinking.
- Experiencing difficulties to control drinking (cutting down or stopping).

- Neglecting other activities in favour of drinking alcohol.
- Spending time drinking or recovering from the effects of alcohol.
- Drinking despite physical or psychological problems.
- Feeling the craving for alcohol when not drinking.
- Consuming alcohol in larger amounts or over longer periods than was intended.
- Failing to fulfil major professional or personal role obligations.
- Recurrently using alcohol in hazardous situations.
- Continuing to drink alcohol despite social or interpersonal problems.

Depending on the number of criteria fulfilled by a person over a period of one year, the severity of AUD can be established. If two or three criteria are met, it is a mild AUD. If four or five criteria are met, it is a moderate AUD. And if six or more criteria are met, it is a severe AUD [17, 19].

Alcohol consumption is dangerous to health because it attacks many parts of the metabolism, including the brain, which is the focus of this study. Fortunately, AUD is treatable, and brain damage is partially reversible with abstinence (see section 2.2). However, there are still a lot of stigmas around alcoholism which results in a low rate of treated patients. On the one hand, people with alcoholism can be seen as dangerous (in relation to the behaviour that drinking can cause) or weak and responsible for their disease, which does not encourage people or doctors to provide help and treatment. On the other hand, alcoholic patients are afraid of this stigma and sometimes prefer not to admit their problems and do not seek help. However, there are effective treatments. These generally revolve around several axes, the combination of which allows an optimal remission and a minimal risk of relapse. Behavioural treatment can be provided by psychologists and therapists by giving advice, seeking to change patients' behaviour through reinforcement approaches, self-control training or mindfulness techniques. All with the same goals, to boost motivation, to encourage abstinence, to overcome withdrawal and to avoid relapse in the short or long term. Medication support can be provided to stop or reduce consumption and prevent relapse. Finally, mutual support groups between patients allows them to help and motivate each other in the recovery process in a less formal way [18, 17, 19].

2.2 Biological impacts of AUD

As previously mentioned, alcohol exerts numerous effects on the human body, and AUD is associated with a significant burden of disease. Various components of the digestive system, which directly interact with alcohol during ingestion, can be susceptible to multiple diseases. The liver, for instance, is notably vulnerable resulting in cirrhosis, fibrosis or sclerosis. Damage to the pancreas is also observed, such as pancreatitis. Furthermore, alcohol consumption has been linked to the development of several cancers, including colorectal cancer and breast cancer in women. The cardiovascular system is not spared, as

AUD can contribute to conditions like strokes, hypertensive and ischaemic heart diseases, as well as dysrhythmias. Finally, AUD can heighten the risk of tuberculosis, respiratory issues like pneumonia, psoriasis, type 2 diabetes, epilepsy, among many others disorders [20].

Alcohol also has a wide range of adverse effects on the brain by altering its microstructure. It is sometimes even difficult to distinguish between neurological features that are part of the causes or consequences of AUD. Nevertheless, it is undeniable that the relationships between alcoholism and brain structures are numerous and complex.

2.2.1 Anatomical content

The nervous system is a complex and organised system of cells, tissues and organs that plays an essential role in the functioning of the body. The nervous system is divided into two main parts: the central nervous system (CNS) and the peripheral nervous system (PNS). The CNS consists of the brain and spinal cord, which are protected by the skull and spine, respectively. It is responsible for the coordination and regulation of all body functions. It is also the seat of thought, memory, learning, sensory perception, motor skills and many other functions. The spinal cord is responsible for the transmission of sensory and motor information between the brain and the rest of the body. The PNS consists of nerves and ganglia connecting the CNS to peripheral organs [21].

The CNS is organised into two types of tissue: grey matter (GM) and white matter (WM). GM is made up of the cell bodies of neurons. It is mainly found in the brain, cerebellum and spinal cord. WM consists of nerve fibres called axons that transmit information between neurons. It is found in all parts of the nervous system, but is particularly abundant in the brain. WM is so called because the fibres are covered with myelin, which gives them a white appearance. The nerve fibres of the WM are organised into bundles, called tracts, connecting different areas of the brain and transmitting information between these areas [21]. Among the WM tracts are the corpus callosum, which connects the two hemispheres of the brain, and the uncinate fasciculus, which connects the temporal lobe to the prefrontal cortex. This study will focus on these two tracts. Their anatomy and roles will therefore be developed in more detail.

Corpus Callosum

The corpus callosum (CC) is a widely studied region of the brain as it connects the two hemispheres (see Figure 2.1). It is the main and largest axonal commissural tract in humans and is composed of up to 300,000,000 fibres of varying size and myelination degree. These mainly connect homotopic regions of the cortex in both hemispheres. Fibres connecting heterotopic regions are much rarer but sometimes present. The CC is located perfectly between the two hemispheres, just above the lateral ventricles [6, 22, 21].

Since the CC is composed of so many fibres, it is subdivided into several sub-regions. There are many different divisions in the literature as there is no obvious macroscopic anatomical division. In this study, the CC division will follow a scheme proposed by S. Hofer and J. Frahm [23] which is inspired by the much better-known scheme of Witelson. This was the result of a study in primates which aimed to separate the CC according to the

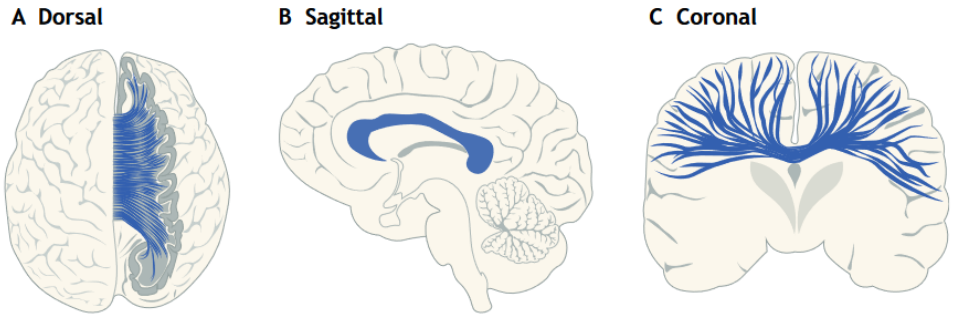


Figure 2.1: Dorsal (A), sagittal (B) and coronal (C) views of the corpus callosum [22].

functional properties of its constituent fibres. Indeed, the organisation of the CC correlates with the organisation of the functional areas of the whole cortex [22, 23]. However, regions are also histologically different. The diameter, the density as well as the myelination of the fibres varies which may, for example, have consequences for the speed of information propagation and conduction. And the two are linked since the distribution of fibres varies according to functional areas [6, 22, 23]. Therefore, the scheme used in this study takes into account the microscopic structural properties and is the result of a study on humans. The scheme divides the CC lengthwise into 5 distinct parts according to precise arithmetic ratios [23]. This division is shown in Figure 2.2.

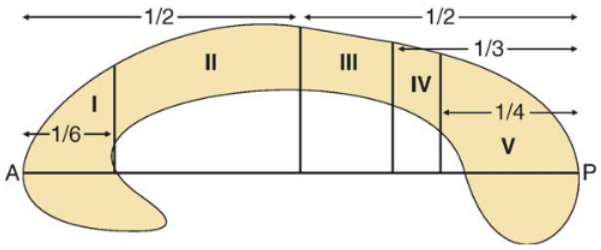


Figure 2.2: CC division scheme proposed by S. Hofer and J. Frahm [23], inspired by the much better-known scheme of Witelson. From anterior to posterior, the regions are respectively the genu (I), the anterior mid-body (II), the posterior mid-body (III), the isthmus (IV) and the splenium (V).

Region I, called the genu, contains the fibres projecting into the prefrontal area and is characterised by dense fibres with a small diameter. Region II, called the anterior mid-body, is the largest and is composed of a lower density of fibres with a larger diameter connecting the premotor and supplementary motor cortical areas. The least dense region is region III, called the posterior mid-body, but the fibres there reach a maximum diameter. It includes the fibres projecting into the primary motor cortex. Region IV, called the isthmus, is the narrowest. These are the primary sensory fibres, of medium diameter and density. Finally, region V, called the splenium, the most posterior, is the region in which the callosal parietal, temporal and occipital fibres are located. These are less dense and of variable diameter [6, 23].

The development of the CC begins during embryonic life and continues through the first years of life. Many callosal projections are refined, i.e. axons and dendrites continue to develop or disappear as needed, for an extended period of life, even into early adulthood. Fibre myelination occurs from the first months of postnatal life and continues until around 9 years of age. Since functional changes can still take place until adulthood, the CC is one of the latest maturing structures in brain development. Moreover, this maturation is content- and activity-dependent meaning that the development of the CC can vary according to many elements including environmental factors, sensory stimuli, etc. This development process proves its high plasticity [22].

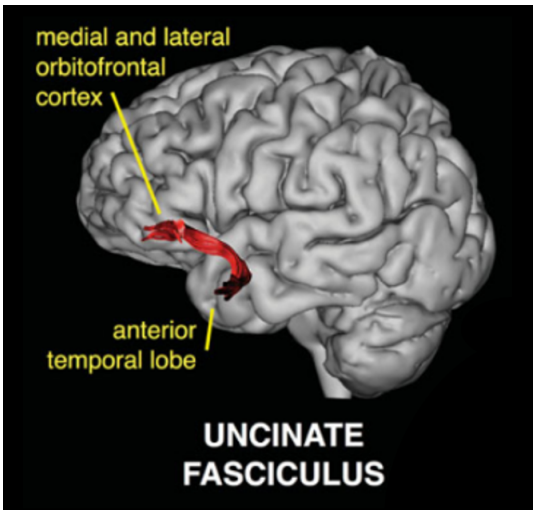
The role of the CC is essential as it allows bilateral sensory integration and as it is involved in many crucial functions such as executive and associative tasks, multidimensional representation of information, coordination of sensory-motor responses, working memory, language, integration of social and emotional stimuli, etc. [22, 24]. This connection between the two hemispheres is particularly important for functional areas not symmetrically present in the brain, such as Broca's area, which is used for language processing and is only present in the left hemisphere. The CC is often affected by neuronal diseases and damages can have serious consequences such as motor difficulties, social or language skills due to the large number of functions in which it is involved [22].

Uncinate Fasciculus

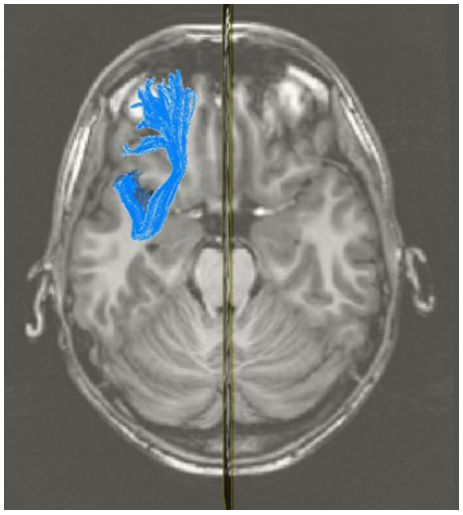
The uncinate fasciculus (UF) is one of the fasciculi of the limbic system, which plays a key role in the relationship between visceral states and emotions with cognition and behaviour. The UF is particularly involved in emotion, memory and language [6, 25].

It consists of two types of fibre. On the one hand, it is composed of association fibres, i.e. fibres with their origins and terminations in the cortex, in the same hemisphere, allowing a postero-anterior connection (in both directions). On the other hand, projection fibres connect regions of the cortex with subcortical regions. The UF is part of the temporal-amygdala-orbitofrontal network. More precisely, it starts in the anterior temporal lobe (temporal pole, uncus, parahippocampal gyrus and amygdala). Then, after a "hook-like" shape, it continues between the insula and the putamen and ends in the medial and lateral orbitofrontal cortex (see Figure 2.3). Actually, it divides into a ventro-lateral branch, which joins the anterior part of the insula and the lateral orbitofrontal cortex, and an antero-medial branch which connects the cingulate gyrus and the frontal lobe [6]. The size of the bundle is approximately of 3 to 7 mm in width and 2 to 5 mm in height [25].

The human brain is composed of two UFs, one in each hemisphere. However, these are asymmetrical in terms of volume and fibre density. Indeed, studies have shown that in most people, the right UF is up to 30% larger than the left UF (volume 27% higher and 33% more fibres in both sexes). This might indicate a higher connectivity in the right sided fronto-temporal region than on the left. These observations emerge from post-mortem dissection studies analysing the macrostructure of the WM [25]. Other studies based on DTI measurements, analysing the microstructure, provided much more variable results. Some found higher FA values in the left UF while others found higher values in the right UF. Still others reported no significant asymmetry between the two UFs [27].



(a) Sagittal view [6]



(b) Axial view [26]

Figure 2.3: 3D reconstruction of the left uncinate fasciculus using diffusion tensor tractography.

The UF is one of the last nervous fasciculus to develop. Moreover, its maturation continues until around the age of 30 [27]. There are many neurological disorders linked to UF, including depression, schizophrenia, dementia, Alzheimer's, autism spectrum disorders, substance abuse and problems relating to reward and valuation computation as well as impulsive decision and memory decision-making [6, 25, 27]. Given the long development of the UF and, moreover, which continues throughout the early life, socio-emotional elements during childhood and adolescence (social deprivation and maltreatment, autism spectrum disorders, conduct disorder, stress) can have important implications for the UF development and therefore long-term behavioural, social, emotional and neurocognitive deficits [27]. In a nutshell, UF-related disorders may in fact be as much consequences as causes of poor UF development.

2.2.2 Microstructural modifications due to alcohol

Alcoholism has been extensively studied and a multitude of articles have been published in the scientific literature. The changes in brain microstructure due to AUD can be analysed in a variety of ways. The main change throughout the whole brain is a decrease in FA, and an increase in MD, AD and RD in alcoholic patients compared to controls [28, 29]. Some studies report greater differences for men than for women. For example, decreases in total WM volume have been reported in men but were not significant in women [28]. However, gender differences remain a controversial issue as the results vary greatly between studies. Older studies speak of a "telescoping effect" in women for whom the age of initiation is generally later but the whole timeline of the disorder (from initiation to treatment) is somehow compressed. Nevertheless, this finding seems to be less and less demonstrated in more recent studies [28, 30].

The CC is often mentioned as one of the most affected regions. The damage appears similar to what is observed throughout the entire brain, characterised by reduced fractional anisotropy (FA) and increased mean diffusivity (MD) accompanied by a decrease in WM volume, as shown on Figure 2.4. Actually, de Souza et al.'s study indicates that the CC undergoes alterations in all forms of alcohol consumption, even in the absence of AUD. However, the importance of these changes becomes more pronounced with higher levels of alcohol consumption, particularly in the context of AUD [31]. The regions affected also vary slightly. Many studies agree on a "frontal brain vulnerability hypothesis" : the frontal brain regions seem to be more affected by alcohol than the more posterior regions. This also applies to the CC, where the genu or body are more damaged than the isthmus or splenium [31, 32, 33, 34].

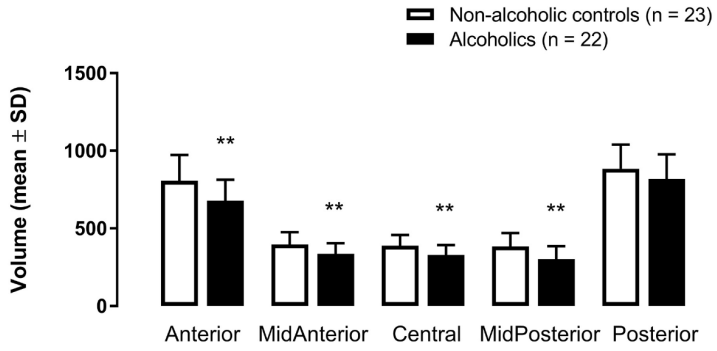


Figure 2.4: Volume differences in 5 CC regions between alcoholic patients and controls. The 5 regions mentioned in this graph were obtained by dividing the CC into 5 parts of equal width in an antero-posterior direction. Only the posterior region shows no significant difference (** p-val < 0.01) [31].

Yeh et al. [29] found an increase in RD in the body of the CC, a metric less frequently analysed and less often significant in studies. The splenium is still affected by alcoholism. For example, Lui et al. [35] reported that drinking duration was significantly associated with FA in regions connecting the bilateral parts of the parietal and temporal cortex. They also found no difference between alcoholic patients and controls in the part of the CC connecting to the motor cortex, which corresponds to the posterior mid-body region in the CC division adopted earlier.

Age may be an important factor in studying microstructural changes in the brain. Pfefferbaum et al. [33] found a correlation between age and values of FA (negative correlation) and MD (positive correlation) in the body of the CC and a negative correlation between age and WM volume in the genu and splenium. As mentioned above, alcohol damage is also related to the amount and duration of consumption [29, 35], which in turn may be related to the age of the patient. The effects of AUD on the brain microstructure are therefore the result of a combination of numerous factors that need to be taken into account in researches.

In addition to the commissural regions, of which the CC is a part, the frontal and temporal regions are strongly affected. Although the UF is located in these two regions and allows them to be linked, this structure is much less studied in alcoholism. Very few

articles focus entirely on it. It is more usually generalised studies in which the UF is mentioned. Yeh et al. [29] studied about 20 brain regions including the left and right UF. They found a decrease in FA and MD and an increase in AD and RD in the UFs of both hemispheres in alcohol-dependent patients compared to controls. They also reported a small area at the junction between the UF and the infero-frontal-occipital fasciculus in the right amygdalo-hippocampal complex where AD values were decreased compared to controls. Tridedi et al. [32] found no difference in MD between alcoholic patients and controls. They noted a decrease in FA, but this could not be considered as significant.

The limbic system of which the UF is part is generally known to be affected in the AUD. Trivedi et al. [32] found FA deficits in the limbic system and Harris et al. [36] report damage to fronto-limbic connections with decreased FA. Other parts of the limbic system are studied. de Souza et al. [34] noted a decrease in FA in the thalamus and fornix. These regions as well as the cingulum have also been cited by Schulte et al. [37] as being significantly affected by alcoholism.

Several studies have reported different results between the two hemispheres. Many agree on a "lateralisation hypothesis" indicating that areas and functions related to the right hemisphere are more likely to be affected by neurobiological damage due to alcoholism and in particular the limbic system [32, 36, 38].

2.2.3 Benefits of abstinence

Abstinence recovers most of the damage caused by alcoholism, at least partially. The benefits of abstinence vary over time. Indeed, the results of recent abstinence are not the same as the improvements observed after several months or years without drinking alcohol. The majority of studies showed an increase in brain volume, particularly in WM, and improvements in microstructural metrics [39].

Gazdzinski et al. [39] observed in one-week abstinent patients, still high MD values in frontal, temporal and parietal WM. But they also noticed that an increase in FA was often accompanied by a decrease in MD in all regions from 1 month of abstinence. Zorlu et al. [40] studied patients with more than 6 months of abstinence. They found that the total volume of tissue in the brain increased with abstinence. They also noted still elevated values of RD and AD in the frontal, temporal and parietal areas (which may indicate no or low recovery) but there was no difference in FA (which may indicate a total recovery) between the abstinent AUD patients and the control ones. They interpreted the elevated AD values as a result of the ongoing repair process and the elevated RD values as the consequences of myelin degradation. These two phenomena together resulted in unchanged FA values compared to controls. However, they concluded their study by drawing attention to the small sample size of the study, which may make the results less relevant. Furthermore, Monnig et al. [34] found results diverging from those of Zorlu et al. [40]. They studied the effects of one year of abstinence. Abstinent patients no longer showed differences in MD, AD and RD compared to healthy patients. They did, however, show lower FA values with lower values in the right hemisphere than in the left hemisphere which supports the lateralisation hypothesis. The areas most marked by low FA were the

parietal lobe, the superior and posterior corona radiata and the body and splenium of the CC.

Abstinence related improvements can be highly variable depending on several factors. The severity or duration of AUD, the amount of drinking before starting abstinence, the age, the history of relapse following previous periods of abstinence are examples of parameters influencing the possibilities, mechanisms, or speed of recovery. Gazdzinski et al. [39] also noted differences between smoking and non-smoking patients. Smoking patients showed a significant increase in WM volume in the frontal and temporal lobes not seen in non-smokers.

Studies specifically analysing CC have reported a decrease in FA in the body and splenium in alcoholic patients abstinent for 1 year, indicating a good recovery [34]. Studies on the effect of abstinence in specific regions of the CC and UF are scarce. The focus of research often revolves around the evolution of cognitive functions, with certain functions being closely related to specific brain regions, including the regions of interest investigated in this study. This aspect will be explored in greater detail in the following section 2.4.

2.3 Psychological impacts of AUD

In addition to physical health problems, AUD can cause a wide range of psychological dysfunctions. These may include depression, fatigue, anxiety, problems in cognitive functioning, social relationships, emotional states, speech impairments as well as memory and thinking disorders [41].

2.3.1 Objective psychological state assessment

It is complicated to assess the psychological state of a patient in an objective and reproducible way. It can be quite subjective and depends on the patient but also on the examiner. There are two kinds of psychological testing : objective and projective. This study use objective tests requiring the respondent to answer in a structured set of instructions. They are reproducible and validated by studies demonstrating a relationship between the test and what it purports to measure. They allow inter-subject comparisons and their results can be used in scientific studies. This study is based on four validated self-reported questionnaires to assess five psychological dimensions that can be affected by AUD : depression, obsession, compulsion, anxiety and fatigue.

Beck Depression Inventory (BDI)

The BDI is one of the most widely used test in psychiatry to assess depression. It is employed both in the clinical and research field. The BDI is based on a list of 21 statements to which the patient is asked to give a score from 0 to 3 (0 being the minimum score and 3 the maximum), in relation to his or her feelings over the last 2 weeks. The total score of the BDI is thus a value between 0 and 63, increasing with the intensity level of depression. Above 25, the patient is considered as severely depressed. The factors included in the test relate to symptoms of depression such as disturbed mood, negative self-image,

wishes for self-punishment, despair or suicidal desires. The advantages of this test are that it is generally considered reliable and consistent in many areas of psychology. Several studies have proven its validity for the study of addictive or substance abuse behaviour, particularly in alcoholism. In addition, it allows the identification of subtle changes in depressive states, which makes it very interesting for an evolutionary study over a defined period of time [42].

Obsessive Compulsive Drinking Scale (OCDS)

The OCDS is a self-rated questionnaire used to evaluate an individual's thoughts about alcohol and his/her attempts to control his/her drinking. Craving can be defined as an intense, addictive, obsessional or compulsive desire to drink alcohol. The OCDS consists of 14 items assessing various symptoms of obsessive-compulsive craving behaviour, such as the need to drink at specific times, difficulties in controlling the urge to drink, the tendency to think obsessively about drinking or the automaticity of drinking. It uses a 5-point scale, with responses ranging from 0 (no symptoms) to 4 (severe symptoms). The scores for each item are added together to give a total score, which can range from 0 to 56, with higher scores indicating greater severity of obsessive-compulsive symptoms related to alcohol use. The OCDS can help mental health professionals better understand the nature and extent of a patient's drinking problem. It can also be used to monitor the progression of symptoms over time and to evaluate the effectiveness of different AUD treatments [43].

Compulsive and obsessive behaviour are two terms associated and often correlated in the notion of craving. Obsessive behaviour is characterised by recurrent, persistent and often unwanted thoughts. Compulsive behaviour, on the other hand, refers to a repetitive behaviour sometimes performed without even being aware of it. It may acquire a certain ritual or routine nature. In this study, these two aspects were therefore distinguished from each other in two different behavioural metrics.

State-Trait Anxiety Inventory (STAI)

The version of the STAI used in this study was developed by Charles Spielberger in 1983. It is a 40-item self-complete questionnaire assessing state anxiety and trait anxiety separately, with 20 items each. It is more precisely the part on state anxiety that is used here in order to assess the temporary anxiety influenced by the patients' current situations. This differs from trait anxiety, which refers to a more permanent personality characteristic predisposing individuals to exhibit anxiety in certain situations. The form of the test is quite similar to the two previous tests discussed above, consisting of a list of statements to which the patient must give a score from 1 (for "not at all" or "almost never") to 4 (for "very much so" or "almost always"). The sum gives a score between 20 and 80 (score for the state STAI only). Each interval indicates a higher degree of severity: 20-39 corresponds to low state anxiety, 40-59 to moderate state anxiety and 60-80 to high state anxiety [44].

Multidimensional Fatigue Inventory (MFI)

The MFI is a fatigue assessment tool based on 20 items questioning the patient about their feelings during the previous days. For each item, a 7-point scale is used whereby a

higher score corresponds to a higher level of fatigue. The term multidimensional refers to the fact that the test investigates 5 dimensions of fatigue. Firstly, general fatigue is assessed on the basis of remarks on the overall functioning of the patient. Secondly, physical fatigue is analysed through items referring to a physical sensation or feeling of tiredness. Thirdly, cognitive symptoms such as difficulties in concentrating are used to measure the level of mental fatigue. Finally, the last two dimensions relate to reduced motivation and reduced activity. In this way, this test provides information on both the intensity and the nature of the experienced fatigue [45]. However, in this analysis, the decision was made to prioritise the total score of fatigue over the different subdimensions.

2.3.2 Behavioural modifications due to alcohol and abstinence

Depression

Alcohol-related disorders are often co-occurring with depressive disorders. Many studies have analysed this and reported a significant correlation between the two since the risk of having one of the two disorders doubles when the first one is present [46]. Onaemo et al. [47] studied the recurrence and persistence of depression disorders and concluded that AUD associated with depression could increase by a factor of 3 the risk of still having depression disorders after 6 and after 16 years. Several hypotheses can be put forward. First, the "overlapping predisposition" theory would argue that AUD and depression disorders have common genetic and/or environmental origins that would favour both disorders at the same time. Boden and Fergusson [46] conducted a review of the literature on the subject and reported that many studies agreed to reject this hypothesis. They were more supportive of a "disorder inducing" theory, stating a causal relationship that is more oriented toward increasing the risk of depression disorders with AUD. A "self-medication" theory is also put forward because many patients try to suppress the symptoms of depression by drinking alcohol. There may be a reciprocal link whereby the presence of AUD leads to depression disorders, which encourages patients to drink more and thus promotes the initial AUD. This correlation between the two disorders also has a vicious character because each disorder exacerbates and maintains the other. This means that treating the two disorders independently is not effective. A joint treatment approach is needed to avoid unnecessary effort. Finally, Borden and Fergusson [46] highlighted several studies (including the one of Oneamo et al. [47]) that noted a gender difference. The correlation between AUD and depression disorders as well as the increased risk of comorbidity was greater in women.

Obsession and compulsion

There are many different ways to define craving even though most of the time the notions of obsession and compulsion are mentioned. Studying these concepts and, even more, comparing and resuming the results of multiple studies are also difficult. The level of craving is evaluated in different ways, according to slightly varying criteria. This inevitably leads to differences in result interpretations. Withdrawal symptoms are often accompanied by anxiety and distress which are therefore considered as a form of craving by patients. There is therefore a mixture and a relationship that is created between the different behavioural parameters evaluated. This makes their study complex. Nevertheless, craving

is a phenomenon that is experienced by alcoholic patients to a much greater extent than by control patients [48]. Heinz et al. [49] added to these observations that different pathways could lead to different types of craving including obsession, control impairments and interference with social and work functioning, each with different neurobiological correlations.

Modell et al. [48] studied the correlation between craving and obsession and compulsion independently. Craving was positively correlated with obsessive thoughts and with compulsive drinking behaviour. However, the authors suggested that compulsive behaviour may reflect a consequence of craving more than a fundamental characteristic of craving itself. They also noted that treatment outcomes with cue exposure response prevention methods used in obsessive-compulsive disorders were quite similar when this type of treatment was used in AUD. They interpreted this as a strong correlation between craving and obsessive-compulsive behaviour.

Finally, the OCDS is regularly used as a predictor of relapse. Again, the results of studies on this topic may differ. Kranzler et al. [43] did not find a significant correlation between the test score at the end of treatment and drinking behaviours after 3 months of follow-up. Conversely, Bottlender and Soyka [50] reported a significant difference in scores at the beginning of treatment between those who relapsed before the end of treatment and those who were still abstinent. This is illustrated on Figure 2.5. Similarly, a consistently significant correlation in end-of-treatment scores was noted between abstainers and relapsers within one year of the end of treatment.

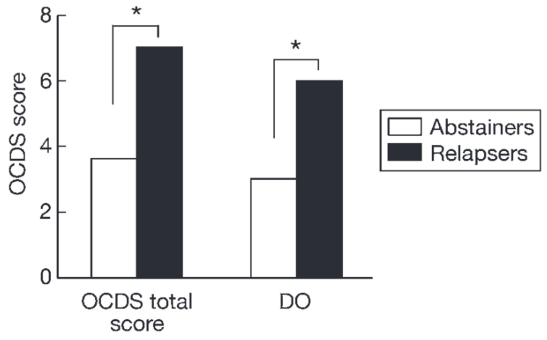


Figure 2.5: Differences in total OCDS score and drinking obsession subscore (DO) between abstainers and relapsers 12 months after the completion of a treatment phase. Adapted from [50].

Anxiety

A review of the literature makes it easy to realise that the relationship between AUD and anxiety is complex. Some studies have put forward a theory of self-medication of anxiety by alcohol as described above for depression [51]. Nevertheless, other authors have argued that the objective evidence is weak and have shown that modest doses of alcohol can instead increase feelings of anxiety and tension [52]. More than half of the patients with AUD have high state anxiety scores. However, it is often difficult to distinguish between substance-induced (including alcohol) and independent mood and anxiety disorders. The disorders are defined as independent when the symptoms have appeared before the symptoms of substance use disorders or when they persist for several weeks or months of abstinence [51, 53]. Unfortunately, it is not always possible to obtain this type of information when the duration of a study is limited.

Several studies have noted that when patients with AUD and anxiety disorders are asked which disorder they think appeared first, about half say it is the anxiety disorders. However, when a more objective and vigorous approach (including documentation and information from external and professional advice) is applied to the same patients, it was found in most cases that it was actually the opposite [51]. This is consistent with the result of several studies showing that the rate of patients developing AUD after anxiety disorders is not more significant than the rate of AUD in the general population. Most studies have suggested a bijective relationship, showing that AUD increases the risk of anxiety disorders but not vice versa [51, 52, 53, 54]. Finally, anxiety is strongly correlated with withdrawal. High rates of anxiety symptoms are observed in the first weeks of withdrawal, especially in protracted abstinence, but they decrease with time [51, 52, 53]. Schuckit and Hesselbrock [51] reported particularly high levels of anxiety in AUD patients who subsequently returned to heavy drinking behaviours. This may suggest a correlation between anxiety level and risk of relapse.

Fatigue

Sleep is strongly impacted by alcohol, both during acute consumption and in the case of chronic alcoholism. Everyone who consumes alcohol will have sleep disturbances, the severity of which may vary with the duration and amount of alcohol consumed. Alcohol has a sedative effect, but the resulting sleep is generally of poor quality with disturbed cycles, more frequent awakenings or breathing disturbances. Although some AUD chronic patients eventually develop a tolerance for these symptoms, most experience them on a regular or daily basis. Insomnia is often correlated with AUD. Withdrawal can also bring its share of fatigue-related symptoms with an increase in insomnia or hypersomnia for some as well as fragmentation and excessive sleep stage shifts. Many studies agree that most symptoms eventually disappear after a period of 9 to 12 months of abstinence. It is also notable that the sedative effects of alcohol tend to induce cravings and the urge to drink again, thus promoting relapse and difficulty in quitting drinking [55].

2.4 Neurocognitive and functional impacts of AUD

Many studies have examined the impact of alcoholism on cognitive functions and their potential recovery after periods of abstinence. Schulte et al. [56] conducted a review of the literature on this subject. They reported improvements or even total recovery of several functions including visual memory, verbal IQ, verbal fluency and episodic memory. Conversely, no improvement was reported for visuospatial skills, divided and sustained attention, verbal memory, craving, decision-making and emotional facial expression recognition. Finally, they reported inconsistent results for processing speed, working memory, selective attention, inhibition and flexibility. Multiple studies [32, 38, 57, 58] even noted more marked impacts of AUD in the reward system and memory function in the right hemisphere, which can be linked to the lateralisation hypothesis already discussed previously 2.2.2.

A question that recurs in many studies is whether the impairments are the result of alcoholism or are pre-existing conditions of alcoholism that actually promote the development of AUD. Impulsivity problems, poor response inhibition and reaction-time as well as impaired verbal and working memory skills are presumed to be premorbid impairments. Decreased neurocognitive function also represents higher risk factors for relapse [56, 59]. Beck et al. [57] studied the differences between permanent abstainers and relapsers. They found that relapsers had more significant atrophy of the bilateral orbitofrontal cortex, right medial prefrontal cortex and anterior cingulate cortex which were associated with impairments in error monitoring, behavioural control, reward processing, impulsivity and risk-taking.

Correlations with microstructural data of the brain have also been demonstrated. Among other things, an increase in hippocampal volume during a period of abstinence was positively correlated with better visual memory results, as was a positive correlation between lateral ventricular volume and memory [56]. Shulte et al. [37] also analysed a decrease in FA values in the brain that were associated with a decrease in processing speed. This is consistent with the fact that metric FA is often related to the level of myelination of neuronal fibres. Pfefferbaum et al. [33] and Yeh et al. [29] focused on the CC and found a significant correlation between decreased FA and increased MD in the genu and splenium with low scores on tests of visual analysis and problem-solving, working memory and mobility skills. Still other studies [32, 58] report neuronal damage related to neurocognitive deficits mainly related to frontal and temporal regions, citing in some cases the limbic system in particular [38].

It is important to note that other factors influence the recovery of cognitive functions. The presence of other disorders or addictions can alter recovery mechanisms. For example, Schulte et al. [56] reported that smoking leads to decreased recovery of certain memory and executive functions. In addition, the number of detoxifications already performed by AUD patients correlates with poorer recovery results [56].

Part II

Analysis

Chapter 3

Objectives and Methods

3.1 Objectives

This master thesis is a continuation of Faustine Falyse and Manon Dausort's master thesis entitled "Identifying the microstructural changes for alcoholic patients during short-term abstinence via diffusion Magnetic Resonance Imaging" [60]. This focused on the impact of short-term abstinence on the microstructure of the brain and the potential reversible damages of alcohol in AUD. They highlighted two tendencies among the patients which enabled to divide them into two clusters. The first cluster did not show significant evolution after abstinence. The second cluster showed several rearrangements in the structures of the limbic system, the cerebellum, its peduncles and the cortico-ponto cerebellar pathway. Two hypotheses to explain these rearrangements were proposed : a disinflammation of the extra-axonal space in those structures, suggesting a recovery process, or an inflammation of the fibres, suggesting a continued progression of the damages.

This work used the same data as this previous master thesis with the aim of finding relationships between the evolution of the brain microstructure and the evolution of different psychological states in alcoholic patients. This evolution was analysed in patients who have undergone a 18-day period of abstinence. In addition, the studied regions are two specific brain regions, namely the CC and the UF. To date, no other study covering this topic with the same points of interest and characteristics has been conducted and published in the scientific literature.

3.2 Data

3.2.1 Data acquisition

As mentioned before, the data used in this study are the same as those used in the master thesis of Faustine Falyse and Manon Dausort [60]. These data were acquired by Melissa Salavrakos in the context of her PhD. The 53 subjects, diagnosed with severe AUD, followed an 18-day abstinence and withdrawal programme organised by the *Cliniques Universitaires Saint-Luc* in Brussels, Belgium. A first exclusion criterion discarded patients with severe comorbidities, chronic inflammatory diseases and regular use of anti-inflammatory drugs. The second exclusion criterion concerned contraindications to undergo MRI due to the

presence of metal-containing medical devices in the patient's body. Except in the case where the patient did not return after 18 days, all other patients had an MRI scan on the day of admission (referenced as time T1) and a second scan on day 18 of abstinence (referenced as time T2).

A total of 20 healthy subjects were also recruited as controls, through advertisements on social networks and posters in public places. The selection criteria followed the WHO recommendations of drinking less than 10 units of alcohol [1] per week for women and 15 units for men, drinking no more than 2 glasses of alcohol per day for women and 3 for men, and abstaining from alcohol at least 2 days per week for both sexes. The exclusion criteria were identical to those applied to alcoholic patients.

The MRI unit used for the scan acquisition is a *3T SignaTM Premier, GE Healthcare* and the MRI sequence was an EP-SE sequence (Echo-Planar Spin-Echo sequence). The main parameters used are as follows: an imaging frequency of 127.77 Hz, a slice thickness of 2 mm, a TR of 4.837 s and a TE varying around 79/80 ms depending on the patient. An example `.json` file containing all the acquisition parameters is available in Appendix B. Two data files were acquired per patient at each time (T1 and T2) which means 4 data files per patient in total. Among these, there are 2 T1-weighted contrasted scans of dimension (156 x 256 x 256) named `NAME_T1_Anat3D` and `NAME_T2_Anat3D`. The other 2 files are diffusion scans consisting of 167 volumes with dimension (110 x 110 x 68) of which 7 were acquired with a zero b-value and the other 160 with b-values of 1000, 2000, 3000 or 5000 s/mm^2. These were named `NAME_T1_DTI` and `NAME_T2_DTI`. When some files were missing or errors in preprocessing occurred, the patients concerned were removed from the study.

3.2.2 Data conversion

The 4 data files per patient contain DICOM[2] data. Using the MRIcron software [63], these files were first anonymised and each subject was renamed by `sub##` with a number from 01 to 53 for the alcoholic patients and from 54 to 73 for the controls. This procedure also resulted in the creation of several files. Two files are obtained from the anatomical scan: a `.json` file, containing the MRI sequence parameters, scan options and imaging frequency, and a `.nii.gz` file containing the recorded MRI slices. The diffusion files each resulted in the creation of 4 files: a `.json` file, a `.nii.gz` file and two files (`.bval` and `.bvec`) containing the b-values and b-vectors respectively. This fulfils the requirements in terms of organisation for preprocessing with the ElikoPy pipeline.

[1] An alcohol unit is defined as 10ml or 8g of pure alcohol. This measurement is equivalent to consuming a single shot of spirits or half a pint of lower-strength lager, beer, or cider, which has a volume of 568ml and an alcohol by volume (ABV) of 3.6% [61].

[2] Digital Imaging and Communications in Medicine : international standard format for the storage, exchange, and management of medical images and related information used in radiology and medical imaging [62].

3.2.3 Data preprocessing

All these files were saved in the necessary organisation for the use of the ElikoPy pipeline. The preprocessing of the data was then carried out to remove a series of artefacts and noise from the images as explained in section 1.6. The ElikoPy pipeline also allows calculating the DTI measurements, running the different models (NODDI, DIAMOND and MF) and creating the whole brain tractography (more details about this will be provided in section 3.3.1 and 3.4.1).

3.3 Regions of interest

A series of steps are necessary to obtain the ROIs used to extract the data required for the analyses.

3.3.1 Tractography

The initial step was a complete tractography of the brain. This was done using the ElikoPy pipeline [15]. First, the ODF was calculated from the diffusion scan by performing a Multi-Shell Multi-Tissue Constrained Spherical Deconvolution (MSMT-CSD) [64]. CSD aims to deconvolve the measured diffusion signal to estimate the ODF within each voxel of the brain. MSMT indicates that this method uses diffusion-weighted images acquired with multiple b-values, allowing more accurate distinction of different tissue types and fibre populations per voxel.

Then Elikopy used the `tckgen` command from the *MRtrix3* package [65] to perform the whole brain tractography using the iFOD2 algorithm. This adopts a probabilistic approach with a second-order integration method and trilinear interpolation (see section 1.5 for explanations about these features). iFOD2 uses the ODF amplitudes to calculate the candidate fibre paths. A fibre is more likely to follow a path with high ODF amplitudes, but it also happens rarely that fibres follow paths with lower ODF amplitudes. The termination criterion is a cut-off on the ODF amplitude. This was set at 0.1, i.e. the fibres stop propagating when they reach a voxel where the ODF amplitude is less than 0.1, corresponding to the limit of the WM and GM. The maximum curvature angle was set to 25 degrees to allow a better tracking of the fibres belonging to the UF pathway. And the seed points were randomly positioned in the expanded brain mask (the file `sub##_E#_brain_mask_dilated.nii.gz` computed by ElikoPy during preprocessing). The parameter indicating the number of different fibres was set to two different values: 200,000 streamlines for the tractography used to isolate the ROIs of the CC and 250,000 for the ROIs of the UFs. An example of the resulting tractography is shown in Figure 3.1.

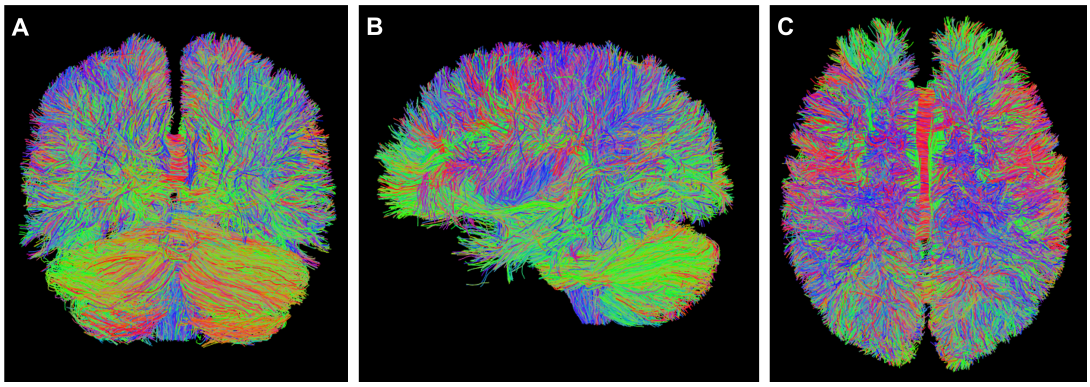


Figure 3.1: Visualisation of a whole brain tractography : frontal **(A)**, sagittal **(B)** and axial **(C)** views. Colours have been assigned based on the main direction of the fibres : vertical fibres in blue, horizontal fibres in green and left to right in red.

3.3.2 Brain parcelation

FreeSurfer

In order to isolate the fibres which are part of the two studied regions, the whole brain was partitioned into neuroanatomically distinct regions using FreeSurfer. This is a free and open-source package allowing many analyses to be performed on structural MRI images [66].

In particular, the function used in this study was the reconstruction of the cortical surface called with the `recon-all` command. From a T1-weighted image which is a 3D representation of a volume, `recon-all` constructs 2D surfaces corresponding to the pial surface (the innermost layer of the meninges covering the entire brain) and the boundary between WM and GM. Then, an atlas is used to parcellate the entire brain volume. In this study, The Desikan-Killiany atlas [67] were used. Figure 3.2 shows the obtained `recon-all` output in which each colour corresponds to a specific region with assigned labels and codes.

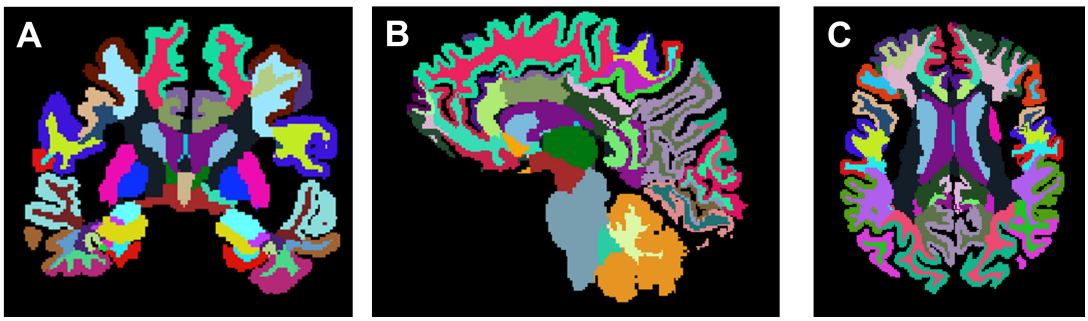


Figure 3.2: Illustration of the whole brain parcelation obtained with the `recon-all` command of FreeSurfer : frontal **(A)**, sagittal **(B)** and axial **(C)** views. Each colour corresponds to a specific region with assigned labels and codes.

CC division

One of the brain areas where parcelation is very important is of course the CC. However, The Desikan-Killiany atlas used by FreeSurfer only makes a simplified division by segmenting the CC into 5 parts of equal length. The length of each segment (in the anterior-posterior direction) measures exactly 1/5 of the total CC length (see Figure 3.3 A). As mentioned in the section on CC anatomy (section 2.2.1), this division does not respect the functional and histological properties of the CC. The obtained parcelisation has therefore been corrected to respect the division scheme proposed by S. Hofer and J. Frahm [23] (see Figure 3.3 B). Specifically, the codes assigned to each voxel in the CC were changed to match the new division and new codes were chosen to avoid confusion between the new division and the old one or any other part of the brain. The new codes are therefore : Genu = 2555, Anterior Mid-Body = 2554, Posterior Mid-Body = 2553, Isthmus = 2552 and Splenium = 2551.

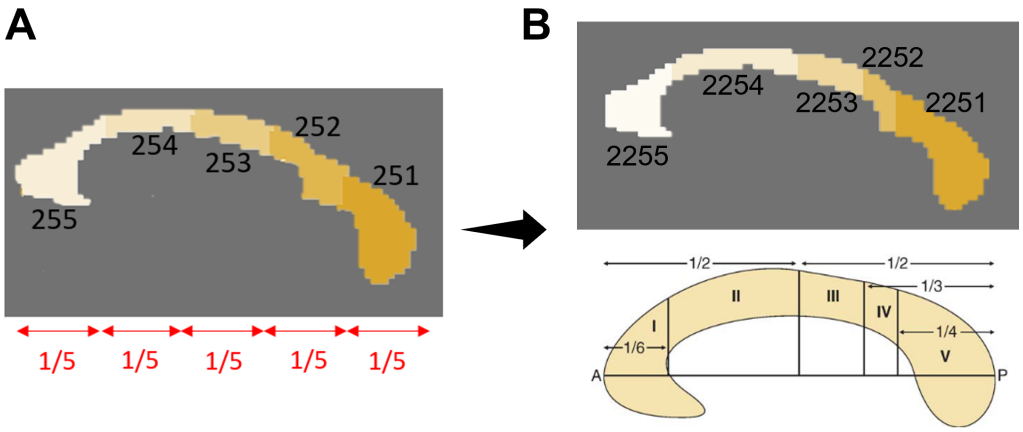


Figure 3.3: Adaptation of the FreeSurfer parcelation of the CC to match with the proposed scheme of CC division (see section on the CC anatomy 2.2.1). From the initial parcelation of FreeSurfer which divided the CC in 5 regions of the same width **(A)** to the adapted division whose geometrical characteristics correspond to the proposed scheme **(B)**.

3.3.3 Tracts isolation

From the complete tractography of the brain, only the fibres belonging to the two studied regions were kept. For this, the White Matter Query Language (WMQL) [68] package was used. This method is based on the descriptions of the studied regions which are constructed in terms of relationships between the different brain areas as segmented by the FreeSurfer parcelation. WMQL uses instructions on anatomical zones in which the fibres must pass or stop and instructions on positions relative to certain anatomical zones in relation to which the fibres must be situated (superior, medial, posterior and their opposites). In addition, there are logical operations (conjunction, disjunction, exclusion) involving both types of instructions. The instruction files used to isolate the studied regions

are available in Appendix C. These definitions correspond to those proposed by WMQL, modified to improve the isolation of the tracts and to correspond to the adopted CC division.

It should be noted that for each subject, a total of 9 files are obtained. For the CC, there are one file for each segment and one file for the complete CC (collecting the tracts of the 5 segments) and for the UF, there are the left UF, the right UF and one file collecting both. Figure 3.4 shows the tracts of the 5 CC segments and Figure 3.5 of the 2 UFs for a control patient.

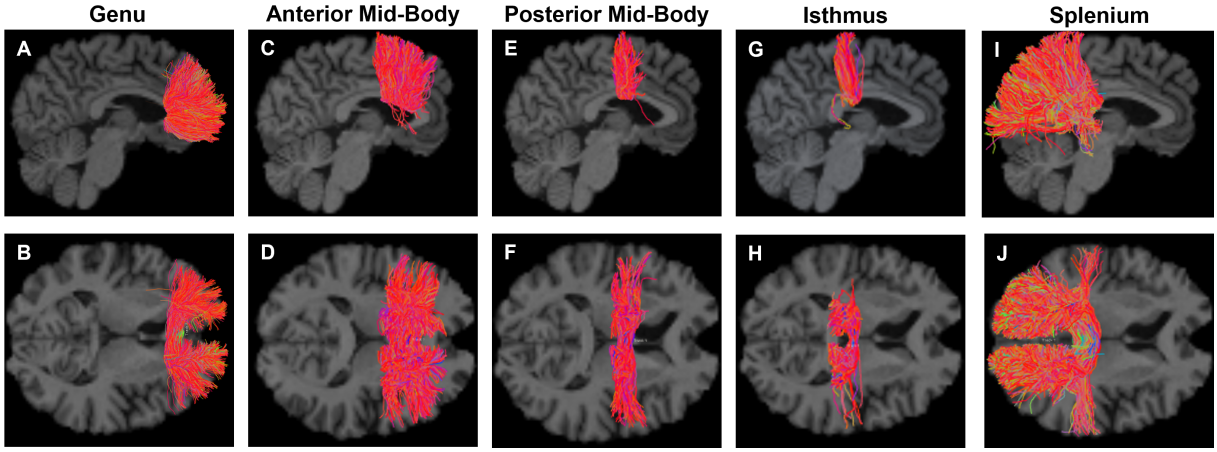


Figure 3.4: Tracts of the CC obtained with WMQL. Sagittal **(A)** and axial **(B)** view of the genu, sagittal **(C)** and axial **(D)** view of the anterior mid-body, sagittal **(E)** and axial **(F)** view of the posterior mid-body, sagittal **(G)** and axial **(H)** view of the isthmus, sagittal **(I)** and axial **(J)** view of the splenium.

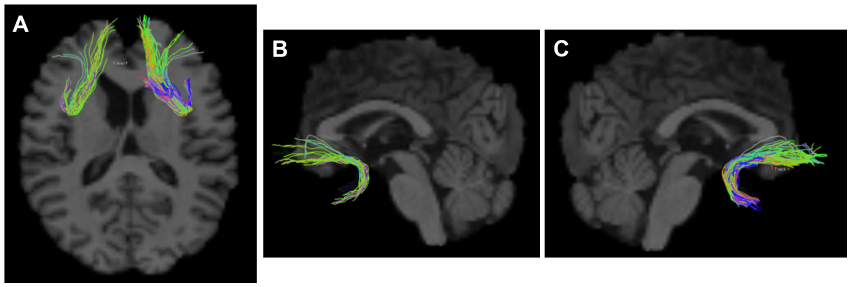


Figure 3.5: Tracts of the UF obtained with WMQL. Axial view of both tracts **(A)**, sagittal view of the left UF **(B)** and sagittal view of the right UF **(C)**.

3.3.4 ROI and fibre density

Finally, the ROIs for each studied region were derived from the corresponding tracts. This transformation is done using the `tract_to_ROI()` and the `get_streamline_density()` functions of the TIME.utils package developed by Nicolas Delinte [69]. The `tract_to_ROI()` function creates a binary image where the voxels are set to 1 if one or more fibres pass through them, the other voxels remain at 0. The `get_streamline_density()` function does the same but weights each voxel by the density of fibres passing through it. In this

way, voxels located for example in the interior of the CC itself will have more weight in the final computed data than voxels located near the outer surface of the brain in which few fibres pass. Moreover, the isolation of the tracts is not always perfect and some isolated fibres are included in the tracts even though they do not form part of the studied regions. Using a weighting according to the number of fibres reduces the impact they have on the final data used for the statistical analysis. Figure 3.6 shows an example of a weighted ROI for the complete CC.

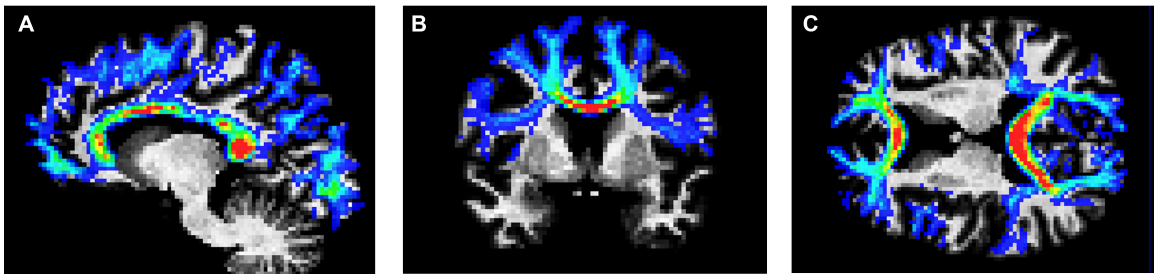


Figure 3.6: Example of a complete CC ROI for a control subject, weighted by the density of fibres (the blue indicates low fibre density and the red high fibre density). Sagittal **(A)**, frontal **(B)** and axial **(C)** views.

3.4 Metrics

3.4.1 Microstructural metrics

The microstructural analysis of the studied regions is performed using the DTI metrics (see section 1.3.2) and metrics extracted from the more advanced diffusion models (NODDI, DIAMOND and MF) already described in the section 1.4. For each metric, the ROIs of the studied regions were superimposed on the maps of the whole brain metrics. The mean of each metric for each ROI was then extracted.

DTI

The DTI metrics used are those already described in section 1.3.2. Examples of whole brain maps used for each metric are shown in Figure 3.7. As a reminder, the 4 metrics were as follows:

- `FA` : Fractional Anisotropy (Figure 3.7 A & B)
- `MD` : Mean Diffusivity (Figure 3.7 C & D)
- `AD` : Axial Diffusivity (Figure 3.7 E & F)
- `RD` : Radial Diffusivity (Figure 3.7 G & H)

NODDI

As described in section 1.4.1, the NODDI model distinguishes three different compartments (intra-cellular, extra-cellular and CSF) in each voxel. The metrics extracted from this model therefore consist of the volume fraction of each compartment in each voxel. In

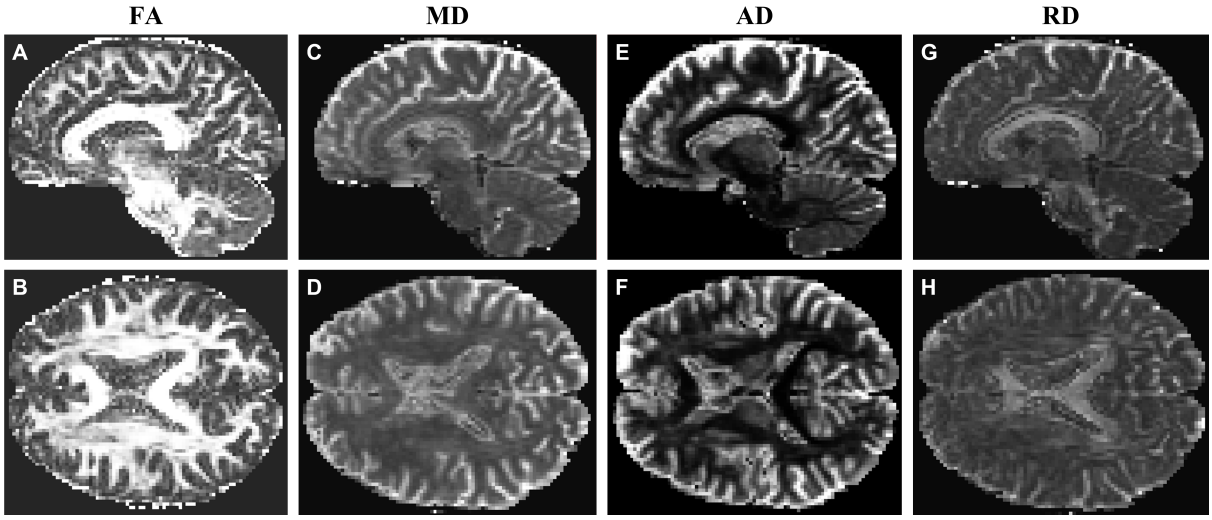


Figure 3.7: Examples of whole brain maps of each DTI metrics. Sagittal **(A)** and axial **(B)** views of a `FA` map, sagittal **(C)** and axial **(D)** views of a `MD` map, sagittal **(E)** and axial **(F)** views of a `AD` map, sagittal **(G)** and axial **(H)** views of a `RD` map.

addition, the `ODI` metric measures the level of fibre orientation dispersion in each voxel. Examples of whole brain maps used for each metric are shown in Figure 3.8. The 4 metrics are the following:

- **`fintra`** : intra-cellular volume fraction (Figure 3.8 A & B)
- **`fextra`** : extra-cellular volume fraction (Figure 3.8 C & D)
- **`fiso`** : free water volume fraction (with an isotropic diffusion) (Figure 3.8 E & F)
- **`ODI`** : fibre orientation dispersion index (Figure 3.8 G & H)

DIAMOND

One of the main characteristics of DIAMOND is its ability to distinguish two populations of fibres (`f0` and `f1`) oriented in different directions within the same voxel, in addition to an extra-cellular compartment (see section 1.16). Three files containing the volume fractions of these three components are therefore obtained thanks to the model, respectively named `fractions_f0`, `fractions_f1` and `fractions_csf`. For each of the two fibre populations, the model also provides files named `t0` and `t1` which contain the diffusion tensors $\overline{\overline{D}}$ for each voxel as described in section 1.3.2. From these, the same metrics as the DTI ones can be calculated. This gives 8 new files: `FA_DMD_t0`, `MD_DMD_t0`, `AD_DMD_t0` and `RD_DMD_t0` for the first population of fibres and the same files with `_t1` for the second population. To keep only one measurement per metric for each voxel encompassing the measurements of both populations, a weighted average was calculated for each metric. These weighted metrics are named `wFA`, `wMD`, `wAD`, `wRD` and are calculated according to the following formula:

$$metric_{weighted} = \frac{frac(f0) * metric(f0) + frac(f1) * metrci(f1)}{frac(f0) + frac(f1)} \tag{3.1}$$

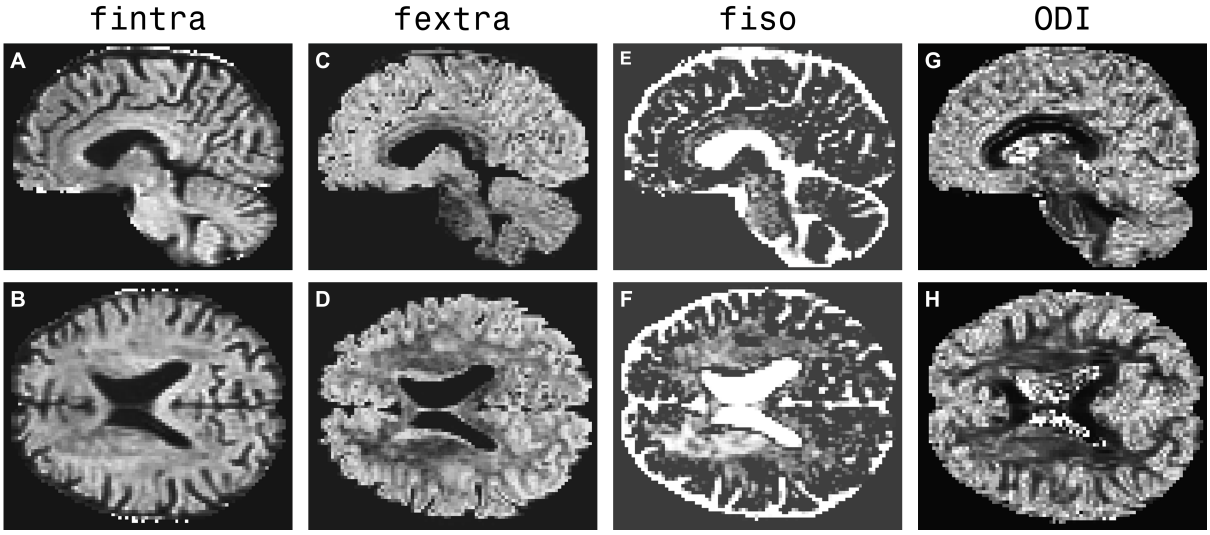


Figure 3.8: Examples of whole brain maps of each NODDI metrics. Sagittal **(A)** and axial **(B)** views of a `fintra` map, sagittal **(C)** and axial **(D)** views of a `fextra` map, sagittal **(E)** and axial **(F)** views of a `fiso` map, sagittal **(G)** and axial **(H)** views of a `ODI` map.

This allows the existence of crossing fibres to be considered and, contrary to what is an important limitation of DTI, not to lose all interpretation of the metrics because of the signal superposition resulting from the two populations. For example, if two populations cross within a voxel, but, in each of them, the fibres are very well aligned, the value of `FA_DMD_t0` and `FA_DMD_t1` will be very close to 1. By calculating `wFA`, a value close to 1 is also obtained whereas DTI considers the orientation of all the fibres at once and the corresponding F`FA` value is much lower.

Finally, the metrics `fractions_csf` and `fractions_ftot` can be calculated. As mentioned previously, `fractions_csf` represents the volume fraction of CSF (free water[3]) while `fractions_ftot` represents the volume fraction of fibres (belonging to both populations) in each voxel calculated from the `f0` and `f1` files. These two metrics are complementary and respect therefore the following equality: `fractions_csf` + `fractions_ftot` = 1.

In summary, the DIAMOND model provides the following 6 metrics:

- **`wFA`** : weighted FA (Figure 3.9 A & B)
- **`wMD`** : weighted MD (Figure 3.9 C & D)
- **`wAD`** : weighted AD (Figure 3.9 E & F)
- **`wRD`** : weighted RD (Figure 3.9 G & H)
- **`fractions_csf`** : free water volume fraction (Figure 3.9 I & J)
- **`fractions_ftot`** : total fibre volume fraction (Figure 3.9 K & L)

Examples of whole brain maps used for each metric are shown in Figure 3.9.

[3]The CSF compartment is used to refer to the free water volume fraction because CSF and free water share similar properties in terms of diffusion. However, it is important to acknowledge that referring to it as such is not entirely accurate and can be considered a misuse of language.

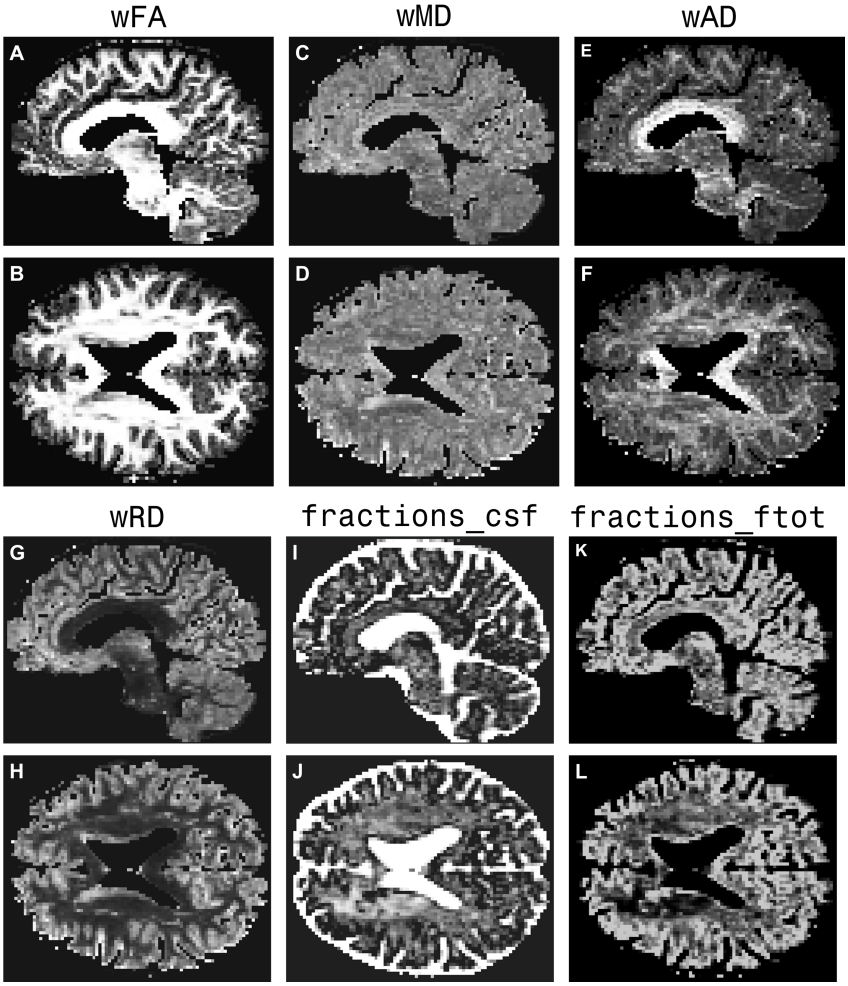


Figure 3.9: Examples of whole brain maps of each DIAMOND metrics. Sagittal **(A)** and axial **(B)** views of a `wFA` map, sagittal **(C)** and axial **(D)** views of a `wMD` map, sagittal **(E)** and axial **(F)** views of a `wAD` map, sagittal **(G)** and axial **(H)** views of a `wRD` map, sagittal **(I)** and axial **(J)** views of a `fractions_csf` map, sagittal **(K)** and axial **(L)** views of a `fractions_ftot` map.

Microstructure Fingerprinting

The MF model also allows for the differentiation of several fibre populations within a voxel whose volume fractions are available in the files named `mf_frac_f0` and `mf_frac_f1`. The combination of these two allows the extraction of a `frac_ftot` metric. In addition, a `frac_csf` metric provides information on the volume fraction of CSF (free water[4]) in the voxel. These two metrics are complementary and therefore sum to 1 : `frac_ftot` + `frac_csf` = 1.

The model also provides 3 other files, `mf_fvf_f0`, `mf_fvf_f1` and `mf_fvf_tot`, which provide the fibre volume fraction of respectively the population f0, the population f1 and both populations together. A metric `fvf_tot` is extracted from the file `mf_fvf_tot` and, in

[4]Same remark as for the CSF compartment in DIAMOND. The term CSF is used to designate free water in general.

the same way as the weighted metrics are calculated for the DIAMOND model (see Equation 3.1), a metric `wfvf` is calculated from the fibre volume fractions of the two populations.

To clarify the difference between `fvf_tot` and `wfvf`, `fvf_tot` provides the fibre concentration in the entire voxel whereas `wfvf` provides the fibre concentration in the compartments of the fibre populations only, regardless of the CSF compartment. This is schematically illustrated in Figure 3.10. `wfvf` is therefore always greater than `fvf_tot` except when there is no CSF compartment in the voxel, in which case `fvf_tot` is equal to `wfvf`.

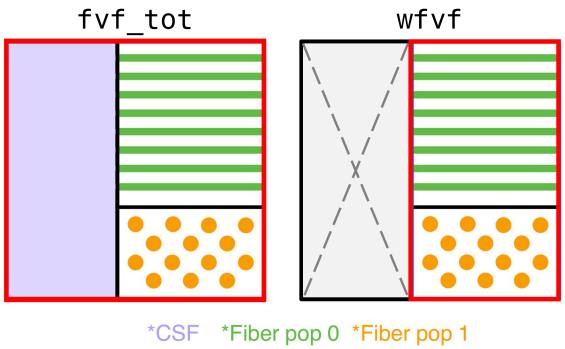


Figure 3.10: Difference between `fvf_tot` and `wfvf` : `fvf_tot` provides the fibre concentration in the entire voxel whereas `wfvf` provides the fibre concentration in the compartments of the fibre populations only, regardless of the CSF compartment. Adapted from [60].

The 4 metrics obtained with the MF model are illustrated with maps of the whole brain in Figure 3.11 and are as follows:

- **`frac_ftot`** : total volume fraction of fibres (Figure 3.11 A & B)
- **`frac_csf`** : free water volume fraction (Figure 3.11 C & D)
- **`fvf_tot`** : fibre volume fraction (Figure 3.11 E & F)
- **`wfvf`** : weighted fibre volume fraction (Figure 3.11 G & H)

3.4.2 Behavioural metrics

The metrics for assessing behaviour used in this study are the metrics already presented in Section 2.3.1. As a reminder, 5 behaviours were examined by means of self-rated questionnaires.

- *Depression* with the **BDI**
- *Compulsion* with the **compulsion-related** statements of the **OCDS**
- *Obsession* with the **obsession-related** statements of the **OCDS**
- *Anxiety* with the **state-related** questions of the **STAI**
- *Fatigue* with the **MFI**

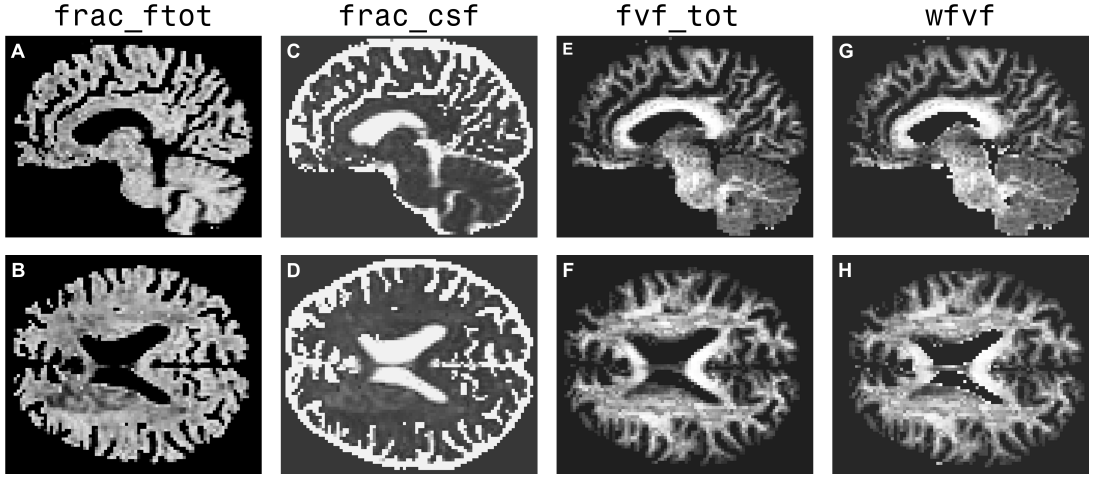


Figure 3.11: Examples of whole brain maps of each MF metrics. Sagittal **(A)** and axial **(B)** views of a `frac_ftot` map, sagittal **(C)** and axial **(D)** views of a `frac_csf` map, sagittal **(E)** and axial **(F)** views of a `fvf_tot` map, sagittal **(G)** and axial **(H)** views of a `wfvf` map.

The alcoholic patients responded to these tests each time they performed brain imaging, i.e. at time T1, at the beginning of the abstinence period, and at time T2, after 18 days of abstinence. The control subjects only responded to these tests at their first T1 imaging. Being healthy controls, their results were considered non-variable over time.

3.4.3 Evolution over time

The evolutions of the metrics between T1 and T2 were measured by means of a difference. The following formula is therefore applied to both the microstructural and behavioural data:

$$evolution(metric, region) = metric(T2, region) - metric(T1, region) \tag{3.2}$$

If the change is positive, it indicates an increase in the value of the metric, whereas if the change is negative, it indicates a decrease.

3.5 Outliers

3.5.1 Behavioural outliers

Outliers were treated on a metric-by-metric basis in the sense that a subject was only removed from an analysis if the value of one behavioural score at one time used for this particular analysis was an outlier. In other analyses, which did not use this score at that time, the subject was retained since it no longer exhibited an outlier value.

The method used to detect outliers is based on quartiles and the interquartile range (IQR) which represents the difference between the first (Q1) and third (Q3) quartile ($IQR = Q3 - Q1$) and corresponds to the height of the coloured part in the boxplot (see Figure 3.12). Outliers can be identified by considering values outside the range [Q1 - 1.5 IQR ; Q3 + 1.5 IQR].

For example, Figure 3.12 shows the spread of the behavioural metrics for the alcoholic subjects at T2. The boxplots allow the identification of outliers represented with ♦. For all analyses on the STAI metric, subjects `sub02` and `sub17` were excluded because their STAI score reaches 70 which is well above the outlier limit set at Q3 + 1.5 IQR = 45 + 1.5*15 = 67.5. Similarly, for all other metrics, the subjects corresponding to the outlier values (♦) were excluded. Among the 53 alcoholic patients, 1 was considered as outlier for the OCDS (obsession) score at T1 and 4 for the BDI and/or STAI scores at T2.

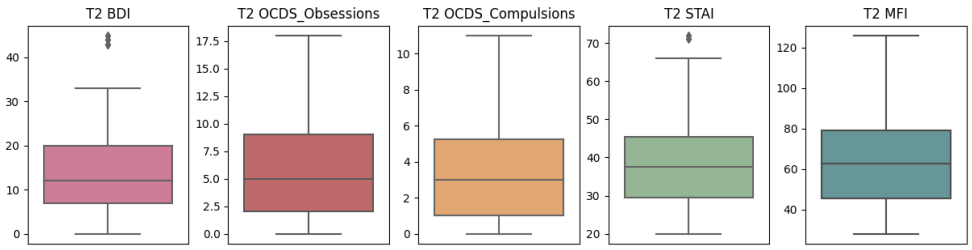


Figure 3.12: Spread of the behavioural metrics for the alcoholic patients at T2. It illustrates the identification of outliers (♦) which correspond to values outside the range Q1 - 1.5 IQR to Q3 + 1.5 IQR where Q1 is the first quartile, Q3 the third and IQR the interquartile range.

The controls were only tested at time T1. Among the 20 control subjects, 4 present an outlier value for at least one of the behavioural metrics with a maximum of 3 outliers per metric 3.13.

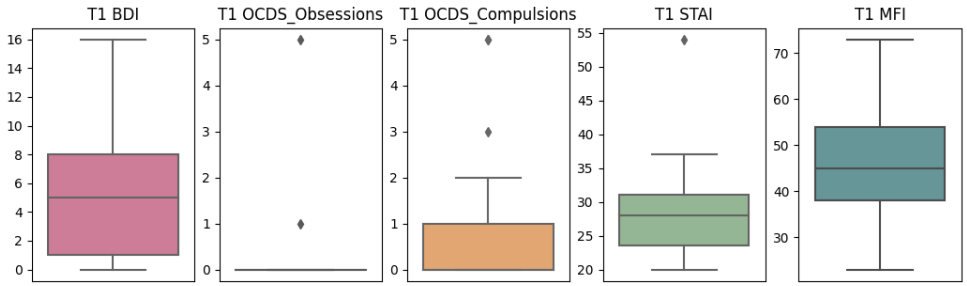


Figure 3.13: Spread of the behavioural metrics at T1 for the control subjects. It illustrates the identification of outliers (♦) which correspond to values outside the range Q1 - 1.5 IQR to Q3 + 1.5 IQR where Q1 is the first quartile, Q3 the third and IQR the interquartile range.

3.5.2 Microstructural outliers

Foremost, 4 subjects (3 alcoholics and 1 controls) were excluded at one of the two times of the study due to the absence of data for certain scans. Subsequently, the detection of subjects to be excluded due to problems in the microstructural data was based on the verification performed by the ElikoPy pipeline. When defects were detected in some scans, the preprocessing could not be achieved.

Then, for all data successfully preprocessed, a screening was carried out according to the amount of noise. All scans with a SNR below 10 were excluded. This corresponds to approximately 12% of all preprocessed scans. A visual inspection of the tracts of each studied region was also performed to identify subjects in whom tract isolation was not successful with the procedure explained in section 3.3. This may have resulted in tracts whose shape does not respect the studied region or tracts with too few or no fibres. The reasons for these unsuccessful isolations can be multiple. It may be due to the anatomy of the subject itself which is more deviated from the norm or the anatomy of other subjects (e.g. a CC with a particularly thin or irregular thickness or a particularly high curvature of a certain tract) resulting in difficulties to isolate the tracts. Issues may also arise from the parameters selected for tractography (see section 3.3.1) which have been optimised for all subjects but which result in defects in some subjects. In some alcoholic patients, swelling of the CSF results in higher curvature of the CC and the fibres can no longer be correctly tracted with a maximum angle of 25. Also, the cut-off was set at 0.1 but the ODF values are sometimes quite low in some patients compared to the average of all subjects. The tracking of the fibres is then restricted and this leads to the presence of many short fibres in length. It becomes difficult to isolate correctly the studied regions with WMQL.

It should be noted that when only certain regions were affected, but others had been correctly isolated, the subject was retained for analysis not including the defecting regions. In addition, the estimation of the metrics from the MF model on subject 67 failed, they were therefore excluded from the study for this subject. A table summarising all cases of exclusion of certain data with a short justification is available in Appendix D.

3.6 Statistical analysis

All statistical analyses presented in this section were performed using the `stats` module of the open-source software SciPy [70].

Patients/controls comparison

First, a comparison between the alcoholic patients and the control subjects was made. For this purpose, a Welch's t test was performed for all ROIs, for all metrics and for all times. As behavioural data were only acquired at time T1 for the control subjects, the behavioural data of the alcoholics at time T1 and T2 were compared with the T1 data of the controls. The Welch's t-test is a variation of the Student's t-test determining if there is a statistically significant difference between the means of two groups with unequal variance and unequal sample size. In each case, the independent two-sample t-test calculates a

t-score according to the following formula:

$$t = \frac{\bar{X}_1 - \bar{X}_2}{\sqrt{\frac{s_1^2}{n_1} + \frac{s_2^2}{n_2}}} \tag{3.3}$$

where $\bar{X}_i$ is the mean of the sample i, s_i the standard deviation of the sample i and n_i the sample size. The test compares the means of two groups and evaluates the corresponding p-value which indicates whether the observed difference between them is statistically significant or could be due to random chance. The formula of the p-value is the following :

$$p = Pr(T \geq t \text{ or } T \leq t | H_0) \tag{3.4}$$

It can be understood as the probability of obtaining a t-score at least as extreme as the one observed with this dataset. A difference was considered statistically significant if the p-value was smaller or equal to 5% (0.05), indicating that the chance of erroneously declaring the difference to be significant is less than 5%.

Evolution comparison

In a second step, the comparison of the metric evolution between T1 and T2 was done in patients and controls. This analysis aimed to detect changes truly caused by AUD and not due to simple scan/rescan variations also observed in healthy subjects. Several factors can influence the reproducibility of DTI measurements including acquisition parameters, data processing (both of which remain constant in this study) but also subject movement, physiological changes and MRI signal variations. These last three factors are not controllable and can lead to large variations in the measurements obtained at different times. The variations also differ according to the studied ROIs [71]. The coefficient of variation in WM is generally between 3 and 10% depending on the study, with values often lower for FA and higher for RD [72, 73]. The reproducibility is even worse in patients with traumatic brain injury than in healthy controls [72]. Andica et al. [74] as well as Grussu et al. [73] studied the NODDI model and reported similar variations as with DTI for the metrics `fintra`, `fextra` and `ODI`. The `fiso` metric, on the other hand, showed larger variations.

To focus on the metrics and regions where variations are significant in alcoholic patients in the sense that they are larger than those observed in controls, the absolute value of percentage change between T1 and T2 was used. As demonstrated by this formula, this is the absolute value of the difference normalised to T1 :

$$Abs_change[\%] = abs\left(\frac{metric(T2) - metric(T1)}{metric(T1)}\right) * 100 \tag{3.5}$$

The mean over all controls is used as a threshold above which the mean of all patients must lie for variations in this metric-region pair to be considered due to alcohol and not to common scan/rescan variabilities.

For the behavioural metrics, there can be no comparison of the evolution between patients and controls since only data at T1 are available for controls. The evolution

was therefore simply analysed within the patients. In this type of analysis, there is a relationship between the T1 and T2 data for each patient. A Paired-Samples or dependent Student's t-test should be used. The formula to calculate the t-score is the following :

$$t = \frac{\bar{X}_D - \mu_0}{s_D/\sqrt{n}} \tag{3.6}$$

where $\bar{X}_D$ and s_D are the mean and standard deviation of the differences between all pairs and the constant μ_0 is here zero as we want to test the null hypothesis considering that the sample means are equal. Again, the p-value corresponding to the t-score is calculated (with the same formula as in Equation 3.4), and the difference is considered statistically significant if the p-value is smaller than or equal to 5%.

Correlation between the evolution of microstructural and behavioural metrics

The correlation between the evolution of microstructural and behavioural metrics was carried out by calculating the Pearson correlation coefficient which measures the linear correlation between 2 sets of data. The formula used to calculate the Pearson coefficient between two random variables X and Y is as follows:

$$\rho = \frac{cov(X,Y)}{\sigma_X \sigma_Y} \tag{3.7}$$

where *cov* is the covariance and σ the standard deviation. The value of ρ is always between -1 and 1, with 0 meaning no correlation, and a positive or negative value meaning a positive or negative correlation respectively.

A p-value could also be calculated indicating the probability of an uncorrelated system producing datasets which have a Pearson correlation at least as extreme as the one computed from these datasets. If the p-value is smaller than or equal to 5%, the correlation is considered statistically significant.

3.7 Technical resources

In addition to software tools and packages already mentioned in this section, MisterI [75] and TrackVis [76] were used to visualise the data. Computational resources have been provided by the Center for High Performance Computing and Mass Storage of the Université catholique de Louvain (CISM/UCL) [77] and the Consortium des Équipements de Calcul Intensif (CÉCI) [78]. The Python computer language [79] was adopted throughout this study for data processing, statistical analyses and graph creation, using the Spyder IDE [80]. In respect to rules of the faculty (Louvain School of Engineering), writing tools such as Deepl [81] and ChatGPT [82] assist the writing of this master thesis. Finally, Overleaf [83] using the Latex language [84] was employed as text editor.

Chapter 4

Results

4.1 Patients and controls comparison

4.1.1 Behavioural comparison

Alcohol-dependent patients and controls were compared for each behavioural metric at time T1 and time T2. As a reminder, the behavioural scores of the controls were only measured at T1. The patients' scores at T1 and T2 were therefore both compared with the T1 scores of the controls. As shown in Figures 4.1(a) and (b), all comparisons demonstrated statistically[1] significant differences. It is interesting to note that the differences are greater at T1 than at T2, demonstrating an evolution of the behavioural scores towards the values measured in healthy subjects. A table with the p-values of these analyses is available in the Appendix E (Table E.1).

4.1.2 Microstructural comparison

Alcohol-dependent patients and controls were also compared for each microstructural metric of each model in each ROI, at T1 and T2. Tables 4.1 and 4.2 highlight the metric-region pairs whose means show significant differences between patients and controls at T1 and T2 respectively and are simplifications of Tables E.2a and E.2b in Appendix E, which contain the corresponding p-values.

Comparison at T1

At T1, the differences between the patients and the controls for the metrics[2] coming up as significant for all regions are `FA` from DTI and `wFA` from DIAMOND. The only other metric coming up as significant from the DTI model is `RD` in the complete CC and in the isthmus. Comparatively, in the DIAMOND model, the metric `wRD` is significant for all ROIs of the CC and for the UF left and, the metric `wAD` for the genu. On one

[1] The word "statistically" will regularly be omitted before the adjective "significant" in order to avoid lengthening and weighing down sentences. The term "significant" will therefore be used at all times to express statistical significance (p-val $< 5\%$).

[2] With the same concern to shorten and lighten the text, metric-region pairs will be mentioned as significant to indicate that the difference between patients and controls for that metric in that region is significant without explicitly stating it.

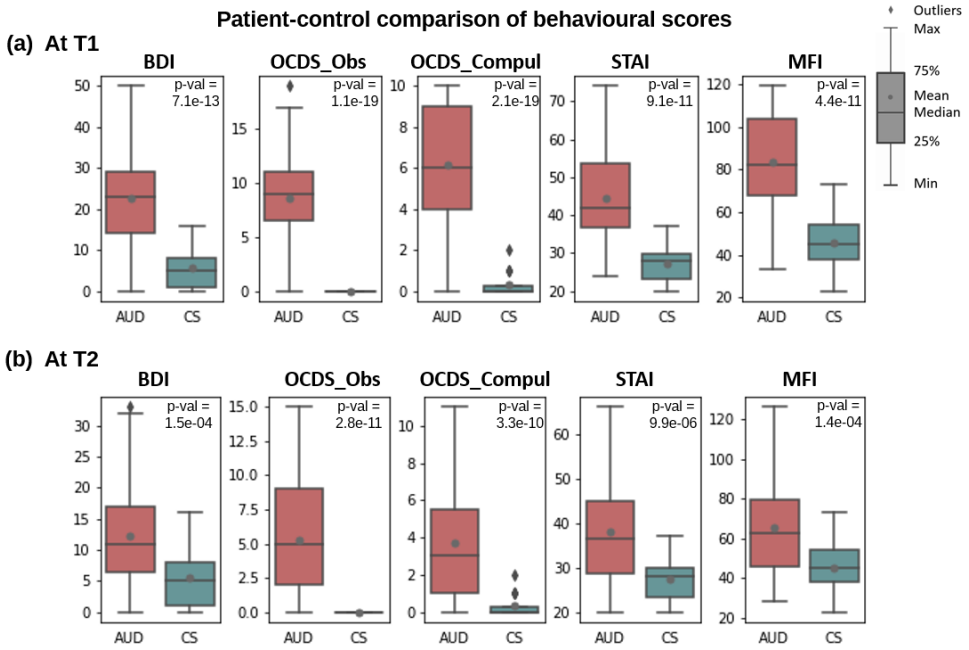


Figure 4.1: Comparison of behavioural metrics between AUD patients and control subjects (CS) at T1 **(a)** and T2 **(b)**. Scores with significant differences (p-val $< 5\%$) are highlighted with more intense colours (all in this case).

side, the metric `frac_csf` and `frac_tot` from DIAMOND are both significant for the genu, the isthmus, the splenium, the UF left and complete UFs. On the other side, the same metrics (`frac_csf` and `frac_tot`) from the MF model are only significant for the isthmus and the splenium. The metric `fvf_tot` is significant for the complete CC and the two most posterior ROIs of the CC (i.e. the isthmus and the splenium) and the metric `wfvf` for the complete CC, the genu, the anterior mid-body and the isthmus. Finally, the NODDI metrics are rarely significant. `fiso` is significant in the isthmus and splenium, `fintra` only in the isthmus and `ODI` only in the complete CC. Looking at the table from the point of view of the regions, it is notable that the isthmus is significant for the majority of the metrics from all 4 models as well as the splenium coming up frequently as significant. Conversely, the posterior mid-body and the UF right are the region with the least regions indicated as significant. The genu is significant for almost all metrics from DIAMOND but not for the other models. Finally, the UF ROIs are only significant in some metrics of the models DTI and DIAMOND but never for any of the metrics from MF and NODDI. The differences of means between controls and patients for each metric-region pair are available in Table E.3a in the corresponding Appendix.

Comparison at T2

AT T2, only one region is significant for one metric from DTI : `FA` in the isthmus. For the DIAMOND model, `wMD` and `wRD` are never significant. `wFA` is significant for almost all ROIs of the CC (except the posterior mid-body and the isthmus) and `wAD` is significant for the complete CC, the genu, the splenium and all three UFs ROIs. The genu, the UF left and the complete UFs show similar significance for `frac_csf` and `frac_ftot`

from both DIAMOND and MF models and also for the metric `fiso` from NODDI. The splenium is also significant for `frac_csf` and `frac_ftot` from the MF model but not from DIAMOND. Finally, the isthmus is significant for the metrics `fvf_tot` and `wfvf` from MF and `ODI` from NODDI. The genu is thus the region which comes up as significant for most metrics while the anterior and posterior mid-body as well as the UF right are never or only one time significant. The complete CC is also significant for only two metrics : `wFA` and `wAD` from DIAMOND. The differences of means between controls and patients for each metric-region pair are available in Table E.3b in the corresponding Appendix.

Table 4.1: Comparison of the microstructural metrics at T1 between AUD patients and controls subjects. Significant differences (p-val $< 5\%$) are highlighted in orange. The same table with the precise p-values is available in Appendix E (Figure E.2a).

	DTI				DIAMOND						MF				NODDI			
Region	FA	MD	AD	RD	wFA	wMD	wAD	wRD	frac csf	frac ftot	fvf tot	frac csf	frac ftot	wfvf	fiso	fintra	fextra	ODI
CC																		
CC Genu																		
CC Ant mid-b.																		
CC Post mid-b.																		
CC Isthmus																		
CC Splenium																		
UF left																		
UF right																		
UF																		

Table 4.2: Comparison of the microstructural metrics at T2 between AUD patients and controls subjects. Significant differences (p-val $< 5\%$) are highlighted in orange. The same table with the precise p-values is available in Appendix E (Figure E.2b).

	DTI				DIAMOND						MF				NODDI			
Region	FA	MD	AD	RD	wFA	wMD	wAD	wRD	frac csf	frac ftot	fvf tot	frac csf	frac ftot	wfvf	fiso	fintra	fextra	ODI
CC																		
CC Genu																		
CC Ant mid-b.																		
CC Post mid-b.																		
CC Isthmus																		
CC Splenium																		
UF left																		
UF right																		
UF																		

Changes between the comparisons at T1 and T2

Numerous metric-region pairs remain significant at T1 and T2: `FA` in the isthmus, `wFA` in the complete CC, the genu, the anterior mid-body and the splenium, `wAD` in the genu, `frac_csf` and `frac_tot` from DIAMOND in the genu, the UF left and the complete UFs, `frac_csf` and `frac_tot` from MF only for the splenium and `fvf_tot` and `wfvf` from MF in the isthmus.

For the DTI model, the only metric remaining significant is `FA` for the isthmus. The metric `wFA` from DIAMOND becomes no significant anymore for the posterior mid-body

and the isthmus of the CC as well as for the three UFs ROIs. The metric `wRD` also loss all its significance. However, the metric `wAD` becomes significant for the majority of the ROIs : the complete CC, the genu (which was already significant at T1), the splenium and the three UFs ROIs. The metric `frac_csf` and `frac_tot` from DIAMOND in the isthmus and the splenium are no more significant at T2. For the MF model, some metric-region pairs were significant at T1 but are not anymore at T2 : `fvf_tot` in the complete CC and the splenium, `frac_csf` and `frac_tot` in the isthmus and the `wfvf` in the complete CC, the genu and the anterior mid-body. Conversely, the metrics `frac_csf` and `frac_tot` in the genu and the left and complete UFs were not significant at T1 but are significant at T2. Finally, in the NODDI model, the metric-region pairs that were significant at T1 are no longer significant at T2 and conversely, pairs that became significant at T2 were not significant at T1 anymore.

The Table E.3c in the Appendix E can be used to analyse the difference between T1 and T2. The main message that can be drawn from it is that the variations in the differences of means do not all point in the same direction. The gap is widening for some metrics, while it is narrowing for others. In most of the cases, the variations observed for the same metric in the different ROIs follow the same direction (with a few exceptions).

To illustrate and bring more detail to some of the more significant comparisons just highlighted by the above tables, boxplots can be seen in Figures 4.2 and 4.3. The boxplots of the metrics values for each region in alcoholic patients (denoted AUD) and in control subjects (denoted CS) are arranged next to each other and the colours used are more intense if the difference is significant and conversely more dull if it is not.

Figures 4.2 shows the boxplots for the `FA` metric from DTI in all studied ROIs. As mentioned above, at T1 it is significant for all ROIs. At T2, however, the differences have strongly diminished, and only the splenium remains significantly different between patients and controls.

Figure 4.3 illustrates the `frac_ftot` metric from the DIAMOND model, in the same way as the Figure 4.2 above does for the `FA` metric. The ROIs of genu, splenium and UF left remain significant at T1 and T2 while isthmus is only significant at T1 and complete UFs only at T2.

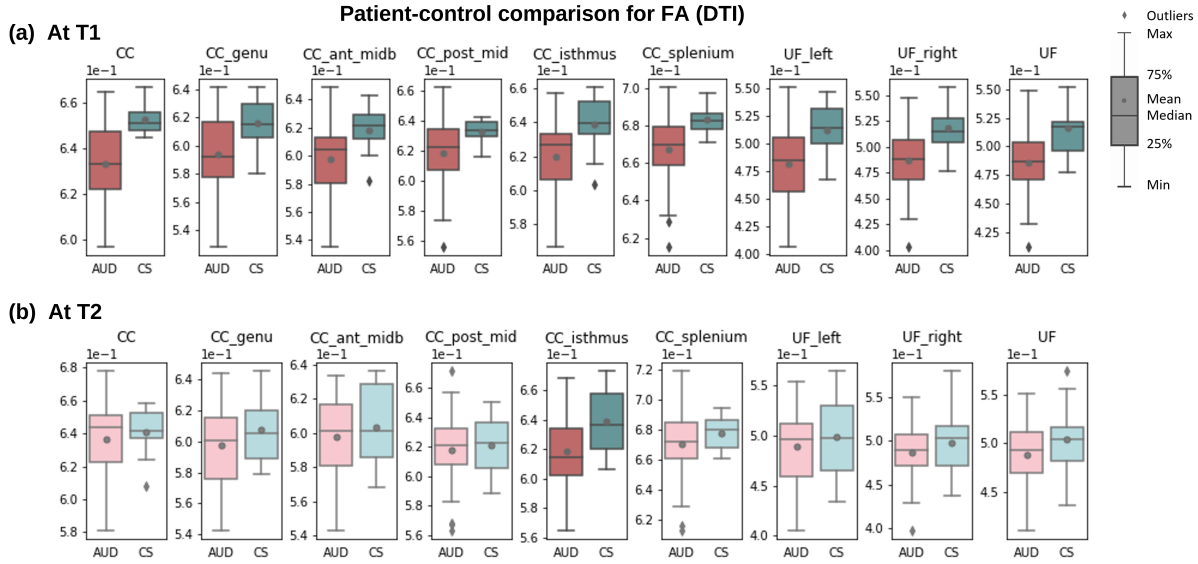


Figure 4.2: Comparison of the microstructural metric `FA` (from DTI) between AUD patients and controls at T1 **(a)** and T2 **(b)**. Regions with significant differences (p-val $< 5\%$) are highlighted with more intense colours.

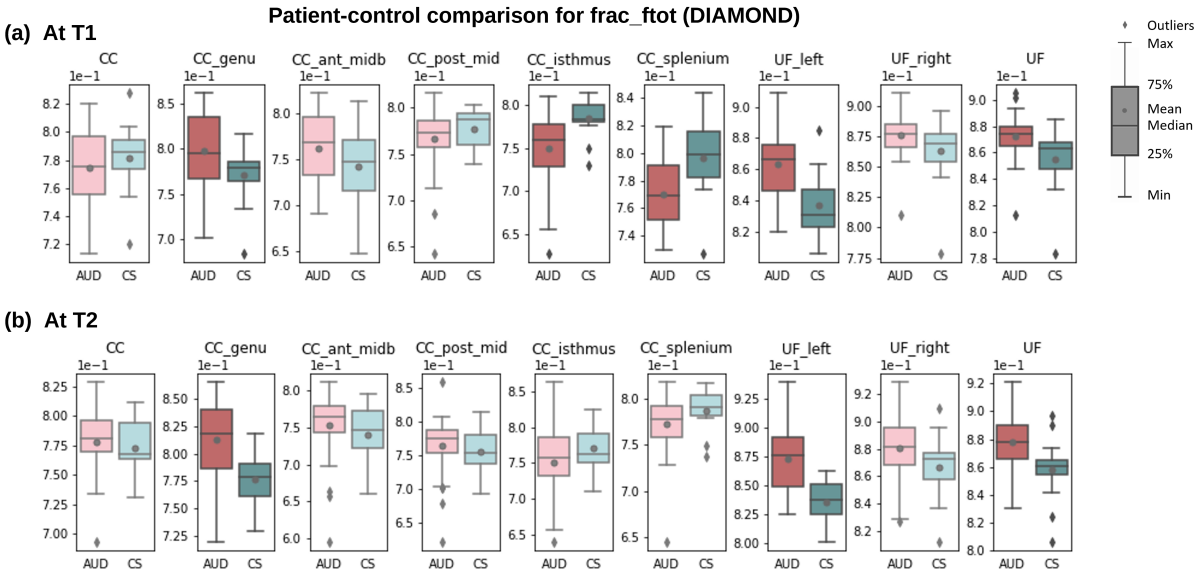


Figure 4.3: Comparison of the microstructural metric `frac_ftot` (from DIAMOND) between AUD patients and controls at T1 **(a)** and T2 **(b)**. Regions with significant differences (p-val $< 5\%$) are highlighted with more intense colours.

4.2 Evolution comparison

4.2.1 Microstructural metrics evolution

In a second step, the evolution of the metrics for each ROI was analysed in the controls and in the patients. As a reminder, the mean of the absolute values of the percentage

changes between T1 and T2 in the controls is used as a threshold to verify that the changes observed in the patients are not the result of normal scan/rescan variations. Table 4.3 summarises this analysis and more details are available in the Tables of the Appendix F. Table F.2a gives the mean percentage of changes for the controls, used as thresholds. Table F.2b gives the mean percentage of changes for the patients. And Table F.2c gives the difference between the two previous tables, indicating how strongly the means of the patients and controls differ from each other or not. In the Table 4.3, if the mean of the absolute values of the percentage changes in patients is well above the control's threshold, the box corresponding to the metric-region pair is coloured green meaning that abnormal variations are observed which can potentially be related to AUD. Conversely, if the average of the patients' changes is below this threshold, the changes are not specific to alcoholics and the box is coloured red. These will therefore be excluded from further analyses.

Table 4.3: Comparison of the evolution of the microstructural metrics between T1 and T2 in AUD patients and controls subjects. The mean of the absolute values of the percentage changes between T1 and T2 in the controls is used as a threshold to verify that the changes observed in patients are not the result of normal scan/rescan variations. The metric-region pairs showing significant changes are coloured green, while the pairs showing non-significant changes are coloured red.

	DTI				DIAMOND						MF				NODDI			
Region	FA	MD	AD	RD	wFA	wMD	wAD	wRD	frac csf	frac ftot	fvf tot	frac csf	frac ftot	wfvf	fiso	fintra	fextra	ODI
CC																		
CC Genu																		
CC Ant mid-b.																		
CC Post mid-b.																		
CC Isthmus																		
CC Splenium																		
UF left																		
UF right																		
UF																		

The analysis of Table 4.3 reveals some readily observed findings. Firstly, the variations observed in the CC ROIs are frequently higher in patients than in controls (the majority of the boxes are green). In particular, the complete CC, the genu and the splenium ROIs as well as all metrics from NODDI (in CC ROIs only) do not show any red boxes meaning that the variations for these metrics/regions are always higher in patients. For DTI, only the `FA` metrics in both mid-bodies and the `RD` metric in the posterior mid-body only show changes with a higher average in controls than in patients. For the DIAMOND model, no average change is lower in the controls for any of the metrics `wFA`, `WMD` and `WAD`. However, the means evolution of the metrics `wRD` and `frac_ftot` in the anterior mid-body are higher for controls than for patients. And for the last metric of DIAMOND, `frac_csf`, the mean evolution in the isthmus is lower for patients than for controls. This observation is also valid for the same metric and the same ROI, but in the MF model. Finally, from MF also, the metric `fvf_tot` in the ROIs of the mid-bodies and the metric `wfvf` in the posterior mid-body show higher evolution in controls than in patients.

From the point of view of the UFs ROIs, many of the evolution of metric-region pairs are on average higher in the controls than in the patients. This is the case for the metrics `fvf_tot`, `wfvf` and `fiso` for all three UFs ROIs. This is also the case for the metrics `RD`, `wFA`, `wRD` and `frac_ftot` (from DIAMOND) but only for the complete and the right UFs. Finally, we can also mention `frac_ftot` (from MF) in the UF left, `wAD` in the complete and left UFs, and `MD`, `frac_csf` (from DIAMOND) and `fextra` in the right UF for which the mean evolutions are higher in controls than in patients.

Figure 4.4 shows the percentages of changes in the `fvf_tot` metric in all ROIs for patients and controls. This is the metric with the most ROIs where the controls have a higher average than the patients. It should be noted that in general for all ROIs (and for all metrics even those not represented here), the range of percentage changes for controls and patients are relatively similar. There is no obvious difference between the two. The differences are mainly visible with the means. It also happens that the difference between the means of the patients and the controls is very small, as is the case for the isthmus in Figure 4.4.

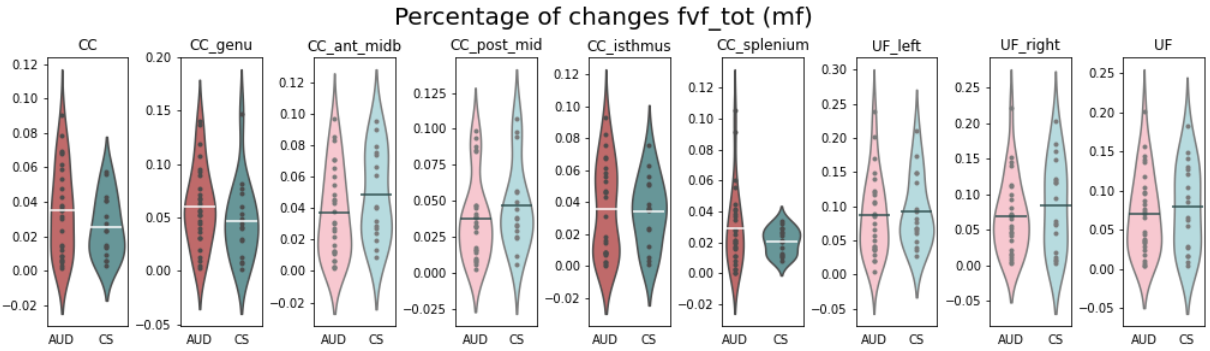


Figure 4.4: Comparison of `fvf_tot` (from the MF model) percentage of changes between patients and controls for all ROIs. The ROIs for which the average evolution is higher in patients than in controls are highlighted with more intense colours. Conversely, the ROIs for which the mean evolution is higher in controls than in patients are shown with less marked colours to indicate that the variations are not particularly abnormal and therefore not due to AUD. The means of all percentages of changes are indicated by small horizontal bars.

Figure 4.5 shows the metric `frac_ftot` calculated by the two models (DIAMOND and MF). As it is the same metric, the results should be identical, but as shown in Table 4.3, this is not the case. DIAMOND indicates that the means in the anterior mid-body and the right and complete UFs are higher in controls than in patients whereas MF indicates this only for the left UF. The two models strongly contradict each other. However, if we analyse the general shapes of the violin plots, we can notice that their shapes are relatively similar in both models, especially in the CC ROIs. This shows a certain coherence that is still present between the two models. Furthermore, the anterior mid-body, the UF left and the complete UF are three ROIs for which the differences in means between patients and controls are very low (see Table F.2c for numerical values). It only takes one or two subjects with values changing between the two models for the patients' mean to fall

below that of the controls or vice versa. Focusing on the UF right, however, we see that the shapes of the violin plots have more changed between the two models and that the differences between the means therefore also vary greatly.

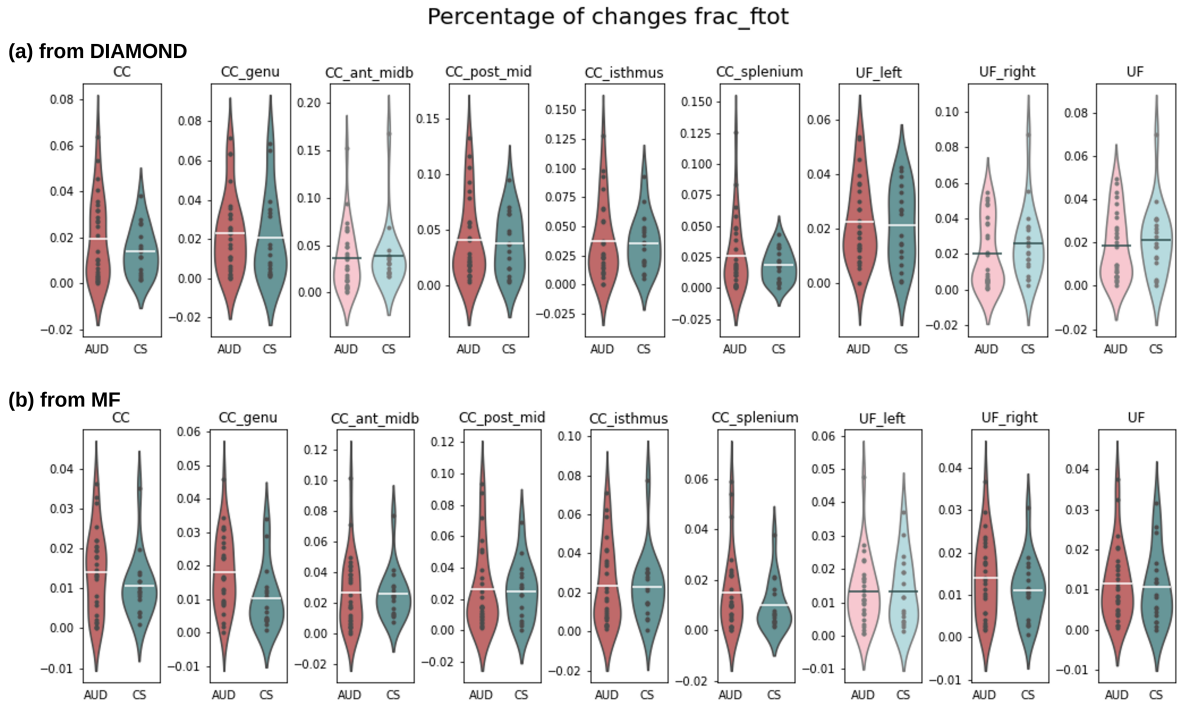


Figure 4.5: Comparison of `frac_ftot` (from both DIAMOND and MF models) percentage of changes between patients and controls in all ROIs. The ROIs for which the average evolution is higher in patients than in controls are highlighted with more intense colours. Conversely, the ROIs for which the mean evolution is higher in controls than in patients are shown with less marked colours. The means of all percentages of changes are indicated by small horizontal bars.

In Tables F.3a and F.3b of the Appendix F, the means of the percentages of change between T1 and T2 are available (these are the means of the **real** percentages of change and **not of the absolute** percentages of change).

4.2.2 Behavioural metrics evolution

The behavioural metrics of alcohol-dependent patients were compared between T1 and T2. As shown in Figures 4.6, all comparisons demonstrated significant differences, with lower scores at T2 than at T1. A table with the p-values of these analyses is available in the Appendix F (Table F.1).

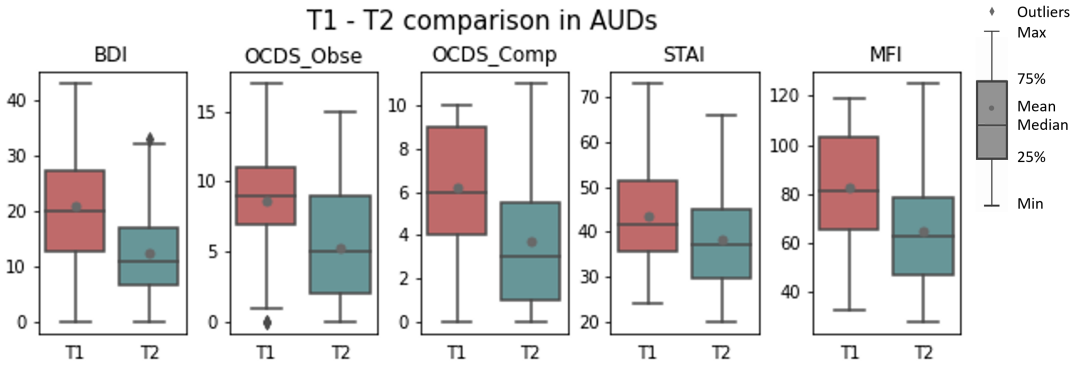


Figure 4.6: Comparison of the behavioural metrics evolution between T1 and T2 in AUDs. The metrics for which the average evolution at T1 and T2 shows significant differences (p-val $< 5\%$) are highlighted with more intense colours (all in this case).

4.3 Correlations between behavioural and microstructural metrics

The central point of interest in this study is the search for correlations between the evolution of behavioural and microstructural metrics. Table 4.4 lists all the behavioural test scores whose evolution can be significantly correlated with one or more metric evolutions in certain ROIs.

Table 4.4: Significant correlation between the evolution of microstructural metrics and behavioural scores. The behaviours for which the correlation of the evolution is significant with the evolution of a certain metric-region pairs are indicated in the table. D for the depression with the BDI test. O for the specific obsession-related statements and C for the specific compulsion-related statements of the OCDS test. A for the anxiety with the STAI test. And F for the fatigue with the MFI test. The cells coloured yellow represent cells that had been excluded because of insignificant evolution (nevertheless some significant correlation were found for these metric-region pairs as shown with the letters O and C).

	DTI				DIAMOND						MF				NODDI			
Region	FA	MD	AD	RD	wFA	wMD	wAD	wRD	frac csf	frac ftot	fvf tot	frac csf	frac ftot	wfvf	fiso	fintra	fextra	ODI
CC	O							O C			O C			O C				
CC Genu				O							O			O		O		
CC Ant mid-b.								OC						O				
CC Post mid-b.								D			OC							
CC Isthmus					D	F	F										F	
CC Splenium					A			C	A	A				C				
UF left																A		
UF right				O							O			O		O		
UF				O							O			O				

BDI

For depression, changes in the BDI score are only significantly correlated with changes in two metrics belonging to the DIAMOND model: `wFA` in the isthmus of the CC and `wRD` in the posterior mid-body of the CC. Figure 4.7 shows the graphs of these correlations. The Pearson correlation coefficients and the corresponding p-values for all metric-region pairs are available in the Tables G.1 of Appendix G.

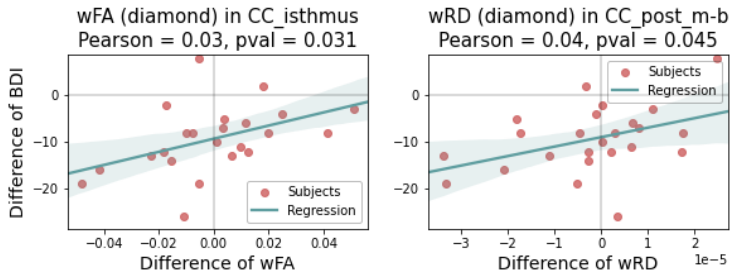


Figure 4.7: Significant correlations between microstructural metrics and BDI score.

OCDS for obsession

For obsession, changes in the obsession-related score of the OCDS are significantly correlated with changes in much more metrics (six different metrics in total). In DTI, `FA` in the complete CC and `RD` in the genu are significantly correlated to OCDS-obsession scores. Only the `wRD` metric[3] is significant in the DIAMOND model for the complete CC. Lots of ROIs are significant for the `fvf_tot` and `wfvf` metrics from MF. `fvf_tot` is significant in the complete CC and the genu. `wfvf` is significant in the complete CC, the genu and the anterior mid-body. Finally, only `fintra` is significant from the NODDI model in the genu and the right UF.

Figure 4.8 shows the graphs of some of these significant correlations. Since the Pearson coefficients of the correlations of a single metric for the different significant ROIs are very close, only the graphs of one of these ROIs for each metric is shown. The other graphs of significant correlations are available in Figure G.6 in Appendix G. Furthermore, the Pearson correlation coefficients and the corresponding p-values for all metric-region pairs are available in the Tables G.2 of the same Appendix.

OCDS for compulsion

For compulsion, changes in the compulsion-related score of the OCDS are significantly correlated with changes in three metrics. For the DIAMOND model, only the `wRD` metric is significant in the complete CC and the splenium. For the MF model, `fvf_tot` is significant in the complete CC and `wfvf` is significant in the complete CC and the splenium. Once again, the correlation coefficients of one metric are very close in the different significant

[3]With the same concern to shorten and lighten the text, metric-region pairs will be mentioned as significant to indicate that they are significantly correlated with the behavioural metrics without explicitly stating it.

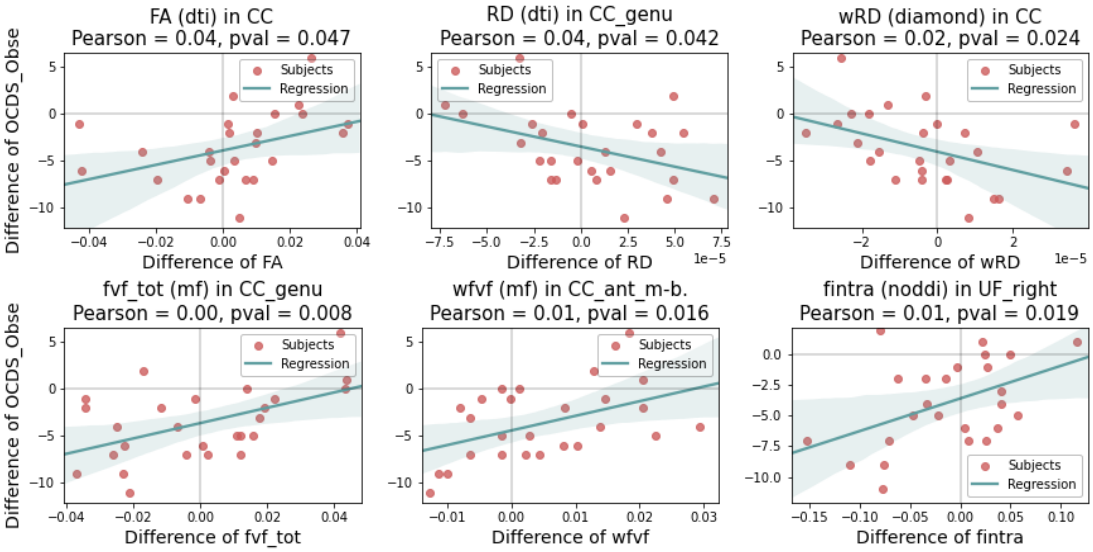


Figure 4.8: Significant correlations between microstructural metrics and OCDS score (obsessions-related statements).

ROIs. Only the graphs of one of these ROIs for each metric is shown in Figure 4.9 and the other ones are available in Figure G.7 in Appendix G. The Pearson correlation coefficients and the corresponding p-values for all metric-region pairs are also available in the Tables G.2 of the same Appendix.

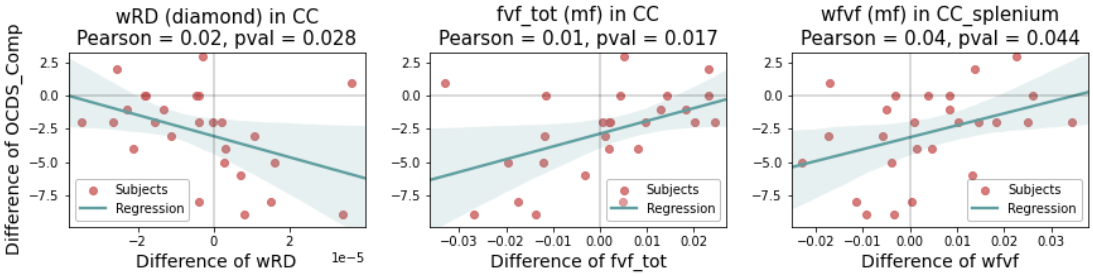


Figure 4.9: Significant correlations between microstructural metrics and OCDS score (compulsion-related statements).

STAI

For anxiety, changes in the STAI score are significantly correlated with changes in four metric-region pairs belonging to the DIAMOND and the NODDI models. The isthmus shows significant correlation for `wFA`, `frac_csf` and `frac_ftot` from DIAMOND and the left UF for `fintra` from NODDI. Figure 4.10 shows the graphs of these correlations. The Pearson correlation coefficients and the corresponding p-values for all metric-region pairs are available in the Tables G.4 of the Appendix G.

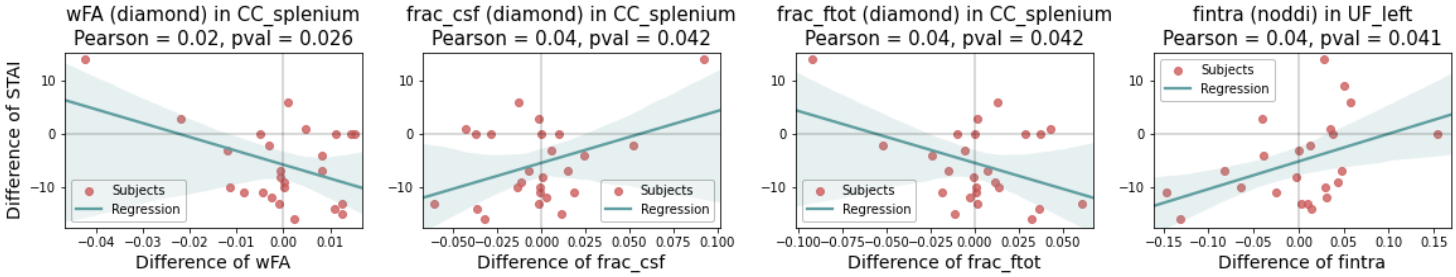


Figure 4.10: Significant correlations between microstructural metrics and STAI score.

MFI

Finally, for fatigue, changes in the MFI score are significantly correlated with changes in three metrics, only in the isthmus : `wMD` and `wAD` from DIAMOND and `fextra` from NODDI. Figure 4.11 shows the graphs of these correlations. The Pearson correlation coefficients and the corresponding p-values for all metric-region pairs are available in the Tables G.5 of the Appendix G.

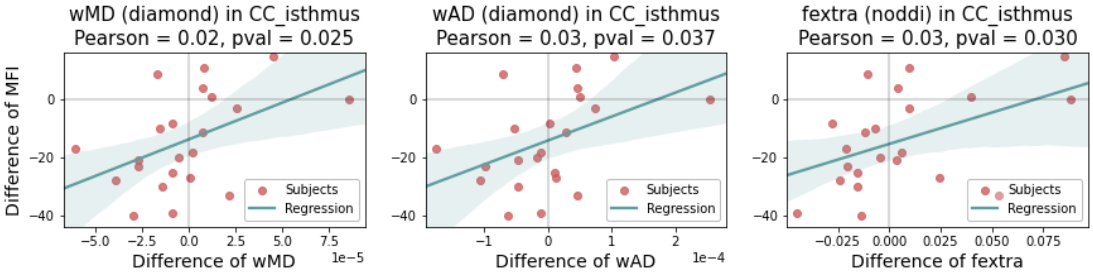


Figure 4.11: Significant correlations between microstructural metrics and MFI score.

Chapter 5

Discussion

5.1 Coherence of the metrics

It is worth beginning the discussion of the results by summarising some of the conclusions drawn by Manon Dausort and Faustine Falyse in their previous study on the same dataset [60], and more particularly on the consistency of the different models and metrics used.

Firstly, from the point of view of the intra-model assessment of the metrics, it has already been mentioned that the `frac_ftot` and `frac_csf` metrics from DIAMOND and MF and the `fintra`, `fextra` and `fiso` metrics from NODDI must be complementary within each model and summed to 1. This property was verified for the NODDI and MF models but not for DIAMOND.

Secondly, from the point of view of the inter-model assessment of the metrics, `frac_csf` (from DIAMOND and MF) and `fiso` (from MF) are defined in the same way, i.e. the volume fraction of the free water compartment. The changes in these metrics between T1 and T2 are therefore expected to be consistent with each other, and this is indeed what was observed. In addition, the metrics `wFA` (from DIAMOND) and `ODI` (from NODDI) represent two contradictory concepts : fibre anisotropy and fibre dispersion orientation respectively. Their tendencies are supposed to be opposite. However, the study of Manon Dausort and Faustine Falyse reported inconsistencies in 14% of the regions whose changes were considered significant in alcohol-dependent patients. Finally, a comparison of the `FA` and `wFA` metrics from DTI and DIAMOND respectively shows consistency, but the amplitude of the variations in these metrics reveals inconsistencies that can be very marked depending on the studied regions. Theoretically, DIAMOND is expected to be more accurate given that the model considers several fibre populations per voxel. However, considering the results of the coherence analyses presented just above, it is important to remain vigilant and critical with regard to the results and their interpretations.

5.2 Behavioural comparison

5.2.1 Patients-Controls comparison

The comparison between patients and controls showed that the averages were always significantly different at both T1 and T2 (see Figures 4.1). At both time points, patients had higher (worse) scores than controls. This clearly indicates a deterioration of the psychological state due to alcoholism. However, a positive evolution was noted after 18 days of abstinence as the scores differences decreased between T1 and T2 by around 30% to 60%, depending on the studied behaviour.

5.2.2 T1-T2 comparison

A comparison of the behavioural scores of patients between T1 and T2 (see Figures 4.6) clearly showed significant differences, with a decrease in all scores at T2. This confirms that the behavioural state of alcoholics tends to improve with abstinence.

Unfortunately, these analyses do not allow differentiating between states pre-existing AUD or caused by AUD. Whichever hypothesis is correct, it suggests that alcohol leads to or reinforces harmful behavioural states that probably maintain AUD and therefore make recovery difficult.

5.3 Microstructural comparison

5.3.1 Patients-Controls comparison

Means of microstructural metrics were compared for all ROIs between patients and controls at T1 and T2 (see Tables 4.1 and 4.2). At T1, 33% (53 out of 162) of metric-region pairs showed significant differences, including 38% for the CC ROIs and 20% for the UFs ROIs. At T2, this value decreased to 19% (31 out of 162) including 17% for the CC ROIs and 24% for the UFs ROIs. This shows a clear impact of alcoholism on the microstructure of the brain. The CC is strongly impacted at T1 and less at T2. Conversely, the UFs are less affected at T1 but more severely at T2.

In the CC, the isthmus shows differences in most of the metrics at T1 indicating a high sensitivity of this region to alcoholism. The splenium and genu are other regions strongly affected at T1. However, it is important to note that the isthmus is a very narrow ROI with a length equal to 1/12 of the entire CC length. This is very low compared with, for example, the splenium and the genu, whose lengths are respectively 1/4 and 1/6 of the CC. In ROIs made up of a small number of voxels, more or less extreme values in a few voxels have a strong influence on the overall average, which is not the case in large ROIs where these extreme values would be drowned out by the large number of voxels. This may therefore explain the fact that the isthmus very often appears significant, indicating a potential overestimation of the impact of alcohol on this region, what should be kept in mind when analysing the results.

The isthmus and splenium show a good evolution between T1 and T2 since numerous metrics are no longer significant at T2 and the gaps between the means of patients and controls also decrease between T1 and T2 (see Tables E.3c in Appendix E). This is also the case for other CC ROIs (the complete CC and the two mid-bodies). Although they were less significant at T1, they are even less significant at T2 with a decrease in the gaps between patients and controls. This is not true for the genu, which shows more significant metrics at T2 than at T1, and increases in the gaps between patients and controls for metrics significant at T2.

To sum up, this would indicate that the CC in general is strongly affected by alcoholism, particularly in the posterior regions. A period of abstinence quickly triggers positive changes, particularly in the posterior regions also. Meanwhile, the genu seems to follow a different pattern, with the harmful effects of alcohol continuing to increase even during periods of abstinence.

In the UFs, the tendencies are rather opposite to those of the CC in general. The number of significant metrics is increasing at T2. In addition, most of the metrics show a raise of the gaps between the means of patients and controls at T2. The UFs therefore appear to be affected by alcoholism, with prolonged effects even during abstinence. Finally, the left and right UFs do not show similar tendencies. The right UF is very rarely significant, whereas the left UF is. This is consistent with the UF asymmetry hypothesis, which will be discussed further below.

With regard to the intra-model consistency of the metrics, `frac_csf` and `frac_ftot` (from DIAMOND and MF) are consistent with each other at both times since they are always significant in pairs. In terms of the inter-model consistency, the metrics `frac_csf` and `frac_ftot` (from DIAMOND and MF) and `fiso` (from MF) are consistent at T2 but less so at T1 where DIAMOND indicates significant ROIs that are not in the other models. This confirms what Manon Dausort and Faustine Falyse [60] had concluded, namely that we should remain critical regarding the DIAMOND model. In addition, it can be noted that the `FA` and `wFA` metrics are consistent at T1 but not as much at T2 where the significant ROIs diverge. There is also inconsistency between the `wFA` and `ODI` metrics as the latter is very rarely significant. However, their tendencies remain consistent, with gaps between patients and controls of opposite signs at both time (consistent with the opposite definitions of these metrics) and both metrics showing positive evolutions with a reduction in the gaps between patients and controls over time.

5.3.2 T1-T2 evolution comparison

Results interpretation

As exposed in the presentation of the results (see Table 4.3 in section 4.2), some metric-region pairs show lower means of absolute evolution for patients as compared to controls. These changes in individual patients are therefore due to common scan/rescan variations and cannot be considered as caused by the AUD. Since this is precisely the purpose of this study, the pairs highlighted in this section (corresponding to the red box in Table 4.3) were discarded from further analyses.

At the CC level, the changes in metrics for patients were mostly greater than those for controls. The ROIs presenting certain metrics for which this is not the case are the two mid-bodies and, to a lesser extent, the isthmus. The significant evolution of all other pairs confirms that alcoholism has a real impact on the cerebral microstructure of the CC. Since only the absolute value of the changes is considered, it is difficult to see whether the changes are improving or deteriorating the CC. However, it is possible to combine these observations with those previously discussed on the comparison between patients and controls at T1 and T2. Given that the differences are reduced at T2, this would mean that the changes in the CC during the 18 days of abstinence are beneficial for the patient, tending towards a return to a normal, healthy state.

For the ROIs of the UFs, the results are very different. Indeed, many metrics show lower mean absolute percentages of change in patients than in controls. This is mainly the case for the right and complete UFs. To explore this difference between the ROIs of the UFs and the CC somewhat further, we can look at the threshold values imposed by the controls (see Table F.2a). For the CC, the thresholds are on average around 5%, whereas for the UFs, the thresholds reach averages of around 9%, with extreme values up to 30%. Thus, the percentages of changes in patients must be much larger in the UFs than in the CC to exceed these thresholds, and some changes in patients, despite being rather robust, are considered as simply due to scan/rescan variations and not to alcohol. These were therefore not considered in the correlation analysis.

General remarks

Generally speaking, if we compare these results with the arbitrary threshold of 8% that Manon Dausort and Faustine Falyse [60] used in their study to distinguish significant variations from others, we can see that applying the same threshold in this study would have produced very different results. Far fewer metric-region pairs would have been considered significant in the CC and a fairly similar number in the UFs but with different pairs from those mentioned here. In fact, the 8% threshold value here appears to be a fairly general and restrictive limit (especially in the CC), whereas the scan/rescan variations seem to depend very much on the studied metrics and ROIs and do not exceed 3-4% for many metric-region pairs.

In addition, as we have already seen from the violin plots in Figures 4.5 and 4.4, there is no marked superiority of the mean percentages of absolute changes of patients over the controls. The graphs show a relatively similar distribution of the evolution measures in the two populations, with fairly similar averages. This implies that the difference between both populations is sometimes very small and that it only takes one subject with slightly higher or lower values to bring the mean of the patients above or below the threshold set by the controls and for the change to be considered as due to alcoholism or due to common scan/rescan variations.

Although subjects with too low SNR in their scans were excluded from the analyses, there is still considerable noise in the studied dataset. Such noise can increase the variations measured, and this has not been taken into account in this analysis. The challenge of isolating UF tracts, especially in alcohol-dependent patients, may also result in variable measurements of metric evolutions depending on the individual, causing averages to diverge from the biological truth. These results therefore need to be examined in greater depth to gain a better understanding of the origin of the measured variations. This could enable more accurate conclusions to be drawn, with the hope of being able to include more metric-region pairs in the correlation analysis if the results presented here do not fully represent reality.

UFs asymmetry

As a reminder, in the state of the art, a 30% difference in fibre volume and density was reported between the two UFs. With all the analyses discussed above, it is already clear that differences are observed between left and right UFs. Analysis of the number of streams and mean stream density on our data is detailed in Appendix H. In short, this analysis also revealed significant differences between the left and right UFs within patients, within controls and within all subjects when studied together. A clear superiority of the right UF is observed at both time, T1 and T2. From the point of view of comparing the left and right UFs on the basis of metrics, there are also marked differences. At T1, about half of the metrics were significantly different between UF left and right, with a reduction in the number of significant metrics at T2 in patients but not in controls. This only confirms a clear asymmetry between the left and right UFs.

Metrics consistency

It is worth pointing out the consistency of the metrics and making the link with Manon Dausort and Faustine Falyse's conclusions [60] summarised at the beginning of the discussion (see section 5.1). They had used the mean percentage of change to check that the evolutions in the `frac_csf` and `frac_ftot` metrics (from DIAMOND and MF) and the `fintra`, `fextra` and `fiso` metrics (from NODDI) compensated each other inside each model. This proved to be the case for MF and NODDI, but not for DIAMOND. In this study, the mean percentage of change were also calculated for the 9 ROIs (see Tables F.3a for controls and F.3b for patients in Appendix F). The consistency of the metrics is not verified for any of the models.

Actually, this is not very surprising given the way in which the ROIs were isolated and the means on these ROIs calculated. Variations regarding the voxels included in each ROI between T1 and T2 had already been mentioned as a limitation by Manon Dausort and Faustine Falyse [60]. Their ROIs were created from identical atlases at T1 and T2. In this study, the final ROIs obtained are the result of numerous steps which lead to greater differences between the ROIs at T1 and T2. The parcelation of the brain as well as the complete tractography of the brain can vary slightly over time. Combining these two sources to isolate tracts with WMQL further amplifies the differences between ROIs. In addition, fibre densities are not the same at both times. Calculating density-weighted

means implies that the voxels do not have the same weight and their contribution varies from T1 to T2. As a result, these variations in ROIs do not allow observing any consistency in the evolution of the metrics.

5.4 Correlation between microstructural and behavioural evolution

In this section, each behaviour will be reviewed in order to detail the significant correlations associated with it. As we have seen in the comparisons including behaviour scores (comparison between patients and controls, section 5.2.1, and comparison between T1 and T2 of patients, section, 5.2.2), all means scores decreased over time. All the analyses and correlations will therefore be presented on the basis of a reduction in scores, since this is also one of the goals sought by patients following a period of abstinence : a return to normality, a reduction towards values close to those observed in controls. Thus, a positive correlation with a microstructural metric means that the behavioural score decreases more when the metric also decreases, whereas a negative correlation indicates that the score decreases more when the metric increases. However, it should be kept in mind that some patients show inverse tendencies with an increase in behavioural scores. In the correlations described below, these increases are therefore favoured by inverse tendencies in microstructural metrics.

5.4.1 Correlations with BDI, STAI and MFI

A first general observation can be made from the correlation summary table (see Table 4.4): scores for depression, anxiety and fatigue (from BDI, STAI and MFI respectively) are significantly correlated with much less metric-region pairs than the OCDS score including obsession and compulsion. However, their correlations are concentrated in the posterior ROIs of the CC. The discussion will first focus on these first 3 behaviours.

BDI

The BDI score was only significantly correlated with two metric-region pairs. On the one hand, it correlates positively with the `wFA` metric from DIAMOND, in the isthmus. A decrease in this metric indicates, at the biological level, a loss of structural organisation of the fibres and a decrease in the integrity of the WM. Although counter-intuitive, according to this correlation, this (in this ROI) would favour the reduction of a depressive state. On the other hand, BDI is positively correlated with `wRD` (from DIAMOND) in the posterior mid-body. This indicates that an increase in axon density, a fibre packing, in this ROI is associated with a reduced depressive state.

STAI

The STAI score correlated significantly with 4 metric-region pairs, 3 of which related to the splenium ROI. In this ROI, the correlation is negative for wFA, positive for `frac_csf` and negative for `frac_ftot`, three DIAMOND metrics. Contrary to what was seen for the BDI, a correlation between a decrease in STAI and an increase in wFA indicates that a structural reorganisation and an improvement in the integrity of the WM accompanies a less anxious state. The opposite sign correlations for `frac_csf` and `frac_ftot` are consistent since these two metrics are complementary and must therefore evolve in opposite proportions to maintain balance. This correlation indicates that a volume increase in the fibre compartment and a volume reduction in the one reserved for free water are associated with a decrease in anxiety.

Finally, we should also mention that, in the UF left, STAI is positively correlated with NODDI's `fintra` metric. Degeneration or injury in the intra-axonal compartment in the left UF is therefore correlated with reduced anxiety.

MFI

The MFI score is only correlated with metrics in the isthmus. The metrics `wMD`, `wAD` and `fextra` are all positively correlated. `wMD` is calculated from `wAD` (among others). It seems therefore that the significance of `wMD` is mainly due to the significance of `wAD`. A decrease in `wAD` is explained by axonal degeneration or deletion. The positive correlation found here suggests that axonal deterioration in the isthmus is associated to a reduction in fatigue. A reduction in `fextra` indicates a reduction in the extra-axonal space with a deterioration in the integrity of the myelin sheath and a depletion in glial cells surrounding axons, which is also associated with a reduction in fatigue.

Preliminary conclusion

As a first general conclusion on these 3 behaviours, we can note that analyses including BDI and MFI showed unexpected correlations. The interpretation of the metric indicates that increasing damage to the WM in the isthmus is associated with positive changes in depression and fatigue. Firstly, it should be noted that the isthmus is the narrowest ROIs in the CC. As discussed previously, due to size-effect, variations in small ROIs can be more sensitive to important variation in certain voxels and be more easily considered as significant in a slightly overestimated way. Secondly, the interpretation of the correlations includes only one metric each time. However, the interpretation of a single metric is not always unambiguous, and discrete evolutions in certain directions can lead to different conclusions.

As already mentioned by Manon Dausort and Faustine Falyse [60], an inflammation hypothesis could explain a decrease in `fextra` in the isthmus for the correlation with MFI. More details are needed on `fintra` and `fiso` because, as the 3 metrics are complementary, an increase in the volume of the extra-cellular compartment necessarily implies a decrease in the volume of the intra-cellular and/or free water compartment. As the correlations

involving these two other metrics were not significant, we can suspect, without certainty, that the decrease would have occurred in both compartments. Even after stopping the drink of alcohol, inflammation would thus continue to increase in the isthmus. However, explanations linking this to a reduction in depression and fatigue have yet to be identified.

Finally, it is also important to note that the ROIs studied include fibres that extend beyond the inter-hemispheric boundary of the CC. These fibres then cross other fibres belonging to other structures. The measure of `wFA` or `wAD` may therefore be influenced by these other fibres with an impact on the interpretation of the results.

5.4.2 Correlation with OCDS (obsession and compulsion)

Significant correlations for compulsion and especially obsession are much more numerous. However, a large proportion of them include metric-region pairs excluded from the analysis because their evolution were non-significant. As shown in summary Table 4.4, the principal affected regions are the complete CC for both obsession and compulsion, the genu for obsession only and the splenium for compulsion only. Generally speaking, for all the correlations with the OCDS score (including compulsion and obsession), the signs of the correlation coefficients of one metric are identical for all ROIs (even when they are not significant). Moreover, when they reach significance, their values are very close. The metric-region pairs whose correlation is significant for both obsession and compulsion can therefore be discussed simultaneously.

In the complete CC, compulsion and obsession are negatively correlated with `wRD` (from DIAMOND) and positively with `fvf_tot` and `wfvf` (from MF). An increase in `wRD` denotes disruption of the myelin sheath or a lost in fibre density whereas a decrease in `fvf_tot` and `wfvf` also indicates a decrease in fibre density. These observations are therefore consistent with each other. However, at first glance, this interpretation does not correspond to what was expected. Referring to the inflammation hypothesis and, at variance with what was hypothesised for the isthmus (swelling due to inflammation), the actual correlation in the complete CC could indicate a reduction in inflammation associated with a decrease in feelings of compulsion and obsession.

The `wRD` and `wfvf` metrics are also significantly correlated with compulsion in the splenium. The same conclusions can thus be drawn for this region including a decrease in compulsion only.

In the genu, a reduction in obsession is significantly correlated with an increase in `RD` (from DTI), a decrease in `fvf_tot` and `wfvf` (from MF) and a decrease in `fintra` (from NODDI). These correlations are again similar to what has already been discussed for the CC complete above. Indeed, the `RD` is the equivalent metric of `wRD` but derived from DTI and not DIAMOND and the correlation is negative, as for the complete CC. The correlations are also the same for `fvf_tot` and `wfvf`. And finally, the correlation including `fintra` is positive, meaning that the decrease in obsession is associated with a volume reduction in the intracellular compartment. All of these factors provide additional

arguments supporting the hypothesis that early abstinence reduces inflammation. A correlation was also observed between obsession and an increase in wRD in the anterior mid-body and a decrease in `fintra` in the right UF. Although this is not confirmed by significant correlations with other metrics, it may also be part of the hypothesis calling for a inflammation reduction.

In addition, in the complete CC, decrease in `FA` (from DTI) is positively correlated with obsession which implies that disorganisation and degradation of the WM is associated with better scores in obsession. This constitutes a new correlation that was not initially envisaged. As already mentioned above for the correlation between BDI and `wFA`, the measurement of the metric is potentially affected by the presence of crossing fibres that are not part of the CC fibres. This observation is particularly relevant in this case because DTI cannot differentiate between various fibre populations within the same voxel as do DIAMOND. As a result, the FA value can be strongly affected.

The main observations and hypotheses regarding the correlation between behaviours and microstructure in the CC are schematically summarised in Figure 5.1.

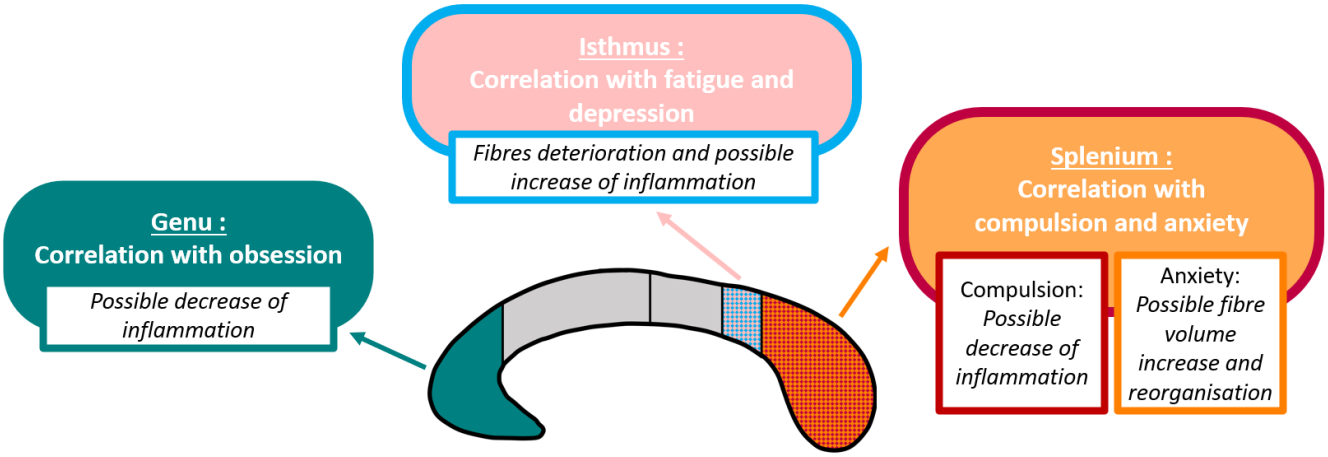


Figure 5.1: Schematic overview of the main observations and hypotheses regarding the correlation between behaviours and microstructure in the CC. Correlations including the isthmus must be interpreted critically, as the narrowness of this region can have a noticeable size effect, inducing a possible overestimation of the correlation significance.

5.4.3 General remarks

Firstly, many correlations are observed. However, these analyses do not explain the reasons or origins of these correlations. In particular, it is not possible to deduce the existence of a causal relationship, nor to know the direction of this causal relationship if it exists.

Secondly, correlation was only studied on the basis of Pearson's coefficient, which quantifies linear correlations between two variables. One can not exclude that other correlations exist and follow other types of non-linear correlations (quadratic, exponential, monotonic or not, etc.).

Thirdly, a large number of metric-region pairs in the complete and right UFs showed significant correlations with obsession. However, these correlations were not discussed because evolutions of these microstructural metrics were not significant. As UFs are part of the limbic system which is itself involved in the reward circuitry, it was indeed not surprising to find correlations with changes in feelings of obsession. As mentioned in the previous section (see section 5.3.2), it would be interesting to analyse the evolution of the metrics more deeply before definitively ruling out the potential involvement of UF in behavioural changes.

5.5 Limitations

This study has a number of limitations linked to the research topic and the methods used. It is necessary to be aware of these limitations and to take them into account when analysing and interpreting the results. Some of these limitations have already been highlighted in the discussions hereinabove. In this section, additional limitations will also be outlined.

Firstly, this is a study on the effects of a period of abstinence in AUD patients. However, the assurance that this abstinence was respected cannot be fully confirmed. Some of the patients declared having consumed alcohol during the 3rd week of the programme (i.e. a few days before data acquisition at T2). When this consumption remained low, the patients were kept in the study. This does not rule out the possibility that other patients also drank alcohol without mentioning it, or that they were not accurate in the information they provided about the quantity of alcohol they drank (whether voluntarily or not).

Secondly, quantifying behavioural states is difficult. In the interests of objectivity, recognised and validated self-report questionnaires were used. Unfortunately, the scores obtained can sometimes be biased by the patient and the context or precise moment at which they were performed. From one day to another, responses may change simply as a result, for example, of the quality of the patient's night just before running the test. In addition, certain behavioural states may not be linked to AUD but may be the result of different character traits in each individual or other external factors.

Thirdly, the study only provides a limited view of the AUD's complete timeline. Only information collected over 2 days is considered, whereas AUD is a disorder that generally spans over several years. In particular, no data is available for the period before the onset of AUD. The results obtained allow conclusions to be drawn about correlations between certain factors without explaining their causal relationship. Specifically, we cannot deduce from our analyses whether certain behavioural states are caused by AUD, whether, on the contrary, it is AUD that causes them to decline or whether any other link exists between the two. The severity of AUD at the time of the study also depended on a large number of antecedent factors, ranging from genetic factors to the age of onset of alcohol consumption, family history, the quantity of alcohol drunk during the year(s) preceding the study, the number of periods of abstinence already completed, etc. Furthermore, abstinence is generally medically assisted. This medication can have significant impacts on patients' behaviour and therefore biased the scores analysed in this study. Although

some data were collected, none of them were included in the analyses.

Fourthly, the sample sizes of the control subjects and alcohol-dependent patients were not equal. Although this was taken into account in the statistical analyses, it may have several implications, such as lower precision in the controls because there were fewer of them, or lower generalisability. The quality of the data between the two samples is not the same either. This can be seen not only in the SNR values, which are lower on average in patients, but also in the quality of tract isolation, which was much more often insufficient in the patients. Insulating UF tracts in particular is a difficult challenge. The fascicle has a fairly complex shape and, moreover, exhibits asymmetry between the two hemispheres. In the end, the number of patients excluded from the analyses was proportionally much greater than controls.

Fifthly, the use of an automated pre-processing pipeline, despite the facilities it brings, also leads to limitations. Checking all the outputs obtained is not an option, as it is far too time-consuming. In addition, the parameters used for this pre-processing are the result of choices made with the aim of obtaining the best results for all the subjects. These parameters are not especially appropriate for all subjects, each of whom has a unique brain with different anatomical particularities and for whom acquisition conditions inevitably vary slightly. In particular, the tractography parameters and the definitions of the different tracts used with WMQL were made manually by observing the outputs at each step. For instance, the definitions of the UF tracts contain instructions of the type *superior_of(region)* which refers to the entire area above a horizontal line placed at the top of that region. However, with different inclinations of the patient's head in the MRI scanner during acquisition, the areas considered as superior may vary slightly from one patient to another, which will have repercussions on the quality of tract isolation.

Sixthly, the choice of the methodology used to measure evolution is open to debate. In this study, mainly the difference between T1 and T2 was used for the majority of the analyses. This choice was initiated by the desire to use the same methodology to measure evolutions in microstructural and behavioural metrics. However, some subjects exhibit zero values for certain behaviours at T1, which, in the case of non-zero evolution, translates into an infinite percentage of change. This value cannot be used, among other things, to obtain correlation coefficients. An offset in behavioural data (on all or only on the zero values) could have been applied, but this would have biased the results in some way, and the percentages of change obtained would not be a true reflection of reality. It was therefore decided to use the absolute difference for all analyses. The only exception was for the comparison of the evolutions, between patients and controls. It was intended to match the methodology most often used in the literature. It is also the methodology that Manon Dausort and Faustine Falyse have used for their study on the same dataset [60]. Focusing on the percentage of change for this particular analysis therefore makes it possible to compare the different results obtained.

However, it is crucial to be aware that this choice has significant consequences on the results. For example, the evolutions considered to be higher in patients than in controls would have been slightly different. It was also noted that the tendencies of the average

evolutions over all the subjects can be interpreted in very different ways depending on the methodology. This is illustrated by the example of three subjects whose evolution for an arbitrary metric can be seen in Table 5.1. It is easily noticeable that appreciating changes in absolute or relative value can lead to tendencies going in different directions. This is because, for the same differences in absolute value, the value at T1 can have a significant impact on the value measured in percentage of change (as is the case for subjects A and B).

Subject	**T1**	**T2**	**Difference**	**% change**
sub A	0.4	0.2	-0.2	-50%
sub B	0.8	1.0	+0.2	+25%
sub C	0.6	0.7	+0.1	+16%
Mean evolution			+0.033	-3%

Table 5.1: Example of the consequences of using the difference or the percentage of changes to measure the average evolution for the same metric between T1 and T2.

Seventhly, among the limitations of DTI outlined in the state of the art (see section 1.3.3), two of them reveal a particular importance in this study. On the one hand, tractography does not allow an exact quantification of the axonal connection density. The use of fibre density weighted averages for the metrics in each ROI is an approximation that does not fully reflect reality. On the other hand, although the DIAMOND and MF models allow the differentiation of several fibre populations within a single voxel, the final value of the metrics for each voxel is still a weighted average over the multiple fibre populations present in that voxel. In this study, specific fibre tracts were studied. However, the final ROIs included all the voxels crossed by these specific tracts and they also included other fibres crossing these voxels. Fibres belonging to the tracts of interest, as well as other fibres passing through the same voxels, influence in this way the value of the metrics measured. The observed correlations and their interpretations may therefore be altered. Possible solutions to overcome these limitations will be proposed in the next section about future perspectives.

Finally, all the interpretations presented in this discussion are, for the moment, only hypotheses supported by these analyses. However, they must be the subject of more detailed future research in order to be confirmed or refuted. The analysis of the biological samples from subjects or additional imaging to analyse the inflammation could, for example, provide interesting information about the hypothesis of inflammation in neuronal tissues. The involvement of health professionals, particularly neurologists and alcoholism specialists, would provide invaluable support for further studies.

5.6 Further perspectives

The limitations mentioned above indicate the necessity to seek alternatives or make corrections to the employed methods. The analyses also raised new questions for which additional studies could be conducted. Here are some perspectives.

Firstly, it was noted that a large number of patients were excluded from the analyses, often because of poor tract isolation. In many cases, reasons for these issues were found (see Tables in Appendix D). Modifications in the tract isolation protocol could be made to resolve these issues, most of which being patient-specific. For example, alcoholism can lead to an increase in the volume of the lateral ventricles, with a consequent alteration in the curvature of the CC. The maximum angle parameter used for the tractography is then not high enough to allow the fibres to follow this non-standard shape. The outlier patients could therefore be treated individually in order to adjust the parameters of the methods and to be able to include a larger number of patients in the study. However, this approach could reduce the objectivity and consistency between all the patients, which would have to be taken into account.

Secondly, many available data on patients and controls were not used. Age, sex, feces analysis, cognitive test results and biological samples are information that could be included in the analyses as additional influencing factors. The analysis of data collected at a third time point (T3, after 3 months) could also extend the scope of this study. As this third dataset had not yet been acquired for the controls, this was not yet possible. These additional researches could help to complete the results obtained previously and, in particular, to understand the mechanisms involved in the correlations we have discussed.

Thirdly, the correlations only included one microstructural metric at a time. However, it would not be surprising to find that the behaviour could be associated with several or a combination of metrics. Correlations should therefore be analysed, including the evolution of several metrics at the same time. Adapting this study by including a PCA (Principal Component Analysis) technique could also represent an interesting prospect that would allow reducing the dimensionality of the data (presently composed of 18 metrics) in order to extract the essential information. This should constitute a very interesting approach to consider for this type of research since some of the metrics currently used are redundant with each other (for example, MD can be calculated from AD and RD). Unfortunately, this could reduce the interpretability of the results since all the metrics would be combined.

Furthermore, more accurate axonal density measurements should be used to weight the means of the metrics on each ROI (and to compare UFs). To this end, a method has been proposed by Smith et al. [85] allowing to determine "*an appropriate cross-sectional area multiplier for each streamline*". In other words, it consists in a calculation of weights associated with each streamline that can be used to extract fibre densities reflecting the true density of WM tracts.

In addition, to prevent the values of the metrics being influenced by crossing-fibres that are not part of the tracts of interest, a framework was developed by Dhollander et al. [86]. In a nutshell, the FBA (Fixel-Based Analysis) framework uses tractography to isolate the fixels (an individual fibre population in a voxel) aligned with the tracts of interest in order to extract the metrics of this specific fixel without mixing the signal and thus the properties from intersecting tracts.

Finally, Manon Dausort and Faustine Falyse [60] had analysed the patients by dividing them into 2 clusters. These clusters were defined by the analysis of their microstructural properties in order to deduce different tendencies. The present study could consequently be combined to the previous one in order to focus on microstructure-behaviour correlations within the clusters already identified. Indeed, since several tendencies have been discovered at the level of the WM microstructure, several patterns of evolution could also exist at the level of behaviour and analyses taking this into account could bring to light additional significant correlations.

Conclusion

AUD has several and diverse consequences, ranging from impaired mental health, social and interpersonal problems to alterations in brain microstructure, weakened cognitive functioning, motor difficulties or even digestive system diseases. The interplays between all these symptoms are also numerous and complex. This master's thesis aimed at investigating the relationships between behavioural and microstructural evolution in the corpus callosum and the uncinate fasciculus in abstinent alcoholic patients, using dMRI.

More specifically, a total of 18 metrics from 4 different models (DTI, NODDI, DIAMOND and MF) were used to explore WM microstructure. In addition, self-reported questionnaires were used to assess 5 behaviours: depression, obsession, compulsion, anxiety and fatigue. After comparing the data obtained in patients and controls at T1 and T2, linear correlations were finally measured between the evolution of microstructural and behavioural metrics after 18 days of abstinence.

The findings of this thesis confirmed the existence of significant alterations in the microstructural organisation and integrity of the corpus callosum and the uncinate fasciculus in alcoholic patients compared to healthy controls. In most regions of the CC, the differences observed between both populations on the first day of abstinence appeared to have decreased at day 18, suggesting a microstructural normalisation in patients during early abstinence. Only the genu does not follow this pattern, as it does not show particular changes at T2 compared to T1. Conversely, in the UFs, a deterioration in their microstructure is observed during the 18 days of abstinence, suggesting a persisting effect of alcohol. In addition, most of the evolutions of the metrics in the UFs of controls were very marked and even higher than what was found in patients. Variations in patients' UFs having therefore been assumed to be due to common scan/rescan variations and not to AUD, very few correlations including UFs could be analysed.

More noteworthy results were found in the different regions of the CC. First, a reduction in anxiety was correlated with a normalisation in the integrity and in the organisation as well as an increase in volume for the splenium fibres. Then, for the 4 other behaviours, different regions of the CC showed less expected changes. Fatigue and depression were correlated with changes in the isthmus suggesting that fibre deterioration and an increase of the inflammation could be associated to a decrease of the fatigue and depressive states. Nevertheless, one must remain critical of the very narrow width of this ROI, which may therefore have a significant size effect. Finally, obsession and compulsion were correlated with an overall reduction of the fibre density in different CC regions. A possible reduction in inflammation was then hypothesised to explain a reduction in the volume of the

intra-axonal compartment. Obsession was associated with changes in the complete CC and more particularly in the genu, while compulsion was associated with changes in the complete CC and more particularly in the splenium.

A number of improvements can be made to this study in order to achieve more precise results. These mostly involve enhancing the way ROIs are obtained, including more rigorous isolation of tracts and more accurate measurement of the fibre density. Future research could also provide insights into the mechanisms involved in the correlations highlighted in this study and could potentially enable the hypotheses put forward to be confirmed. In addition, a more detailed analysis of the changes observed in the UFs of patients and controls could help to understand the origin of the large variations observed in controls and whether there could exist a correlation between UFs and certain behaviours in alcohol-dependent patients.

Nevertheless, this thesis underscores the importance of dMRI studies in understanding the relationships between microstructural changes and behavioural alterations in abstinent alcoholic patients. The findings may have significant implications for the diagnosis, the development of treatment strategies and interventions or for the follow-up of treatment, promoting successful rehabilitation and long-term sobriety. By elucidating the neural involvement of recovery, this research contributes to the broader goal of improving the lives of individuals affected by AUD and reducing the burden of alcohol-related disorders in our society.

Bibliography

[1] *Alcohol Use Disorder (AUD) Statistics | Facts About Alcohol Use*. en-US. URL: https://www.arkbh.com/alcohol/alcohol-use-disorder/statistics/ (visited on 04/26/2023).

[2] *Goal 3 | Department of Economic and Social Affairs, Sustainable Development Goals*. United Nations. URL: https://sdgs.un.org/goals/goal3 (visited on 05/31/2023).

[3] Bruno Kastler and Daniel Vetter. *Comprendre l'IRM: Manuel d'auto-apprentissage*. fr. 7e. Collection d'imagerie médicale diagnostic. Elsevier Masson, 2011. ISBN: 978-2-294-72168-7.

[4] Leonard Bond et al. "Evaluation of Non-Nuclear Techniques for Well Logging: Technology Evaluation". In: (Mar. 2023). DOI: 10.2172/1006309.

[5] *Free interactive course on Magnetic Resonance Imaging | e-MRI*. en. URL: https://www.imaios.com/en/e-mri (visited on 03/07/2023).

[6] Marco Catani and Michel Thiebaut de Schotten. *Atlas of Human Brain Connections*. en. OUP Oxford, June 2012. ISBN: 978-0-19-954116-4.

[7] Lauren J. O'Donnell and Carl-Fredrik Westin. "An Introduction to Diffusion Tensor Image Analysis". en. In: *Neurosurgery Clinics of North America*. Functional Imaging 22.2 (Apr. 2011), pp. 185–196. ISSN: 1042-3680. DOI: 10.1016/j.nec.2010.12.004.

[8] Cognitive Neuroscience Compendium. *MRI-based diffusion tensor imaging (DTI) and tractography*. Apr. 2019. URL: https://www.youtube.com/watch?v=nZU_5TH1CWs (visited on 04/06/2023).

[9] Kathleen M. Curran, Louise Emsell, and Alexander Leemans. "Quantitative DTI Measures". en. In: *Diffusion Tensor Imaging: A Practical Handbook*. Ed. by Wim Van Hecke, Louise Emsell, and Stefan Sunaert. New York, NY: Springer, 2016, pp. 65–87. ISBN: 978-1-4939-3118-7. DOI: 10.1007/978-1-4939-3118-7_5.

[10] Andrew W. Barritt et al. "Emerging Magnetic Resonance Imaging Techniques and Analysis Methods in Amyotrophic Lateral Sclerosis". In: *Frontiers in Neurology* 9 (2018). ISSN: 1664-2295. URL: https://www.frontiersin.org/articles/10.3389/fneur.2018.01065.

[11] Hui Zhang et al. "NODDI: Practical in vivo neurite orientation dispersion and density imaging of the human brain". en. In: *NeuroImage* 61.4 (July 2012), pp. 1000–1016. ISSN: 1053-8119. DOI: 10.1016/j.neuroimage.2012.03.072.

[12] Benoit Scherrer et al. “Characterizing brain tissue by assessment of the distribution of anisotropic microstructural environments in diffusion-compartment imaging (DIAMOND)”. en. In: *Magnetic Resonance in Medicine* 76.3 (2016), pp. 963–977. ISSN: 1522-2594. DOI: 10.1002/mrm.25912.

[13] Gaëtan Rensonnet et al. “Towards microstructure fingerprinting: Estimation of tissue properties from a dictionary of Monte Carlo diffusion MRI simulations”. en. In: *NeuroImage* 184 (Jan. 2019), pp. 964–980. ISSN: 1053-8119. DOI: 10.1016/j.neuroimage.2018.09.076.

[14] Ben Jeurissen et al. “Diffusion MRI fiber tractography of the brain”. en. In: *NMR in Biomedicine* 32.4 (2019), e3785. ISSN: 1099-1492. DOI: 10.1002/nbm.3785.

[15] Quentin Dessain and Mathieu Simon. *Introduction to ElikoPy — ElikoPy documentation*. 2021. URL: https://elikopy.readthedocs.io/en/latest/introduction.html (visited on 04/11/2023).

[16] *DIPY : Docs 1.7.0 - What is DIPY?* URL: https://dipy.org/ (visited on 05/19/2023).

[17] *Understanding Alcohol Use Disorder*. Apr. 2021. URL: https://www.niaaa.nih.gov/publications/brochures-and-fact-sheets/understanding-alcohol-use-disorder (visited on 04/26/2023).

[18] Andre F. Carvalho et al. “Alcohol use disorders”. eng. In: *Lancet (London, England)* 394.10200 (Aug. 2019), pp. 781–792. ISSN: 1474-547X. DOI: 10.1016/S0140-6736(19)31775-1.

[19] K. Witkiewitz, R. Z. Litten, and L. Leggio. “Advances in the science and treatment of alcohol use disorder”. In: *Science Advances* 5.9 (Sept. 2019). Publisher: American Association for the Advancement of Science, eaax4043. DOI: 10.1126/sciadv.aax4043.

[20] Jürgen Rehm et al. “The relation between different dimensions of alcohol consumption and burden of disease: an overview”. en. In: *Addiction* 105.5 (2010), pp. 817–843. ISSN: 1360-0443. DOI: 10.1111/j.1360-0443.2010.02899.x.

[21] *Brain-inter-atlas | atlas interactif de neuroanatomie*. URL: https://sites.uclouvain.be/braininteratlas/fr (visited on 03/27/2023).

[22] Noelia S. De León Reyes, Lorena Bragg-Gonzalo, and Marta Nieto. “Development and plasticity of the corpus callosum”. In: *Development* 147.18 (Sept. 28, 2020). ISSN: 0950-1991. DOI: 10.1242/dev.189738.

[23] Sabine Hofer and Jens Frahm. “Topography of the human corpus callosum revisited—Comprehensive fiber tractography using diffusion tensor magnetic resonance imaging”. en. In: *NeuroImage* 32.3 (Sept. 2006), pp. 989–994. ISSN: 1053-8119. DOI: 10.1016/j.neuroimage.2006.05.044.

[24] Patrick Friedrich et al. “The Relationship Between Axon Density, Myelination, and Fractional Anisotropy in the Human Corpus Callosum”. In: *Cerebral Cortex* 30.4 (Apr. 2020), pp. 2042–2056. ISSN: 1047-3211. DOI: 10.1093/cercor/bhz221.

[25] J. Robin Highley et al. “Asymmetry of the Uncinate Fasciculus: A Post-mortem Study of Normal Subjects and Patients with Schizophrenia”. In: *Cerebral Cortex* 12.11 (Nov. 2002), pp. 1218–1224. ISSN: 1047-3211. DOI: 10.1093/cercor/12.11.1218.

[26] Costanza Papagno. “Naming and the Role of the Uncinate Fasciculus in Language Function”. en. In: *Current Neurology and Neuroscience Reports* 11.6 (Dec. 2011), pp. 553–559. ISSN: 1534-6293. DOI: 10.1007/s11910-011-0219-6.

[27] Ingrid R. Olson et al. “Development of the uncinate fasciculus: Implications for theory and developmental disorders”. en. In: *Developmental Cognitive Neuroscience* 14 (Aug. 2015), pp. 50–61. ISSN: 1878-9293. DOI: 10.1016/j.dcn.2015.06.003.

[28] Adolf Pfefferbaum, Elfar Adalsteinsson, and Edith V. Sullivan. “Supratentorial Profile of White Matter Microstructural Integrity in Recovering Alcoholic Men and Women”. en. In: *Biological Psychiatry* 59.4 (Feb. 2006), pp. 364–372. ISSN: 0006-3223. DOI: 10.1016/j.biopsych.2005.06.025.

[29] Ping-Hong Yeh et al. “Tract-based spatial statistics (TBSS) of diffusion tensor imaging data in alcohol dependence: Abnormalities of the motivational neurocircuitry”. en. In: *Psychiatry Research: Neuroimaging* 173.1 (July 2009), pp. 22–30. ISSN: 0925-4927. DOI: 10.1016/j.pscychresns.2008.07.012.

[30] Katherine M. Keyes et al. “Telescoping and Gender Differences in Alcohol Dependence: New Evidence From Two National Surveys”. In: *American Journal of Psychiatry* 167.8 (Aug. 2010). Publisher: American Psychiatric Publishing, pp. 969–976. ISSN: 0002-953X. DOI: 10.1176/appi.ajp.2009.09081161.

[31] Rodrigo Stênio Moll de Souza et al. “Anterior to Midposterior Corpus Callosum Subregions Are Volumetrically Reduced in Male Alcoholics but Only the Anterior Segment Is Associated to Alcohol Use”. In: *Frontiers in Psychiatry* 10 (2019). ISSN: 1664-0640. URL: https://www.frontiersin.org/articles/10.3389/fpsyt.2019.00196.

[32] Richa Trivedi et al. “White matter damage is associated with memory decline in chronic alcoholics: A quantitative diffusion tensor tractography study”. en. In: *Behavioural Brain Research* 250 (Aug. 2013), pp. 192–198. ISSN: 0166-4328. DOI: 10.1016/j.bbr.2013.05.001.

[33] Adolf Pfefferbaum, Elfar Adalsteinsson, and Edith V. Sullivan. “Dysmorphology and microstructural degradation of the corpus callosum: Interaction of age and alcoholism”. en. In: *Neurobiology of Aging* 27.7 (July 2006), pp. 994–1009. ISSN: 0197-4580. DOI: 10.1016/j.neurobiolaging.2005.05.007.

[34] Mollie A. Monnig et al. “Diffusion tensor imaging of white matter networks in individuals with current and remitted alcohol use disorders and comorbid conditions”. In: *Psychology of Addictive Behaviors* 27 (2013). Place: US Publisher: American Psychological Association, pp. 455–465. ISSN: 1939-1501. DOI: 10.1037/a0027168.

[35] I-Chao Liu et al. “The microstructural integrity of the corpus callosum and associated impulsivity in alcohol dependence: A tractography-based segmentation study using diffusion spectrum imaging”. en. In: *Psychiatry Research: Neuroimaging* 184.2 (Nov. 2010), pp. 128–134. ISSN: 0925-4927. DOI: 10.1016/j.pscychresns.2010.07.002.

[36] Gordon J. Harris et al. “Frontal White Matter and Cingulum Diffusion Tensor Imaging Deficits in Alcoholism”. en. In: *Alcohol: Clinical and Experimental Research* 32.6 (2008), pp. 1001–1013. ISSN: 1530-0277. DOI: 10.1111/j.1530-0277.2008.00661.x.

[37] Tilman Schulte et al. “Neurocircuitry of emotion and cognition in alcoholism: contributions from white matter fiber tractography”. In: *Dialogues in Clinical Neuroscience* 12.4 (Dec. 2010), pp. 554–560. ISSN: null. DOI: 10.31887/DCNS.2010.12.4/tschulte.

[38] Marlene Oscar-Berman and Ksenija Marinković. “Alcohol: Effects on Neurobehavioral Functions and the Brain”. en. In: *Neuropsychology Review* 17.3 (Sept. 2007), pp. 239–257. ISSN: 1573-6660. DOI: 10.1007/s11065-007-9038-6.

[39] Stefan Gazdzinski et al. “Cerebral white matter recovery in abstinent alcoholics—a multimodality magnetic resonance study”. en. In: *Brain* 133.4 (Apr. 2010), pp. 1043–1053. ISSN: 1460-2156, 0006-8950. DOI: 10.1093/brain/awp343.

[40] Nabi Zorlu et al. “Abnormal white matter integrity in long-term abstinent alcohol dependent patients”. en. In: *Psychiatry Research: Neuroimaging* 224.1 (Oct. 2014), pp. 42–48. ISSN: 0925-4927. DOI: 10.1016/j.pscychresns.2014.07.006.

[41] Andriy V. Samokhvalov et al. “Disability Associated With Alcohol Abuse and Dependence”. en. In: *Alcohol: Clinical and Experimental Research* 34.11 (2010), pp. 1871–1878. ISSN: 1530-0277. DOI: 10.1111/j.1530-0277.2010.01275.x.

[42] A. McPherson and C. R. Martin. “A narrative review of the Beck Depression Inventory (BDI) and implications for its use in an alcohol-dependent population”. In: *Journal of Psychatric and Mental Health Nursing* 17 (2010). DOI: 10.1111/j.1365-2850.2009.01469.x.

[43] Henry R. Kranzler et al. “Validity of the Obsessive Compulsive Drinking Scale (OCDS): Does Craving Predict Drinking Behavior?” In: *Alcohol: Clinical and Experimental Research* 23.1 (1999). DOI: 10.1111/j.1530-0277.1999.tb04030.x.

[44] Petros Skapinakis. “Spielberger State-Trait Anxiety Inventory”. en. In: *Encyclopedia of Quality of Life and Well-Being Research*. Ed. by Alex C. Michalos. Dordrecht: Springer Netherlands, 2014, pp. 6261–6264. ISBN: 978-94-007-0753-5. DOI: 10.1007/978-94-007-0753-5_2825.

[45] E. M. A. Smets et al. “The multidimensional Fatigue Inventory (MFI) psychometric qualities of an instrument to assess fatigue”. en. In: *Journal of Psychosomatic Research* 39.3 (Apr. 1995), pp. 315–325. ISSN: 0022-3999. DOI: 10.1016/0022-3999(94)00125-O.

[46] Joseph M. Boden and David M. Fergusson. “Alcohol and depression”. en. In: *Addiction* 106.5 (2011), pp. 906–914. ISSN: 1360-0443. DOI: 10.1111/j.1360-0443.2010.03351.x.

[47] Vivian N. Onaemo, Timothy O. Fawehinmi, and Carl D’Arcy. “Alcohol Use Disorder and the Persistence/Recurrence of Major Depression: Le trouble de l’usage de l’alcool et la persistance/récurrence de la dépression majeure”. en. In: *The Canadian Journal of Psychiatry* 65.9 (Sept. 2020). Publisher: SAGE Publications Inc, pp. 652–663. ISSN: 0706-7437. DOI: 10.1177/0706743720923065.

[48] Jack G. Modell et al. “Obsessive and Compulsive Characteristics of Craving for Alcohol in Alcohol Abuse and Dependence”. en. In: *Alcohol: Clinical and Experimental Research* 16.2 (1992), pp. 272–274. ISSN: 1530-0277. DOI: 10.1111/j.1530-0277.1992.tb01375.x.

[49] Andreas Heinz et al. “Reward Craving and Withdrawal Relief Craving: Assesment of Different Motivational Pathways to Alcohol Intake”. In: *Alcohol and Alcoholism* 38.1 (Jan. 2003), pp. 35–39. ISSN: 0735-0414. DOI: 10.1093/alcalc/agg005.

[50] Miriam Bottlender and Michael Sokya. “Impact of Craving on Alcohol Relapse during, and 12 Months Following, Outpatient Treatment”. In: *Alcohol and Alcoholism* 39.4 (July 2004), pp. 357–361. ISSN: 0735-0414. DOI: 10.1093/alcalc/agh073.

[51] Marc A. Schuckit and Victor Hesselbrock. “Alcohol Dependence and Anxiety Disorders”. In: *FOCUS* 2.3 (July 2004). Publisher: American Psychiatric Publishing, pp. 440–453. ISSN: 1541-4094. DOI: 10.1176/foc.2.3.440.

[52] Marc A. Schuckit and Maristela G. Monteiro. “Alcoholism, Anxiety and Depression”. en. In: *British Journal of Addiction* 83.12 (1988), pp. 1373–1380. ISSN: 1360-0443. DOI: 10.1111/j.1360-0443.1988.tb02551.x.

[53] Bridget F. Grant et al. “Prevalence and Co-occurrence of Substance Use Disorders and IndependentMood and Anxiety Disorders: Results From the National Epidemiologic Survey on Alcohol and RelatedConditions”. In: *Archives of General Psychiatry* 61.8 (Aug. 2004), pp. 807–816. ISSN: 0003-990X. DOI: 10.1001/archpsyc.61.8.807.

[54] Dirk Wedekind et al. “Attachment style, anxiety coping, and personality-styles in withdrawn alcohol addicted inpatients”. In: *Substance Abuse Treatment, Prevention, and Policy* 8.1 (Jan. 2013), p. 1. ISSN: 1747-597X. DOI: 10.1186/1747-597X-8-1.

[55] Michael V. Vitiello. “Sleep, alcohol and alcohol abuse”. en. In: *Addiction Biology* 2.2 (1997), pp. 151–158. ISSN: 1369-1600. DOI: 10.1080/13556219772697.

[56] Mieke H. J. Schulte et al. “Recovery of neurocognitive functions following sustained abstinence after substance dependence and implications for treatment”. en. In: *Clinical Psychology Review* 34.7 (Nov. 2014), pp. 531–550. ISSN: 0272-7358. DOI: 10.1016/j.cpr.2014.08.002.

[57] Anne Beck et al. “Effect of Brain Structure, Brain Function, and Brain Connectivity on Relapse in Alcohol-Dependent Patients”. In: *Archives of General Psychiatry* 69.8 (Aug. 2012), pp. 842–852. ISSN: 0003-990X. DOI: 10.1001/archgenpsychiatry.2011.2026.

[58] Elke R. Gizewski et al. “The impact of alcohol dependence on social brain function”. en. In: *Addiction Biology* 18.1 (2013), pp. 109–120. ISSN: 1369-1600. DOI: 10.1111/j.1369-1600.2012.00437.x.

[59] Jennifer M. Glass et al. “Effects of alcoholism severity and smoking on executive neurocognitive function”. en. In: *Addiction* 104.1 (2009), pp. 38–48. ISSN: 1360-0443. DOI: 10.1111/j.1360-0443.2008.02415.x.

[60] Manon Dausort and Faustine Falyse. “Identifying the microstructural changes for alcoholic patients during shortterm abstinence via diffusion Magnetic Resonance Imaging”. In: *Ecole Polytechnique de Louvain, Université Catholique de Louvain* (2022). Prom. : Macq, Benoît ; Dricot, Laurence. http://hdl.handle.net/2078.1/thesis:35541. URL: http://hdl.handle.net/2078.1/%20thesis:35541.

[61] *Alcohol units*. en-GB. URL: https://alcoholchange.org.uk/alcohol-facts/interactive-tools/check-your-drinking/alcohol-units (visited on 05/11/2023).

[62] *About DICOM- Overview*. en. URL: https://www.dicomstandard.org/about (visited on 05/14/2023).

[63] *NITRC: MRIcron: Tool/Resource Info*. URL: https://www.nitrc.org/projects/mricron/ (visited on 05/11/2023).

[64] J-Donald Tournier and Ben Jeurissen. *dwi2fod — MRtrix 3.0 documentation*. URL: https://mrtrix.readthedocs.io/en/latest/reference/commands/dwi2fod.html (visited on 05/12/2023).

[65] J-Donald Tournier and Robert E. Smith. *tckgen — MRtrix 3.0 documentation*. URL: https://mrtrix.readthedocs.io/en/latest/reference/commands/tckgen.html (visited on 05/12/2023).

[66] Andy Jahn. *FreeSurfer Short Course — Andy's Brain Book 1.0 documentation*. 2019. URL: https://andysbrainbook.readthedocs.io/en/latest/FreeSurfer/FreeSurfer_Introduction.html (visited on 05/09/2023).

[67] Rahul S. Desikan et al. "An automated labeling system for subdividing the human cerebral cortex on MRI scans into gyral based regions of interest". en. In: *NeuroImage* 31.3 (July 2006), pp. 968–980. ISSN: 1053-8119. DOI: 10.1016/j.neuroimage.2006.01.021.

[68] Demian Wassermann et al. "The white matter query language: a novel approach for describing human white matter anatomy". en. In: *Brain Structure and Function* 221.9 (Dec. 2016), pp. 4705–4721. ISSN: 1863-2661. DOI: 10.1007/s00429-015-1179-4.

[69] Nicolas Delinte. *API — TIME 2022 documentation*. 2022. URL: https://unravel.readthedocs.io/en/latest/api.html#module-unravel.utils (visited on 05/09/2023).

[70] SciPy community. *Statistical functions (scipy.stats) — SciPy v1.10.1 Manual*. URL: https://docs.scipy.org/doc/scipy/reference/stats.html (visited on 05/13/2023).

[71] Xin Liu et al. "Reproducibility of diffusion tensor imaging in normal subjects: an evaluation of different gradient sampling schemes and registration algorithm". en. In: *Neuroradiology* 56.6 (June 2014), pp. 497–510. ISSN: 1432-1920. DOI: 10.1007/s00234-014-1342-2.

[72] Pashtun Shahim et al. "Test-retest reliability of high spatial resolution diffusion tensor and diffusion kurtosis imaging". en. In: *Scientific Reports* 7.1 (Sept. 2017), p. 11141. ISSN: 2045-2322. DOI: 10.1038/s41598-017-11747-3.

[73] Francesco Grussu et al. "Neurite orientation dispersion and density imaging of the healthy cervical spinal cord in vivo". en. In: *NeuroImage* 111 (May 2015), pp. 590–601. ISSN: 1053-8119. DOI: 10.1016/j.neuroimage.2015.01.045.

[74] Christina Andica et al. "Scan–rescan and inter-vendor reproducibility of neurite orientation dispersion and density imaging metrics". In: *Neuroradiology* 62.4 (2020), pp. 483–494. ISSN: 0028-3940. DOI: 10.1007/s00234-019-02350-6.

[75] *MisterI*. URL: http://www.benoitscherrer.com/MisterI/ (visited on 06/04/2023).

[76] *TrackVis*. URL: http://trackvis.org/ (visited on 06/04/2023).

[77] *Center for High Performance Computing and Mass Storage*. en. URL: https://uclouvain.be/en/research/cism (visited on 06/04/2023).

[78] *CECI - Consortium des Equipements de Calcul Intensif*. URL: https://www.ceci-hpc.be/ (visited on 06/04/2023).

[79] *Welcome to Python.org*. en. May 2023. URL: https://www.python.org/ (visited on 06/04/2023).

[80] *Spyder IDE - The Scientific Python Development Environment*. URL: https://www.spyder-ide.org/ (visited on 06/04/2023).

[81] *DeepL Traduction*. fr. URL: https://www.DeepL.com/translator (visited on 06/04/2023).

[82] *ChatGPT*. URL: https://chat.openai.com (visited on 06/04/2023).

[83] *Overleaf documentation*. en. URL: https://www.overleaf.com/learn (visited on 06/04/2023).

[84] *LaTeX - A document preparation system*. URL: https://www.latex-project.org/ (visited on 06/04/2023).

[85] Robert E. Smith et al. "SIFT2: Enabling dense quantitative assessment of brain white matter connectivity using streamlines tractography". en. In: *NeuroImage* 119 (Oct. 2015). Publisher: Academic Press, pp. 338–351. ISSN: 1053-8119. DOI: 10.1016/j.neuroimage.2015.06.092.

[86] Thijs Dhollander et al. "Fixel-based Analysis of Diffusion MRI: Methods, Applications, Challenges and Opportunities". en. In: *NeuroImage* 241 (Nov. 2021), p. 118417. ISSN: 1053-8119. DOI: 10.1016/j.neuroimage.2021.118417.

Appendix A

Additional details about the gradients used in the signal acquisition process in MRI

This appendix provides additional information on the different gradients used in a spin echo (SE) sequence to obtain spatial localisation information. Figure A.1 shows the complete chronology and components of a SE sequence. Each gradient will be detailed separately.

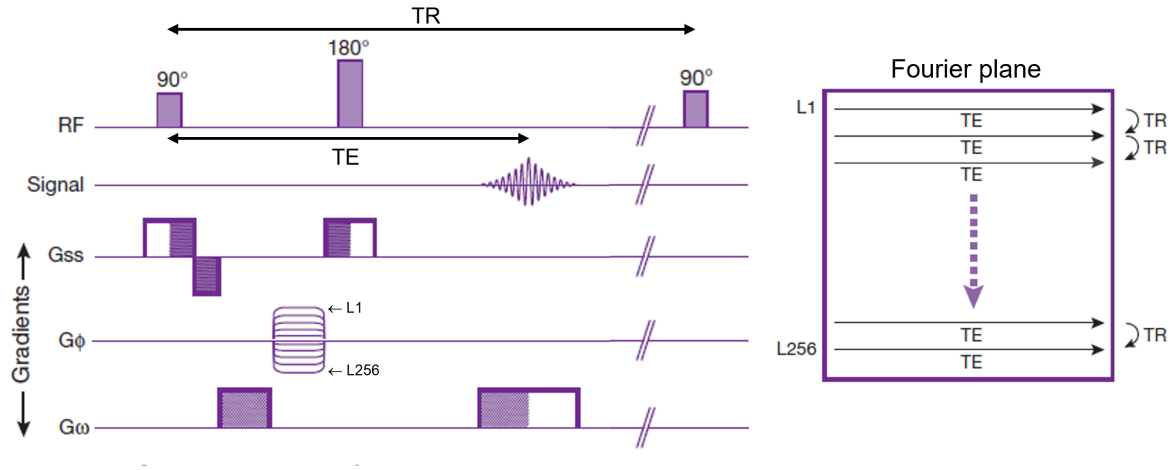


Figure A.1: Complete acquisition chronology with all gradients of the SE sequence. Adapted from [3]

Slice plane gradient Gss

A first magnetic field gradient is created within the total volume to select a slice plane oriented perpendicular to the direction of the gradient. This gradient is added to the $\overrightarrow{B_0}$ field to vary the angular frequencies at which the spins of the protons precess. When an RF wave is applied, only the protons that meet the resonance condition (i.e. only protons with a specific angular frequency) will be excited. Thus, only one slice will be selected since all other protons not belonging to this slice will continue to orientate randomly

(see Figure A.2). This gradient should be applied at the same time as both the 90° and 180° RF pulse. The frequency of the RF pulse is therefore the parameter to be modified to choose the desired slice in the whole volume. The thickness of the slice can also be adjusted according to the frequency band ($\Delta\omega$) and the amplitude of the gradient. This is called spatial coding of the image [3].

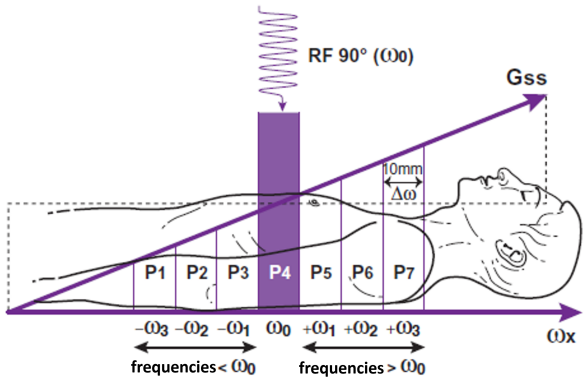


Figure A.2: Spatial coding: the application of a *Gss* gradient allows the angular frequency ω to diverge in each slice. Only protons with the same frequency as the RF pulse will be excited and contribute to the final measured signal [3].

As you can see on the Figure A.1, the *Gss* gradient is composed of several positive and negative lobes. Indeed, the gradients cause phase shifts between the different slices of the volume that persist even after the gradient is stopped. The introduction of a bipolar gradient of proportion +2/-1 compensates for these unwanted phase shifts. At the moment of the 180° RF pulse, the same phenomenon is observed. However, the phases are reversed by the 180° pulse. The last part of the gradient must therefore not be negative, but must remain positive after the pulse to compensate for the phase shifts [3].

After the selection of a specific slice, tall the information necessary to obtain the K-space corresponding to this slice must be obtained. This process involves traversing through all frequencies and phases within the K-space.

Frequency encoding gradient G_ω

The G_ω gradient is applied perpendicular to the slice plane gradient, *Gss*, and is also added to the $\overrightarrow{B_0}$ field. During the application of this gradient G_ω the signal will be read out. As the protons will acquire different precession frequencies, the signal will therefore be composed of several frequencies encoded on one line of the K-space.

The signal is not read out instantaneously, but over a certain period of time. To compensate for this slight time lag, a bipolar gradient of proportion -1/+2 must be applied. For practical reasons, the first negative lobe should be applied before the 180° pulse. Since this pulse will reverse the phases, this negative gradient must become positive [3].

Phase encoding gradient G_ϕ

As the frequency encoding gradient applied to acquire all the information to fill a line in the Fourier plane, this gradient is used to change the line acquired. This gradient is applied perpendicular to the other two gradients, in the last possible direction. In the same way as any gradient, this will modify the precession frequency of the protons and therefore cause a phase shift. No pulse is applied at the same time as the gradient, the differences in precession frequency will thus disappear when the gradient stops. However, the phase shifts will remain. At each acquisition, the characteristics of the other gradients and pulses will remain unchanged. A different phase encoding gradient in amplitude will be applied at each repetition to cause different phase shifts and be able to successively fill all lines of the Fourier plane. The different amplitudes of this gradient (from positive to negative) corresponding to different lines of the Fourier plan are schematically illustrated on Figure A.1 [3].

Appendix B

Example of a `.json` file containing all the acquisition parameters


```
{ "Modality": "MR",
   "MagneticFieldStrength": 3,
   "ImagingFrequency": 127.77,
   "Manufacturer": "GE",
   "ManufacturersModelName": "SIGNA_Premier",
   "InstitutionName": "UCL",
   "DeviceSerialNumber": "000000210036MR03",
   "StationName": "GEHC",
   "BodyPartExamined": "BRAIN",
   "PatientPosition": "HFS",
   "SoftwareVersions": "28_LX_MR_Software_release:RX28.0_R04_2020.b",
   "MRAcquisitionType": "2D",
   "SeriesDescription": "Opt_DTI_4B_64_32_HB3",
   "ProtocolName": "Opt_DTI_4B_64_32_HB3",
   "ScanningSequence": "EP_SE",
   "SequenceVariant": "NONE",
   "ScanOptions":     "CL_GEMS_SAT_GEMS_EDR_GEMS_EPI_GEMS_
      HYPERBAND_GEMS_ACC_GEMS_PFF_FS",
   "ImageType": ["ORIGINAL", "PRIMARY", "OTHER"],
   "SeriesNumber": 4,
   "AcquisitionTime": "13:47:11.000000",
   "AcquisitionNumber": 1,
   "SliceThickness": 2,
   "SpacingBetweenSlices": 2,
   "SAR": 0.12376,
   "EchoTime": 0.0808,
   "RepetitionTime": 4.837,
   "FlipAngle": 90,
   "PhaseEncodingPolarityGE": "Unflipped",
   "CoilString": "48HAP",
   "PercentPhaseFOV": 100,
```

```
    "AcquisitionMatrixPE": 110,
    "ReconMatrixPE": 110,
    "EffectiveEchoSpacing": 0.000752,
    "TotalReadoutTime": 0.081968,
    "PixelBandwidth": 4545.45,
    "PhaseEncodingDirection": "j-",
    "ImageOrientationPatientDICOM": [ 0.999854, 0.0162767, 0.00525461,
       -0.0140324, 0.956288, -0.292091 ],
    "InPlanePhaseEncodingDirectionDICOM": "COL",
    "ConversionSoftware": "dcm2niix",
    "ConversionSoftwareVersion": "v1.0.20190902"
}
```

Appendix C

WMQL file for the CC and the UF

```
#Import the freesurfer label definitions from the Desikan atlas (Desikan et al 2006)
import FreeSurfer.qry

hemisphere.left |= '*.left'
hemisphere.right |= '*.right'
cerebellum.right |= 'Cerebellum_*.right'
cerebellum.left |= 'Cerebellum_*.left'

medulla |= 175
pons |= 174
midbrain |= 173
cerebellarpedoncle |= 178
brainstem_other |= Brain_Stem
brainstem |= (medulla
        or pons
        or midbrain
        or cerebellarpedoncle
        or brainstem_other)

CC_Splenium |= 5251
CC_Isthmus |= 5252
CC_Post_Midbody |= 5253
CC_Ant_Midbody |= 5254
CC_Genu |= 5255

midCC |= (CC_Splenium
        or CC_Isthmus
        or CC_Post_Midbody
        or CC_Ant_Midbody
        or CC_Genu)

middlefrontal.side |= (rostralmiddlefrontal.side
        or caudalmiddlefrontal.side)
```

```
inferiorfrontal.side |= (parsopercularis.side
        or parstriangularis.side
        or parsorbitalis.side)

orbitofrontal.side |= (lateralorbitofrontal.side
        or medialorbitofrontal.side)

cingulate.side |= (caudalanteriorcingulate.side
        or posteriorcingulate.side
        or rostralanteriorcingulate.side
        or isthmuscingulate.side)

frontal.side |= (superiorfrontal.side
        or middlefrontal.side
        or inferiorfrontal.side
        or orbitofrontal.side
        or frontalpole.side
        or precentral.side
        or paracentral.side)

temporal.side |= (entorhinal.side
        or temporalpole.side
        or fusiform.side
        or superiortemporal.side
        or middletemporal.side
        or inferiortemporal.side
        or transversetemporal.side
        or bankssts.side)

parietal.side |= (postcentral.side
        or precuneus.side
        or supramarginal.side
        or superiorparietal.side
        or inferiorparietal.side)

occipital.side |= (lingual.side
        or pericalcarine.side
        or cuneus.side
        or lateraloccipital.side
        or lingual.side)

modbrain=midbrain
```

```
#########################
###       Corpus Callosum       ###
#########################

CC_tract_Genu = (endpoints_in(frontal.left or cingulate.left)
        and endpoints_in(frontal.right or cingulate.right)
        and CC_Genu
        not in (parietal.left or parietal.right
                or temporal.left or temporal.right
                or occipital.left or occipital.right)
        not in brainstem
        not in (Thalamus_Proper.left or Thalamus_Proper.right)
        not in (Putamen.left or Putamen.right)
        not in (pallidum.left or pallidum.right)
        not in (caudate.left or caudate.right)
        not in (choroid_plexus.left or choroid_plexus.right)
        not in (VentralDC.left or VentralDC.right)
        not in CC_Ant_Midbody
        not in posterior_of(CC_Ant_Midbody))

   CC_tract_Ant_Midbody = (endpoints_in(frontal.left or parietal.left or cingulate.left)
        and endpoints_in(frontal.right or parietal.right or cingulate.right)
        and CC_Ant_Midbody
        not in (temporal.left or temporal.right
                or occipital.left or occipital.right)
        not in brainstem
        not in (Thalamus_Proper.left or Thalamus_Proper.right)
        not in (Putamen.left or Putamen.right)
        not in (pallidum.left or pallidum.right)
        not in (caudate.left or caudate.right)
        not in (choroid_plexus.left or choroid_plexus.right)
        not in (VentralDC.left or VentralDC.right)
        not in CC_Post_Midbody
        not in CC_Genu
        not in posterior_of(CC_Post_Midbody)
        not in anterior_of(CC_Genu))

CC_tract_Post_Midbody = (endpoints_in(frontal.left or parietal.left or cingulate.left)
        and endpoints_in(frontal.right or parietal.right or cingulate.right)
        and CC_Post_Midbody
        not in (temporal.left or temporal.right
                or occipital.left or occipital.right)
        not in brainstem
        not in (Thalamus_Proper.left or Thalamus_Proper.right)
        not in (Putamen.left or Putamen.right)
        not in (pallidum.left or pallidum.right)
```

```
        not in (caudate.left or caudate.right)
        not in (choroid_plexus.left or choroid_plexus.right)
        not in (VentralDC.left or VentralDC.right)
        not in CC_Isthmus
        not in CC_Ant_Midbody
        not in posterior_of(CC_Isthmus)
        not in anterior_of(CC_Ant_Midbody))

CC_tract_Isthmus = (endpoints_in(frontal.left or parietal.left or occipital.left
                or temporal.left or cingulate.left)
        and endpoints_in(frontal.right or parietal.right or occipital.right
                or temporal.right or cingulate.right)
        and CC_Isthmus
        not in brainstem
        not in (Thalamus_Proper.left or Thalamus_Proper.right)
        not in (Putamen.left or Putamen.right)
        not in (pallidum.left or pallidum.right)
        not in (caudate.left or caudate.right)
        not in (choroid_plexus.left or choroid_plexus.right)
        not in CC_Post_Midbody
        not in CC_Splenium
        not in anterior_of(CC_Post_Midbody)
        not in posterior_of(CC_Splenium))

CC_tract_Splenium = (endpoints_in(parietal.left or occipital.left or temporal.left
                or cingulate.left)
        and endpoints_in(parietal.right or occipital.right or temporal.right
                or cingulate.right)
        and CC_Splenium
        not in brainstem
        not in (Thalamus_Proper.left or Thalamus_Proper.right)
        not in (Putamen.left or Putamen.right)
        not in (pallidum.left or pallidum.right)
        not in (caudate.left or caudate.right)
        not in (choroid_plexus.left or choroid_plexus.right)
        not in (VentralDC.left or VentralDC.right)
        not in CC_Isthmus
        not in anterior_of(CC_Isthmus))

CC_tract = CC_tract_Genu or CC_tract_Ant_Midbody or CC_tract_Post_Midbody
or CC_tract_Isthmus or CC_tract_Splenium
```

```
#########################
###       Uncinate fasciculus       ###
#########################

UF.side = (endpoints_in((middlefrontal.side
                or inferiorfrontal.side
                or lateralorbitofrontal.side
                or medialorbitofrontal.side)
                and anterior_of(caudalmiddlefrontal.side))
        and endpoints_in(fusiform.side
                or temporalpole.side
                or frontalpole.side)
        not in superior_of(caudalanteriorcingulate.side)
        not in superiorfrontal.side
        not in rostralmiddlefrontal.side
        not in posterior_of(Amygdala.side)
        not in cingulate.side
        not in midCC
        not in brainstem
        not in Thalamus_Proper.side
        not in Putamen.side
        not in pallidum.side
        not in hemisphere.opposite
        not in VentralDC.side
        not in Optic_Chiasm
        not in posterior_of(CC_Ant_Midbody))


UF = UF.left or UF.right
```

Appendix D

Outliers justifications

These tables contain all the data considered as outliers. When the information has been found, the origin or the reasons leading to these exclusions are mentioned.
In red : all data (microstructural or behavioural) at that time are discarded from the analyses.
In green : only the data for the mentioned metric or region are excluded from the analyses.

Outliers in the alcoholic patients :

	T1		T2	
Patient	Behavioural data	Microstructural data	Behavioural data	Microstructural data
sub01		SNR < 10		SNR < 10
sub02			BDI and STAI scores outlier	
sub03		Preprocessing failure		
sub06		No T1-contrasted MRI		
sub07		Preprocessing failure		
sub08		SNR < 10		
sub10		SNR < 10		No data (patient's refusal to undergo MRI)
sub11		CC anterior midbody not properly isolated (CC very thin)		SNR < 10
sub14				No fibres in the UF right tract
sub15			Tests not completed (emotional difficulties)	

	T1		T2	
Patient	Behavioural data	Microstructural data	Behavioural data	Microstructural data
sub16			Excluded from the process, started drinking again	
sub17		SNR < 10	BDI and STAI scores outlier	SNR < 10
sub19		No data		
sub21		SNR < 10		
sub22		CC post mid-body and isthmus not properly isolated (CC very thin) + UF left contains only 1 fibre		
sub23			BDI score outlier	Preprocessing failure
sub24		UF not properly isolated : only in the hook-like part (ODF very low in the frontal area)		UF not properly isolated : only in the hook-like part (ODF very low in the frontal area)
sub25		Preprocessing failure		
sub27		CC not properly isolated (too low max angle and low ODF values in the CC) + UF not properly isolated (very low ODF values in the UF pathway)		
sub29				SNR < 10
sub31		CC not properly isolated (too low max angle)		
sub34		SNR < 10		SNR < 10

	T1		T2	
Control	Behavioural data	Microstructural data	Behavioural data	Microstructural data
sub36		SNR < 10		SNR < 10
sub38				Preprocessing failure
sub40		SNR < 10		
sub42				SNR < 10
sub43		No fibres in the UF left (possibly because of low ODF values in the middle of the UF pathway)		No fibres in the UF left
sub44				Preprocessing failure
sub47		CC and UF not properly isolated (low ODF values, short fibres)		Preprocessing failure
sub48		SNR <10	BDI and OCDS (obsession) scores outlier	CC not properly isolated (too low max angle and very thin and irregular thickness)
sub49		Preprocessing failure		Preprocessing failure
sub50		CC isthmus not properly isolated (shrinking of the thickness at this point)		
sub52				CC and UF not properly isolated

Outliers in the controls subjects :

	T1		T2	
Control	Behavioural data	Microstructural data	Behavioural data	Microstructural data
sub54	STAI outlier			
sub56				No data
sub57	No data			
sub61		CC not properly isolated (possibly too low max angle and low ODF values in the CC)		CC not properly isolated
sub62	OCDS outlier			
sub67		MF model computation failure		MF model computation failure
sub69	OCDS outlier	Few fibres in the UF left (possibly because of low ODF values this hemisphere)		
sub70	OCDS (compulsion) outlier			
sub71		CC not properly isolated (too low max angle and low ODF values in the CC)		CC not properly isolated (too low max angle and low ODF values in the CC)

Appendix E

Additional tables for the patients-controls comparison analysis

Patients-Controls comparison

Behavioural metrics	T1	T2
BDI	7,07E-13	1,48E-04
Total_OCDS	1,59E-20	1,41E-11
OCDS (Obsessions)	1,15E-19	2,79E-11
OCDS (Compulsions)	2,12E-19	3,28E-10
STAI	9,13E-11	9,85E-06
MFI	4,35E-11	1,41E-04

<0,05
Significantly different in patients and controls

Figure E.1: Tables of p-values for the comparison of behavioural metrics between alcoholic patients (at T1 and T2) and control subjects at T1. Student's t-test highlights different means. p-values less than 0,05 indicate a significantly unequal mean between patients and controls.

Patients-Controls comparison at T1

<0,05 Significantly different in patients and controls

Region	DTI				DIAMOND						MF			NODDI			
	FA	MD	AD	RD	wFA	wMD	wAD	wRD	frac csf	frac ftot	fvf tot	frac csf	frac ftot	wfvf	fiso	fintra	fextra	odi
CC	1,4E-06	0,981	0,310	0,046	5,2E-07	0,907	0,055	0,001	0,430	0,431	0,005	0,126	0,126	0,022	0,412	0,387	0,955	0,040
CC Genu	0,004	0,681	0,628	0,084	4,3E-04	0,810	0,021	0,010	0,041	0,041	0,243	0,536	0,534	0,027	0,082	0,714	0,468	0,172
CC Ant mid-b.	0,005	0,997	0,261	0,135	0,001	0,301	0,204	0,002	0,259	0,259	0,227	0,729	0,729	0,039	0,338	0,917	0,257	0,056
CC Post mid-b.	0,003	0,892	0,394	0,294	0,007	0,268	0,972	0,026	0,226	0,226	0,084	0,190	0,190	0,406	0,187	0,212	0,914	0,167
CC Isthmus	5,6E-03	0,548	0,681	0,038	0,012	0,247	0,686	8,6E-03	2,8E-03	2,8E-03	5,4E-05	0,014	0,014	7,7E-03	6,0E-03	8,9E-03	0,995	0,213
CC Splenium	1,5E-04	0,910	0,439	0,079	3,9E-07	0,842	0,111	0,030	0,016	0,016	0,006	0,006	0,006	0,161	0,020	0,100	0,571	0,098
UF left	0,002	0,859	0,334	0,404	0,008	0,564	0,098	0,027	0,003	0,003	0,607	0,183	0,183	0,451	0,223	0,897	0,944	0,184
UF right	0,002	0,970	0,348	0,250	0,039	0,277	0,212	0,075	0,166	0,164	0,547	0,803	0,788	0,462	0,440	0,444	0,899	0,156
UF	0,001	0,967	0,346	0,301	0,025	0,445	0,114	0,061	0,036	0,036	0,564	0,416	0,409	0,432	0,272	0,583	0,859	0,184

(a) At T1.

Patients-Controls comparison at T2

<0,05 Significantly different in patients and controls

Region	DTI				DIAMOND						MF			NODDI			
	FA	MD	AD	RD	wFA	wMD	wAD	wRD	frac csf	frac ftot	fvf tot	frac csf	frac ftot	wfvf	fiso	fintra	fextra	odi
CC	0,452	0,733	0,544	0,921	0,013	0,257	0,031	0,791	0,481	0,481	0,683	0,900	0,900	0,723	0,762	0,425	0,560	0,453
CC Genu	0,227	0,496	0,348	0,829	0,013	0,187	0,010	0,563	4,1E-04	4,1E-04	0,705	0,018	0,018	0,721	0,026	0,079	0,748	0,230
CC Ant mid-b.	0,530	0,921	0,734	0,874	0,040	0,518	0,230	0,772	0,387	0,387	0,899	0,847	0,847	0,921	0,472	0,571	0,829	0,611
CC Post mid-b.	0,723	0,844	0,828	0,897	0,344	0,367	0,362	0,718	0,532	0,532	0,560	0,804	0,804	0,656	0,608	0,797	0,758	0,738
CC Isthmus	0,020	0,690	0,354	0,088	0,109	0,458	0,784	0,092	0,121	0,121	0,015	0,138	0,138	0,042	0,114	0,093	0,989	0,038
CC Splenium	0,135	0,888	0,664	0,266	0,001	0,177	0,024	0,805	0,097	0,097	0,072	0,046	0,046	0,443	0,126	0,608	0,268	0,401
UF left	0,430	0,132	0,070	0,474	0,208	0,197	2,0E-04	0,857	7,2E-06	7,3E-06	0,914	3,6E-04	3,6E-04	0,472	0,007	0,057	0,441	0,534
UF right	0,313	0,563	0,279	0,964	0,668	0,212	0,007	0,724	0,094	0,094	0,918	0,119	0,119	0,647	0,081	0,964	0,557	0,794
UF	0,173	0,449	0,151	0,988	0,345	0,256	0,001	0,982	0,012	0,012	0,964	0,033	0,033	0,610	0,048	0,759	0,583	0,431

(b) At T2.

Figure E.2: Tables of p-values for the comparison of microstructural metrics and regions between alcoholic patients and control subjects (at T1 **(a)** and T2 **(b)**). Student's t-test highlights different means. p-values lower than 0,05 indicate a significantly unequal mean between patients and controls and are shown in red.

Difference of the means between patients and controls at T1

Mean of patients **higher** than mean of controls
Mean of patients **lower** than mean of controls

Region	DTI				DIAMOND					MF			NODDI			
	FA	MD	AD	RD	wFA	wMD	wAD	wRD	frac csf	frac ftot	fvf tot	frac csf	frac ftot	wfvf	fiso	fintra	fextra	odi
CC	0,019	-2,3E-07	2,0E-05	-1,1E-05	0,025	-9,7E-07	3,5E-05	-1,9E-05	-0,007	0,007	0,013	-0,009	0,009	0,010	-0,009	0,010	0,001	-0,009
CC Genu	0,022	-4,7E-06	1,1E-05	-1,3E-05	0,029	-2,6E-06	4,4E-05	-2,6E-05	0,026	-0,026	0,007	0,005	-0,005	0,010	0,029	-0,006	-0,013	-0,009
CC Ant mid-b.	0,021	3,0E-08	2,1E-05	-1,0E-05	0,026	-9,0E-06	2,2E-05	-2,4E-05	0,020	-0,020	0,008	0,004	-0,004	0,012	0,018	-0,002	-0,017	-0,009
CC Post mid-b.	0,015	1,3E-06	1,6E-05	-6,2E-06	0,017	-8,7E-06	5,7E-07	-1,3E-05	-0,011	0,011	0,010	-0,011	0,011	0,004	-0,013	0,015	-0,001	-0,005
CC Isthmus	0,019	-6,4E-06	9,0E-06	-1,4E-05	0,021	-8,9E-06	7,6E-06	-1,7E-05	-0,034	0,034	0,025	-0,023	0,023	0,016	-0,034	0,034	0,000	-0,007
CC Splenium	0,016	-1,2E-06	1,7E-05	-1,0E-05	0,023	1,8E-06	3,2E-05	-1,3E-05	-0,026	0,026	0,015	-0,018	0,018	0,008	-0,027	0,020	0,007	-0,006
UF left	0,031	2,9E-06	2,7E-05	-9,3E-06	0,030	-8,9E-06	4,2E-05	-3,5E-05	0,026	-0,026	0,006	0,008	-0,008	0,009	0,017	0,003	-0,002	-0,017
UF right	0,032	-5,6E-07	2,4E-05	-1,3E-05	0,023	-1,2E-05	1,6E-05	-2,6E-05	0,013	-0,013	0,007	0,001	-0,001	0,008	0,010	0,014	-0,003	-0,013
UF	0,030	6,2E-07	2,4E-05	-1,1E-05	0,023	-9,1E-06	2,5E-05	-2,6E-05	0,018	-0,018	0,006	0,004	-0,004	0,008	0,015	0,010	-0,005	-0,013

(a) Difference at T1.

Difference of the means between patients and controls at T2

Mean of patients **higher** than mean of controls
Mean of patients **lower** than mean of controls

Region	DTI				DIAMOND					MF			NODDI			
	FA	MD	AD	RD	wFA	wMD	wAD	wRD	frac csf	frac ftot	fvf tot	frac csf	frac ftot	wfvf	fiso	fintra	fextra	odi
CC	0,004	3,2E-06	1,1E-05	-6,3E-07	0,015	8,1E-06	2,8E-05	-2,1E-06	0,006	-0,006	0,002	-0,001	0,001	0,002	0,003	-0,009	0,008	-0,003
CC Genu	0,010	1,0E-05	2,6E-05	2,1E-06	0,020	1,7E-05	6,5E-05	-6,9E-06	0,036	-0,036	-0,003	0,014	-0,014	0,003	0,031	-0,030	0,008	-0,008
CC Ant mid-b.	0,005	1,1E-06	6,1E-06	-1,4E-06	0,021	6,0E-06	2,4E-05	-2,7E-06	0,013	-0,013	-0,001	0,002	-0,002	0,001	0,011	-0,008	-0,003	-0,002
CC Post mid-b.	0,003	1,7E-06	3,2E-06	9,1E-07	0,008	-8,4E-06	-1,9E-05	-2,8E-06	0,008	-0,008	-0,004	0,002	-0,002	-0,003	0,007	-0,003	-0,003	-0,001
CC Isthmus	0,021	-3,3E-06	1,5E-05	-1,2E-05	0,016	-6,0E-06	6,2E-06	-1,2E-05	-0,020	0,020	0,020	-0,016	0,016	0,015	-0,020	0,020	-1,4E-04	-0,009
CC Splenium	0,008	-1,1E-06	7,5E-06	-5,5E-06	0,017	9,9E-06	3,3E-05	-1,6E-06	-0,015	0,015	0,008	-0,012	0,012	0,004	-0,015	0,004	0,011	-0,003
UF left	0,010	1,5E-05	3,3E-05	6,3E-06	0,017	1,7E-05	5,8E-05	-3,2E-06	0,037	-0,037	-0,001	0,019	-0,019	0,006	0,029	-0,023	0,014	-0,006
UF right	0,012	8,7E-06	2,5E-05	5,6E-07	0,005	1,7E-05	3,8E-05	6,4E-06	0,014	-0,014	0,001	0,010	-0,010	0,005	0,018	0,001	0,015	-0,002
UF	0,016	9,8E-06	3,0E-05	-1,6E-07	0,012	1,4E-05	4,4E-05	-3,9E-07	0,020	-0,020	4,4E-04	0,012	-0,012	0,005	0,019	-0,005	0,012	-0,006

(b) Difference at T2

Variation of the gap of means between T1 and T2

abs(Table T2) - abs(Table T1)

No difference
Strongly increase from T1 to T2
Strongly decrease from T1 to T2

Region	DTI				DIAMOND					MF			NODDI			
	FA	MD	AD	RD	wFA	wMD	wAD	wRD	frac csf	frac ftot	fvf tot	frac csf	frac ftot	wfvf	fiso	fintra	fextra	odi
CC	-0,015	2,9E-06	-9,6E-06	-9,9E-06	-0,010	7,1E-06	-6,3E-06	-1,7E-05	-0,001	-0,001	-0,011	-0,009	-0,009	-0,008	-0,006	-0,001	0,007	-0,006
CC Genu	-0,013	5,4E-06	1,5E-05	-1,0E-05	-0,009	1,5E-05	2,1E-05	-1,9E-05	0,010	0,010	-0,004	0,009	0,009	-0,007	0,002	0,024	-0,005	-0,001
CC Ant mid-b.	-0,015	1,1E-06	-1,5E-05	-9,0E-06	-0,005	-3,0E-06	2,0E-06	-2,1E-05	-0,006	-0,006	-0,008	-0,002	-0,002	-0,011	-0,007	0,007	-0,014	-0,007
CC Post mid-b.	-0,012	3,8E-07	-1,3E-05	-5,3E-06	-0,009	-2,9E-07	1,9E-05	-1,0E-05	-0,003	-0,003	-0,006	-0,008	-0,008	-0,002	-0,007	-0,012	0,002	-0,004
CC Isthmus	0,001	-3,1E-06	5,8E-06	-1,7E-06	-0,004	-2,9E-06	-1,4E-06	-5,1E-06	-0,014	-0,014	-0,005	-0,008	-0,008	-0,001	-0,013	-0,013	0,000	0,003
CC Splenium	-0,009	-5,3E-08	-9,5E-06	-4,8E-06	-0,006	8,0E-06	9,7E-07	-1,2E-05	-0,012	-0,012	-0,007	-0,006	-0,006	-0,004	-0,012	-0,016	0,004	-0,004
UF left	-0,021	1,2E-05	5,6E-06	-3,0E-06	-0,014	8,3E-06	1,6E-05	-3,1E-05	0,011	0,011	-0,005	0,011	0,011	-0,003	0,012	0,021	0,012	-0,012
UF right	-0,020	8,1E-06	1,3E-06	-1,2E-05	-0,017	4,6E-06	2,2E-05	-2,0E-05	0,001	0,001	-0,005	0,009	0,009	-0,003	0,008	-0,013	0,011	-0,011
UF	-0,015	9,1E-06	5,7E-06	-1,1E-05	-0,011	5,3E-06	1,9E-05	-2,6E-05	0,002	0,002	-0,006	0,008	0,008	-0,003	0,005	-0,005	0,007	-0,007

(c) Variations between T1 and T2

Figure E.3: **(a & b)** Tables of differences of means between patients and controls for each metric-region pairs at T1 **(a)** and at T2 **(b)**. When the difference is positive meaning that the mean of patients is higher than the mean of controls, the value of the difference is written in green. Conversely, the value is written in blue when the mean of patients is lower than the mean of controls. **(c)** Variation of the gaps of means between T1 and T2. The difference is calculated on the absolute values of the values in the Tables **(a)** and **(b)** in order to see either the gap increase, indicated in green or the gap decrease, indicated in red. The more intense the colour of the box, the greater the difference between the gaps.

Appendix F

Additional tables for the evolution comparison analysis

Patients T1-T2 comparison

Behavioural metrics	T1
BDI	5,26E-09
Total_OCDS	3,39E-07
OCDS (Obsessions)	1,20E-06
OCDS (Compulsions)	1,59E-06
STAI	1,12E-03
MFI	5,40E-07

<0,05
Significantly different at T1 and T2

Figure F.1: Tables of p-values for the comparison of behavioural metrics between alcoholic patients at T1 and T2. Paired t-test highlights different means. p-values less than 0,05 indicate a significantly unequal mean between T1 and T2.

Threshold of variations according to the controls (corresponding to the mean of the control's asbolute value of percentage change)

	DTI				DIAMOND					MF			NODDI			
Region	FA	MD	AD	RD	wFA	wMD	wAD	wRD	frac csf	fvf tot	frac csf	frac ftot	wfvf	fiso	fintra	fextra	odi
CC	1,61%	4,77%	5,06%	4,78%	1,12%	1,54%	2,08%	3,53%	5,06%	2,55%	8,25%	1,07%	1,55%	7,36%	3,39%	8,91%	4,49%
CC Genu	2,14%	8,72%	8,83%	9,49%	1,47%	2,85%	2,62%	6,82%	6,60%	4,71%	8,22%	1,05%	4,06%	16,61%	5,66%	24,88%	6,03%
CC Ant mid-b.	2,66%	5,27%	4,66%	7,55%	1,99%	1,53%	2,11%	5,27%	10,79%	4,86%	16,22%	2,60%	2,46%	11,58%	5,74%	9,67%	3,29%
CC Post mid-b	2,87%	4,21%	4,36%	6,36%	2,36%	1,61%	2,57%	3,45%	12,61%	4,64%	18,73%	2,47%	2,32%	16,00%	4,65%	5,85%	4,17%
CC Isthmus	1,72%	4,06%	4,41%	4,53%	2,18%	2,70%	3,17%	3,03%	13,07%	3,42%	17,31%	2,27%	1,57%	14,66%	3,97%	5,37%	3,09%
CC Splenium	1,10%	3,64%	4,17%	3,40%	0,89%	1,72%	1,86%	3,22%	7,23%	2,08%	8,15%	0,99%	1,44%	9,59%	3,09%	6,44%	4,15%
UF left	4,68%	9,64%	10,01%	10,18%	3,27%	3,51%	3,76%	6,46%	11,13%	9,22%	12,30%	1,33%	8,68%	24,47%	7,29%	24,29%	9,19%
UF right	3,65%	9,75%	9,67%	10,16%	3,81%	2,18%	2,21%	7,51%	16,28%	8,43%	12,76%	1,11%	7,90%	30,92%	7,20%	20,46%	7,81%
UF	3,19%	9,49%	9,56%	9,40%	3,25%	2,29%	1,92%	6,58%	12,66%	7,88%	11,32%	1,05%	7,38%	26,61%	6,86%	21,18%	7,74%

(a) For controls (threshold for the patients)

Mean absolute percentage of changes in patients

	DTI				DIAMOND					MF			NODDI			
Region	FA	MD	AD	RD	wFA	wMD	wAD	wRD	frac csf	fvf tot	frac csf	frac ftot	wfvf	fiso	fintra	fextra	odi
CC	2,22%	5,57%	5,98%	6,69%	1,50%	2,24%	2,35%	5,22%	6,72%	3,52%	10,93%	1,42%	2,96%	9,33%	5,26%	12,59%	5,64%
CC Genu	2,59%	12,02%	12,95%	12,56%	1,78%	4,64%	4,47%	8,09%	9,14%	6,01%	16,31%	1,80%	4,29%	17,18%	10,40%	36,20%	9,57%
CC Ant mid-b.	2,50%	7,11%	6,69%	8,41%	2,92%	2,50%	2,53%	5,14%	12,60%	3,69%	20,52%	2,67%	2,67%	17,21%	6,22%	12,65%	4,16%
CC Post mid-b	2,54%	5,03%	5,61%	5,96%	2,83%	3,41%	3,63%	4,25%	13,81%	3,74%	19,17%	2,60%	2,14%	18,28%	4,93%	11,52%	4,45%
CC Isthmus	2,63%	4,69%	5,73%	5,64%	2,23%	2,79%	3,38%	3,37%	11,66%	3,56%	15,40%	2,33%	2,54%	15,38%	4,69%	10,12%	5,84%
CC Splenium	1,69%	4,30%	4,78%	5,05%	1,04%	2,27%	2,46%	4,73%	8,40%	2,88%	10,19%	1,51%	2,76%	11,54%	4,63%	8,16%	4,88%
UF left	6,49%	11,34%	12,62%	10,96%	4,32%	3,72%	2,60%	8,82%	15,09%	8,63%	13,04%	1,31%	7,82%	24,29%	9,20%	31,35%	12,67%
UF right	4,68%	9,56%	10,51%	9,34%	2,78%	2,52%	2,31%	5,33%	14,37%	6,88%	17,26%	1,40%	6,15%	23,67%	8,99%	19,89%	11,14%
UF	4,81%	9,58%	11,18%	9,20%	2,90%	2,74%	1,78%	6,10%	12,87%	7,06%	13,29%	1,15%	6,50%	21,08%	8,00%	22,01%	11,07%

(b) Means for patients

Difference of absolute percentage of changes (Patients - Controls)

	DTI				DIAMOND					MF			NODDI			
Region	FA	MD	AD	RD	wFA	wMD	wAD	wRD	frac csf	fvf tot	frac csf	frac ftot	wfvf	fiso	fintra	fextra	odi
CC	0,61%	0,81%	0,92%	1,92%	0,38%	0,70%	0,28%	1,69%	1,66%	0,97%	2,68%	0,35%	1,41%	1,97%	1,87%	3,67%	1,15%
CC Genu	0,45%	3,30%	4,12%	3,07%	0,31%	1,79%	1,85%	1,27%	2,54%	1,31%	8,10%	0,75%	0,23%	0,57%	4,74%	11,32%	3,53%
CC Ant mid-b.	-0,16%	1,83%	2,03%	0,86%	0,93%	0,97%	0,42%	-0,13%	1,81%	-0,34%	-1,17%	4,29%	0,07%	0,21%	5,63%	0,48%	2,98%	0,87%
CC Post mid-b	-0,33%	0,81%	1,25%	-0,41%	0,47%	1,80%	1,06%	0,80%	1,20%	0,39%	-0,90%	0,45%	0,12%	-0,18%	2,28%	0,28%	5,68%	0,28%
CC Isthmus	0,91%	0,63%	1,32%	1,11%	0,05%	0,09%	0,21%	0,34%	-1,41%	0,17%	0,15%	-1,91%	0,06%	0,97%	0,72%	0,72%	4,75%	2,75%
CC Splenium	0,60%	0,66%	0,61%	1,66%	0,15%	0,55%	0,60%	1,52%	1,17%	0,80%	0,79%	2,03%	0,51%	1,32%	1,94%	1,54%	1,72%	0,73%
UF left	1,82%	1,71%	2,62%	0,78%	1,05%	0,21%	-1,16%	2,37%	3,95%	0,13%	-0,59%	0,75%	-0,01%	-0,87%	-0,18%	1,91%	7,06%	3,49%
UF right	1,03%	-0,19%	0,84%	-0,82%	-1,04%	0,33%	0,10%	-2,18%	-1,90%	-0,58%	-1,54%	4,50%	0,29%	-1,76%	-7,26%	1,79%	-0,57%	3,33%
UF	1,63%	0,09%	1,62%	-0,20%	-0,35%	0,44%	-0,13%	-0,48%	0,21%	-0,28%	-0,82%	1,97%	0,09%	-0,88%	-5,52%	1,14%	0,83%	3,33%

(c) Difference (b - a) (patients - controls)

Figure F.2: **(a & b)** Tables of mean absolute value of percentage changes between T1 and T2 for each metric-region in controls **(a)** and patients **(b)**. The values for the controls are used as thresholds to verify that the changes observed in the patients are not the result of normal scan/rescan variations. Values for the patients that are superior to that of the corresponding threshold are highlighted in green, while the ones that are inferior are highlighted in red. **(c)** Difference between the threshold from the controls and the mean for patients. The more intense the colour of the box, the greater the difference, positively in green (patients have an average above the threshold) and negatively in red (patients have an average below the threshold).

Mean percentage of changes in controls

No difference — Strongly increase from T1 to T2 — Strongly decrease from T1 to T2

Region	DTI				DIAMOND						MF			NODDI			
	FA	MD	AD	RD	wFA	wMD	wAD	wRD	frac csf	frac ftot	fvf tot	frac csf	frac ftot	wfvf	fiso	fintra	fextra	odi
CC	0,34%	2,60%	3,12%	1,75%	-0,13%	-0,21%	0,03%	-1,00%	-0,19%	0,20%	0,21%	2,32%	-0,14%	0,43%	-2,10%	-0,67%	5,86%	-1,81%
CC Genu	0,98%	4,42%	5,43%	3,01%	0,31%	0,37%	0,66%	-0,30%	-3,67%	1,16%	0,00%	-0,02%	0,31%	-0,40%	-8,39%	0,23%	18,90%	-2,71%
CC Ant mid-b.	0,30%	3,45%	3,94%	2,76%	-0,83%	-0,96%	-0,61%	-1,94%	6,08%	-1,40%	-0,28%	10,38%	-1,07%	1,00%	5,20%	-1,94%	4,13%	-2,24%
CC Post mid-b.	0,41%	2,65%	3,24%	1,82%	-0,09%	0,07%	0,23%	-0,40%	2,04%	-0,13%	0,20%	5,85%	-0,36%	0,61%	1,75%	-0,88%	4,13%	-1,71%
CC Isthmus	0,01%	1,61%	1,97%	1,26%	0,09%	-0,21%	0,09%	-1,18%	1,35%	-0,14%	0,34%	3,57%	-0,22%	0,84%	1,44%	-0,44%	2,77%	-0,03%
CC Splenium	0,37%	1,43%	2,00%	0,37%	-0,01%	-0,18%	0,15%	-1,38%	-0,28%	0,26%	0,97%	1,43%	-0,04%	1,03%	-0,09%	0,17%	1,92%	-1,10%
UF left	2,12%	3,75%	4,85%	2,63%	1,76%	-2,41%	-0,98%	-4,64%	-3,05%	0,55%	0,22%	-4,24%	0,53%	-0,57%	-8,52%	0,79%	16,32%	-1,61%
UF right	1,75%	2,19%	2,96%	1,44%	1,09%	-0,43%	0,25%	-1,44%	-0,90%	0,36%	-0,07%	0,65%	0,19%	-0,40%	-7,73%	-1,83%	5,05%	-4,00%
UF	1,57%	2,61%	3,37%	1,86%	0,93%	-0,94%	-0,25%	-1,98%	-2,44%	0,48%	-0,24%	-1,49%	0,33%	-0,72%	-7,84%	-0,89%	7,69%	-2,66%

(a) For controls

Mean percentage of changes in patients

No difference — Strongly increase from T1 to T2 — Strongly decrease from T1 to T2

Region	DTI				DIAMOND						MF			NODDI			
	FA	MD	AD	RD	wFA	wMD	wAD	wRD	frac csf	frac ftot	fvf tot	frac csf	frac ftot	wfvf	fiso	fintra	fextra	odi
CC	-0,81%	2,87%	2,39%	3,79%	-0,72%	0,50%	0,00%	2,37%	2,63%	-0,65%	-1,05%	5,14%	-0,64%	-0,34%	0,51%	-2,55%	5,88%	-0,61%
CC Genu	-1,18%	6,89%	6,25%	7,90%	-0,81%	2,11%	1,24%	4,84%	0,74%	0,05%	-2,89%	5,93%	-0,66%	-2,24%	-7,06%	-4,94%	19,11%	-2,88%
CC Ant mid-b.	-1,60%	3,46%	2,32%	5,35%	-1,12%	0,35%	-0,56%	3,42%	4,04%	-0,83%	-2,15%	7,07%	-0,84%	-1,22%	2,50%	-2,90%	6,25%	0,04%
CC Post mid-b.	-1,23%	2,82%	1,92%	4,50%	-0,87%	0,37%	-0,29%	2,83%	6,54%	-1,67%	-1,97%	10,17%	-1,13%	-0,81%	6,68%	-3,06%	3,31%	0,18%
CC Isthmus	0,12%	2,64%	2,93%	2,21%	-0,90%	-0,50%	-0,81%	0,70%	6,08%	-1,29%	-0,84%	7,65%	-0,79%	0,15%	5,56%	-1,97%	2,37%	-1,63%
CC Splenium	-0,51%	1,80%	1,56%	2,31%	-0,50%	0,29%	-0,08%	1,81%	1,98%	-0,35%	-0,30%	3,61%	-0,37%	0,14%	1,63%	-1,58%	3,89%	-0,16%
UF left	0,24%	7,00%	7,29%	6,74%	0,33%	-0,30%	-0,22%	-0,15%	4,19%	-0,62%	-3,66%	5,23%	-0,35%	-3,40%	-9,00%	-4,36%	19,21%	-3,62%
UF right	-1,24%	4,67%	4,04%	5,42%	-0,72%	1,05%	0,28%	2,73%	3,09%	-0,07%	-2,54%	6,84%	-0,53%	-2,05%	-2,31%	-3,38%	11,83%	-1,06%
UF	-0,74%	5,52%	5,20%	5,87%	-0,48%	0,69%	0,12%	1,84%	2,99%	-0,25%	-3,12%	6,72%	-0,53%	-2,66%	-5,34%	-3,91%	14,25%	-2,19%

(b) For patients

Figure F.3: (a & b) Tables of mean percentage changes between T1 and T2 for each metric-region in controls **(a)** and patients **(b)**. The more intense the colour of the box, the greater the difference, positively in green and negatively in red.

Appendix G

Additional tables and graphs for the correlation analysis

Pearson correlation coefficient (BDI)

Negative correlation: -1, -0,5 — 0 — 0,5, 1 :Positive correlation

	DTI				DIAMOND						MF			NODDI			
Region	**FA**	**MD**	**AD**	**RD**	**wFA**	**wMD**	**wAD**	**wRD**	**frac csf**	**frac ftot**	**fvf tot**	**frac csf**	**frac ftot**	**wfvf**	**fiso**	**fintra**	**fextra**	**odi**
CC	-0,120	0,109	0,071	0,141	-0,114	0,176	0,095	0,155	0,282	-0,282	-0,189	0,205	-0,205	-0,096	0,238	-0,225	0,071	0,029
CC Genu	-0,278	0,068	0,021	0,137	-0,226	0,216	0,129	0,278	0,233	-0,233	-0,217	0,178	-0,178	-0,183	0,158	-0,186	0,076	0,068
CC Ant mid-b.	-0,099	0,120	0,096	0,141	0,039	0,084	0,022	0,137	0,146	-0,146	-0,154	0,041	-0,041	-0,133	0,091	-0,161	0,075	-0,020
CC Post mid-b.	0,044	0,049	0,070	0,007	0,179	0,318	0,220	**0,413**	-0,258	0,258	0,114	-0,255	0,255	-0,103	-0,282	0,077	0,281	-0,028
CC Isthmus	-0,006	0,044	0,009	0,094	**0,448**	0,273	0,199	0,375	-0,266	0,266	0,116	-0,339	0,339	-0,091	-0,283	0,098	0,251	0,013
CC Splenium	-0,171	0,168	0,109	0,237	-0,355	-0,016	-0,025	0,014	0,353	-0,353	-0,284	0,349	-0,349	-0,063	0,319	-0,309	0,030	-0,029
UF left	-0,147	-0,092	-0,125	-0,041	-0,113	0,139	0,067	0,115	0,012	-0,014	0,032	-0,057	0,055	0,041	0,145	-0,016	-0,104	0,089
UF right	0,113	-0,092	-0,038	-0,155	0,064	0,122	0,259	-0,015	-0,242	0,242	0,135	-0,197	0,196	0,128	-0,009	0,182	-0,040	0,037
UF	-0,146	-0,057	-0,078	-0,022	-0,144	0,214	0,165	0,165	-0,098	0,097	-0,022	-0,052	0,050	-0,014	0,103	0,061	-0,029	0,124

(a) Pearson correlation coefficients

<0,05 Significantly correlated

p-val of the correlation (BDI)

	DTI				DIAMOND						MF			NODDI			
Region	**FA**	**MD**	**AD**	**RD**	**wFA**	**wMD**	**wAD**	**wRD**	**frac csf**	**frac ftot**	**fvf tot**	**frac csf**	**frac ftot**	**wfvf**	**fiso**	**fintra**	**fextra**	**odi**
CC	0,566	0,605	0,736	0,501	0,586	0,401	0,652	0,460	0,172	0,171	0,365	0,325	0,325	0,649	0,251	0,279	0,736	0,892
CC Genu	0,178	0,746	0,922	0,515	0,277	0,299	0,538	0,178	0,262	0,262	0,297	0,396	0,395	0,383	0,451	0,374	0,717	0,747
CC Ant mid-b.	0,639	0,568	0,649	0,501	0,853	0,689	0,915	0,514	0,487	0,487	0,464	0,846	0,846	0,526	0,666	0,442	0,722	0,926
CC Post mid-b.	0,839	0,819	0,745	0,975	0,402	0,130	0,302	0,045	0,223	0,223	0,597	0,229	0,229	0,631	0,182	0,722	0,183	0,898
CC Isthmus	0,979	0,843	0,967	0,669	0,032	0,207	0,362	0,077	0,220	0,220	0,597	0,114	0,114	0,681	0,190	0,657	0,249	0,952
CC Splenium	0,413	0,422	0,603	0,255	0,082	0,939	0,905	0,946	0,084	0,084	0,169	0,087	0,087	0,764	0,120	0,133	0,886	0,891
UF left	0,503	0,676	0,571	0,851	0,606	0,527	0,760	0,600	0,957	0,951	0,886	0,795	0,804	0,852	0,510	0,944	0,638	0,688
UF right	0,599	0,668	0,862	0,469	0,768	0,570	0,222	0,944	0,254	0,255	0,529	0,357	0,359	0,552	0,968	0,394	0,854	0,862
UF	0,487	0,788	0,710	0,918	0,491	0,304	0,429	0,430	0,641	0,646	0,919	0,805	0,811	0,948	0,624	0,772	0,889	0,555

(b) The corresponding p-val

Figure G.1: Pearson correlation coefficients **(a)** and the corresponding p-values **(b)** for the correlations between the BDI scores and all metric-region pairs. In **(a)**, the colours correspond to the degree of correlation and the significative ones are highlighted in bold, they correspond to the p-values inferior to 0,05 highlighted in red in **(b)**.

Pearson correlation coefficient (OCDS obsession)

Negative correlation | -1 | -0,5 | 0 | 0,5 | 1 | Positive correlation

Region	DTI				DIAMOND						MF			NODDI			
	FA	MD	AD	RD	wFA	wMD	wAD	wRD	frac csf	frac ftot	fvf tot	frac csf	frac ftot	wfvf	fiso	fintra	fextra	odi
CC	**0,393**	-0,167	-0,029	-0,342	0,349	-0,103	0,172	**-0,441**	-0,021	0,021	**0,483**	-0,060	0,060	**0,546**	0,164	0,226	-0,283	-0,101
CC Genu	0,300	-0,301	-0,222	**-0,401**	0,229	-0,257	-0,145	-0,349	-0,246	0,246	**0,508**	-0,347	0,347	**0,539**	0,174	**0,418**	-0,262	0,251
CC Ant mid-b.	0,290	-0,167	-0,109	-0,228	0,107	-0,314	-0,059	**-0,548**	0,040	-0,040	0,383	0,003	-0,003	**0,466**	0,123	0,175	-0,288	0,013
CC Post mid-b.	0,389	-0,175	-0,022	-0,344	0,192	0,100	0,233	-0,339	-0,249	0,249	**0,407**	-0,217	0,217	0,303	-0,180	0,274	-0,071	-0,119
CC Isthmus	0,074	0,050	0,050	0,032	0,066	0,236	0,265	-0,088	-0,009	0,009	0,175	0,040	-0,040	0,184	0,007	-0,057	0,053	0,000
CC Splenium	0,228	0,135	0,184	0,005	0,122	-0,043	0,112	-0,339	0,152	-0,152	0,229	0,203	-0,203	0,366	0,154	-0,111	-0,036	-0,242
UF left	-0,068	-0,290	-0,269	-0,289	0,000	-0,247	-0,293	-0,111	-0,009	0,006	0,354	-0,330	0,326	0,349	0,230	0,182	-0,322	0,140
UF right	0,242	-0,336	-0,237	**-0,434**	0,144	-0,369	-0,233	-0,314	-0,269	0,269	**0,431**	-0,345	0,345	**0,410**	0,125	**0,463**	-0,255	0,180
UF	0,084	-0,346	-0,280	**-0,407**	0,058	-0,280	-0,260	-0,195	-0,078	0,077	**0,430**	-0,298	0,297	**0,430**	0,290	0,366	-0,323	0,197

(a) Pearson correlation coefficients

p-val of the correlation (OCDS obsession)

<0,05 Significantly correlated

Region	DTI				DIAMOND						MF			NODDI			
	FA	MD	AD	RD	wFA	wMD	wAD	wRD	frac csf	frac ftot	fvf tot	frac csf	frac ftot	wfvf	fiso	fintra	fextra	odi
CC	0,047	0,414	0,888	0,088	0,081	0,617	0,401	0,024	0,918	0,918	0,013	0,771	0,772	0,004	0,422	0,266	0,162	0,623
CC Genu	0,137	0,136	0,275	0,042	0,260	0,205	0,479	0,080	0,226	0,226	0,008	0,082	0,082	0,004	0,394	0,033	0,197	0,216
CC Ant mid-b.	0,150	0,414	0,596	0,263	0,604	0,118	0,773	0,004	0,847	0,847	0,053	0,987	0,987	0,016	0,548	0,393	0,154	0,949
CC Post mid-b.	0,055	0,404	0,917	0,093	0,358	0,636	0,262	0,097	0,230	0,230	0,043	0,297	0,297	0,141	0,390	0,185	0,737	0,570
CC Isthmus	0,731	0,816	0,815	0,883	0,761	0,267	0,210	0,682	0,967	0,967	0,414	0,852	0,852	0,389	0,975	0,793	0,805	0,999
CC Splenium	0,262	0,512	0,369	0,982	0,551	0,835	0,587	0,090	0,458	0,458	0,261	0,320	0,320	0,066	0,453	0,589	0,859	0,233
UF left	0,754	0,169	0,204	0,171	0,999	0,244	0,164	0,607	0,968	0,976	0,089	0,115	0,120	0,094	0,279	0,394	0,125	0,515
UF right	0,244	0,101	0,255	0,030	0,493	0,070	0,262	0,127	0,194	0,194	0,031	0,091	0,091	0,042	0,551	0,020	0,218	0,389
UF	0,683	0,083	0,166	0,039	0,780	0,166	0,200	0,340	0,706	0,710	0,028	0,139	0,141	0,028	0,151	0,066	0,108	0,334

(b) The corresponding p-val

Figure G.2: Pearson correlation coefficients **(a)** and the corresponding p-values **(b)** for the correlations between the OCDS scores for the obsession-related statements and all metric-region pairs. In **(a)**, the colours correspond to the degree of correlation and the significative ones are highlighted in bold, they correspond to the p-values inferior to 0,05 highlighted in red in **(b)**.

Pearson correlation coefficient (OCDS compulsion)

Negative correlation: -1, -0,5 — Positive correlation: 0, 0,5, 1

Region	DTI				DIAMOND						MF			NODDI			
	FA	MD	AD	RD	wFA	wMD	wAD	wRD	frac csf	frac ftot	fvf tot	frac csf	frac ftot	wfvf	fiso	fintra	fextra	odi
CC	0,333	-0,197	-0,087	-0,323	0,344	-0,180	0,076	**-0,429**	-0,020	0,020	**0,462**	-0,087	0,086	**0,512**	0,076	0,243	-0,251	-0,036
CC Genu	0,200	-0,111	-0,063	-0,177	0,223	-0,036	0,054	-0,170	-0,188	0,188	0,293	-0,188	0,188	0,326	-0,030	0,195	-0,049	0,098
CC Ant mid-b.	0,204	-0,102	-0,058	-0,150	0,131	-0,264	-0,082	**-0,405**	-0,073	0,073	0,346	-0,075	0,075	0,348	-0,055	0,186	-0,130	0,032
CC Post mid-b.	0,317	-0,210	-0,081	-0,336	0,254	0,099	0,193	-0,227	-0,364	0,364	**0,452**	-0,337	0,337	0,261	-0,328	0,375	0,008	0,001
CC Isthmus	0,123	-0,073	-0,038	-0,115	0,195	0,101	0,153	-0,210	-0,158	0,158	0,369	-0,142	0,142	0,318	-0,158	0,167	0,016	0,065
CC Splenium	0,203	-0,152	-0,091	-0,230	0,144	-0,343	-0,147	**-0,508**	0,143	-0,143	0,324	0,090	-0,090	**0,397**	0,144	0,107	-0,309	-0,005
UF left	0,026	-0,190	-0,159	-0,212	0,155	-0,147	-0,072	-0,127	-0,194	0,194	0,320	-0,365	0,366	0,296	0,024	0,221	-0,150	0,110
UF right	0,326	-0,117	-0,038	-0,207	0,338	-0,286	0,015	-0,376	-0,066	0,065	0,320	-0,176	0,174	0,317	0,036	0,239	-0,117	-0,017
UF	0,124	-0,149	-0,107	-0,193	0,182	-0,130	0,044	-0,177	-0,016	0,016	0,284	-0,162	0,162	0,287	0,148	0,228	-0,143	0,096

(a) Pearson correlation coefficients

p-val of the correlation (OCDS compulsion)

<0,05 Significantly correlated

Region	DTI				DIAMOND						MF			NODDI			
	FA	MD	AD	RD	wFA	wMD	wAD	wRD	frac csf	frac ftot	fvf tot	frac csf	frac ftot	wfvf	fiso	fintra	fextra	odi
CC	0,096	0,335	0,674	0,108	0,085	0,378	0,712	0,029	0,924	0,924	0,017	0,674	0,674	0,008	0,711	0,232	0,216	0,860
CC Genu	0,327	0,590	0,758	0,388	0,273	0,860	0,792	0,407	0,358	0,358	0,146	0,358	0,358	0,104	0,885	0,339	0,812	0,635
CC Ant mid-b.	0,317	0,618	0,778	0,463	0,525	0,193	0,691	0,040	0,724	0,724	0,083	0,717	0,717	0,082	0,789	0,362	0,527	0,876
CC Post mid-b.	0,123	0,315	0,702	0,101	0,220	0,638	0,355	0,276	0,073	0,073	0,023	0,099	0,099	0,207	0,109	0,065	0,970	0,997
CC Isthmus	0,568	0,735	0,859	0,593	0,361	0,637	0,474	0,325	0,460	0,460	0,076	0,508	0,508	0,131	0,461	0,434	0,939	0,763
CC Splenium	0,321	0,460	0,658	0,257	0,483	0,087	0,472	0,008	0,486	0,486	0,106	0,664	0,663	0,045	0,481	0,604	0,124	0,979
UF left	0,904	0,373	0,457	0,320	0,469	0,493	0,738	0,555	0,364	0,363	0,128	0,079	0,079	0,160	0,910	0,300	0,484	0,609
UF right	0,112	0,578	0,856	0,322	0,099	0,165	0,942	0,064	0,754	0,757	0,119	0,401	0,405	0,123	0,866	0,251	0,576	0,935
UF	0,546	0,468	0,601	0,346	0,373	0,528	0,832	0,388	0,939	0,937	0,160	0,430	0,428	0,156	0,470	0,262	0,486	0,640

(b) The corresponding p-val

Figure G.3: Pearson correlation coefficients **(a)** and the corresponding p-values **(b)** for the correlations between the OCDS scores for the compulsion-related statements and all metric-region pairs. In **(a)**, the colours correspond to the degree of correlation and the significative ones are highlighted in bold, they correspond to the p-values inferior to 0,05 highlighted in red in **(b)**.

Pearson correlation coefficient (STAI)

Negative correlation | -1 | -0,5 | 0 | 0,5 | 1 | Positive correlation

	DTI				DIAMOND						MF			NODDI			
Region	**FA**	**MD**	**AD**	**RD**	**wFA**	**wMD**	**wAD**	**wRD**	**frac csf**	**frac ftot**	**fvf tot**	**frac csf**	**frac ftot**	**wfvf**	**fiso**	**fintra**	**fextra**	**odi**
CC	-0,155	0,083	0,045	0,123	-0,210	0,137	0,015	0,208	0,248	-0,248	-0,151	0,189	-0,189	-0,053	0,219	-0,184	0,031	0,083
CC Genu	-0,159	-0,049	-0,060	-0,028	-0,212	0,094	-0,020	0,241	-0,006	0,006	-0,075	0,005	-0,005	-0,058	0,195	-0,017	-0,042	0,111
CC Ant mid-b.	-0,083	0,040	0,014	0,070	-0,041	-0,047	-0,077	0,035	0,144	-0,144	-0,029	0,069	-0,069	0,062	0,111	-0,070	-0,036	0,022
CC Post mid-b.	-0,073	0,104	0,065	0,129	-0,080	0,046	-0,020	0,209	0,000	0,000	-0,075	0,040	-0,040	-0,093	-0,039	-0,049	0,105	0,065
CC Isthmus	-0,170	0,045	-0,033	0,178	0,075	0,027	-0,036	0,285	0,060	-0,060	-0,015	-0,042	0,042	-0,020	-0,009	-0,048	0,065	0,144
CC Splenium	-0,341	0,223	0,109	0,384	**-0,444**	0,015	-0,089	0,220	**0,409**	**-0,409**	-0,395	0,364	-0,364	-0,173	0,314	-0,386	0,140	0,081
UF left	-0,250	-0,394	-0,390	-0,357	-0,390	0,049	-0,274	0,210	-0,247	0,249	0,298	-0,356	0,359	0,307	0,403	**0,428**	-0,375	0,402
UF right	0,187	-0,042	0,018	-0,117	0,121	0,015	0,235	-0,134	-0,215	0,214	0,141	-0,053	0,052	0,144	-0,043	0,155	-0,064	-0,029
UF	-0,236	-0,153	-0,174	-0,110	-0,299	0,129	-0,095	0,193	-0,267	0,268	0,090	-0,143	0,145	0,096	0,151	0,224	-0,149	0,270

(a) Pearson correlation coefficients

<0,05 Significantly correlated

p-val of the correlation (STAI)

	DTI				DIAMOND						MF			NODDI			
Region	**FA**	**MD**	**AD**	**RD**	**wFA**	**wMD**	**wAD**	**wRD**	**frac csf**	**frac ftot**	**fvf tot**	**frac csf**	**frac ftot**	**wfvf**	**fiso**	**fintra**	**fextra**	**odi**
CC	0,459	0,692	0,832	0,559	0,314	0,514	0,942	0,318	0,232	0,232	0,472	0,366	0,366	0,800	0,294	0,379	0,884	0,694
CC Genu	0,449	0,816	0,774	0,895	0,309	0,656	0,925	0,246	0,978	0,978	0,720	0,981	0,981	0,783	0,349	0,935	0,841	0,598
CC Ant mid-b.	0,695	0,850	0,949	0,741	0,846	0,823	0,715	0,867	0,493	0,493	0,892	0,743	0,743	0,768	0,599	0,739	0,863	0,917
CC Post mid-b.	0,735	0,630	0,763	0,546	0,710	0,830	0,926	0,327	0,999	0,999	0,726	0,854	0,854	0,667	0,858	0,821	0,625	0,762
CC Isthmus	0,438	0,839	0,882	0,416	0,734	0,901	0,870	0,187	0,785	0,785	0,945	0,851	0,851	0,929	0,966	0,828	0,767	0,511
CC Splenium	0,095	0,283	0,603	0,058	0,026	0,944	0,671	0,291	0,042	0,042	0,051	0,074	0,074	0,407	0,126	0,056	0,505	0,699
UF left	0,250	0,063	0,066	0,094	0,066	0,824	0,206	0,337	0,255	0,252	0,167	0,096	0,093	0,155	0,057	0,042	0,078	0,057
UF right	0,382	0,845	0,934	0,586	0,575	0,946	0,269	0,532	0,313	0,314	0,511	0,807	0,810	0,503	0,840	0,470	0,768	0,895
UF	0,255	0,465	0,405	0,600	0,147	0,538	0,653	0,354	0,197	0,195	0,669	0,494	0,488	0,649	0,472	0,282	0,477	0,191

(b) The corresponding p-val

Figure G.4: Pearson correlation coefficients **(a)** and the corresponding p-values **(b)** for the correlations between the STAI scores and all metric-region pairs. In **(a)**, the colours correspond to the degree of correlation and the significative ones are highlighted in bold, they correspond to the p-values inferior to 0,05 highlighted in red in **(b)**.

Pearson correlation coefficient (MFI)

Negative correlation: -1, -0,5 — Positive correlation: 0, 0,5, 1

Region	DTI				DIAMOND						MF				NODDI			
	FA	MD	AD	RD	wFA	wMD	wAD	wRD	frac csf	frac ftot	fvf tot	frac csf	frac ftot	wfvf	fiso	fintra	fextra	odi
CC	0,071	0,282	0,330	0,151	-0,069	0,161	0,233	-0,083	0,152	-0,152	0,116	0,281	-0,281	0,307	0,130	-0,273	0,163	-0,287
CC Genu	0,052	0,225	0,245	0,174	0,005	0,231	0,258	0,102	-0,120	0,120	-0,060	0,095	-0,095	-0,016	-0,037	-0,228	0,203	-0,253
CC Ant mid-b.	-0,017	0,312	0,345	0,243	-0,088	0,017	0,127	-0,194	0,337	-0,337	0,015	0,302	-0,302	0,388	0,220	-0,385	0,169	-0,314
CC Post mid-b.	0,013	0,326	0,338	0,221	-0,105	0,105	0,076	0,125	-0,071	0,071	0,069	0,060	-0,060	0,200	-0,124	-0,170	0,358	-0,200
CC Isthmus	0,270	0,338	0,375	0,141	0,309	**0,474**	**0,445**	0,218	-0,244	0,244	0,291	-0,142	0,142	0,283	-0,276	-0,105	**0,462**	-0,356
CC Splenium	0,051	0,352	0,367	0,233	-0,268	0,048	0,132	-0,162	0,233	-0,233	0,109	0,357	-0,357	0,387	0,217	-0,321	0,173	-0,310
UF left	-0,167	-0,035	-0,074	0,018	-0,143	-0,201	-0,351	-0,024	-0,065	0,062	0,101	-0,215	0,211	0,093	-0,014	0,033	-0,038	0,114
UF right	0,262	0,101	0,172	-0,001	0,193	-0,073	0,156	-0,189	-0,236	0,235	0,024	-0,097	0,096	0,027	-0,208	0,031	0,153	-0,139
UF	-0,014	0,080	0,079	0,074	-0,019	-0,037	-0,019	-0,033	-0,108	0,106	-0,008	-0,041	0,038	0,011	-0,040	0,004	0,105	0,031

(a) Pearson correlation coefficients

p-val of the correlation (MFI)

<0,05 Significantly correlated

Region	DTI				DIAMOND						MF				NODDI			
	FA	MD	AD	RD	wFA	wMD	wAD	wRD	frac csf	frac ftot	fvf tot	frac csf	frac ftot	wfvf	fiso	fintra	fextra	odi
CC	0,742	0,182	0,116	0,482	0,748	0,451	0,273	0,701	0,478	0,477	0,588	0,184	0,184	0,145	0,546	0,197	0,446	0,174
CC Genu	0,808	0,291	0,248	0,415	0,982	0,278	0,224	0,635	0,577	0,578	0,780	0,659	0,658	0,941	0,862	0,285	0,341	0,233
CC Ant mid-b.	0,937	0,138	0,099	0,252	0,683	0,938	0,555	0,363	0,108	0,108	0,943	0,151	0,151	0,061	0,301	0,064	0,430	0,136
CC Post mid-b.	0,952	0,129	0,114	0,311	0,633	0,634	0,730	0,571	0,748	0,748	0,754	0,784	0,784	0,360	0,572	0,439	0,094	0,360
CC Isthmus	0,224	0,124	0,086	0,532	0,162	0,026	0,038	0,329	0,275	0,275	0,190	0,529	0,529	0,202	0,213	0,643	0,030	0,104
CC Splenium	0,814	0,091	0,077	0,273	0,206	0,824	0,539	0,448	0,274	0,274	0,614	0,087	0,087	0,061	0,309	0,127	0,418	0,140
UF left	0,459	0,877	0,743	0,938	0,525	0,371	0,109	0,916	0,774	0,784	0,655	0,337	0,346	0,681	0,950	0,885	0,867	0,613
UF right	0,228	0,645	0,433	0,997	0,378	0,739	0,478	0,387	0,278	0,281	0,914	0,658	0,664	0,902	0,340	0,888	0,485	0,527
UF	0,949	0,709	0,713	0,730	0,931	0,863	0,930	0,877	0,614	0,621	0,970	0,848	0,861	0,961	0,853	0,987	0,626	0,886

(b) The corresponding p-val

Figure G.5: Pearson correlation coefficients **(a)** and the corresponding p-values **(b)** for the correlations between the MFI scores and all metric-region pairs. In **(a)**, the colours correspond to the degree of correlation and the significative ones are highlighted in bold, they correspond to the p-values inferior to 0,05 highlighted in red in **(b)**.

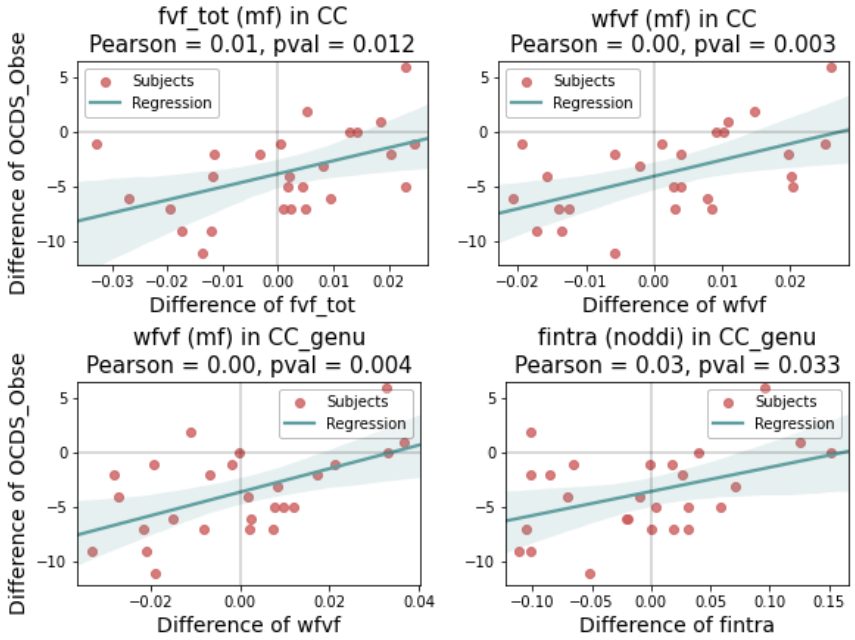


Figure G.6: Graphs of the significant correlations between microstructural metrics and OCDS (obsessions-related statements) score.

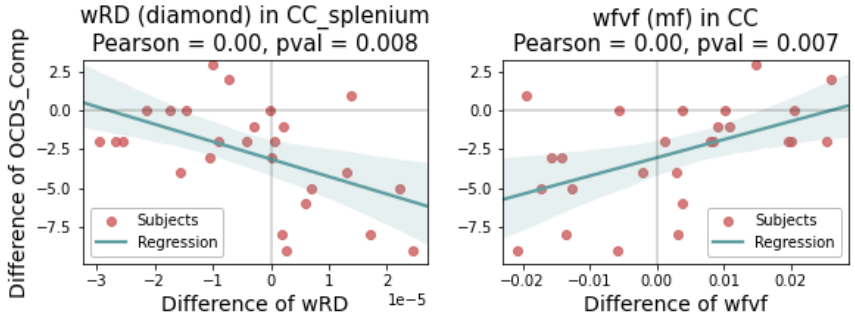


Figure G.7: Graphs of the significant correlations between microstructural metrics and OCDS (compulsion-related statements) score.

Appendix H

UFs asymmetry comparison

Volumetric comparison

The volumetric asymmetry of the UFs was tested by comparing the number and density of fibres in the left and right UFs. A Paired-Samples Student's must be used as for the evolution comparison analysis (see Equation 3.6), because there is a relationship between the size of the UFs left and right for each subject. It is the difference between the two UFs of each patient that needs to be analysed, not the difference between all the left and right UFs of all subjects taken together. Three different populations were analysed to compare the UF asymmetry within patients and within controls separately and finally within all subjects together. The comparison was made at times T1 and T2. Table H.1 presents the results of these analyses. As indicated by the fact that all the boxes are highlighted in red, all the metrics for all the populations at both times are highly significant.

Table H.1: p-values of the comparison between the UFs left and right in patients, controls and all subjects gathered together, at T1 and T2.

	T1		T2	
Population	**Number of stream**	**Mean stream density**	**Number of stream**	**Mean stream density**
Patients	6.38 e-09	5.66 e-08	6.72 e-09	3.07 e-06
Controls	7.17 e-05	2.26 e-04	1.87 e-05	2.44 e-05
All sujects	1.34 e-12	1.46 e-10	4.44 e-13	5.93 e-10

As a reminder, in the state of the art, a 30% difference in fibre volume and density was reported between the two UFs. The present analysis confirms the significant differences between the left and right UFs within patients, within controls and within all subjects studied together. As shown in the graphs of Figure H.1, a clear superiority of the right UF is observed which is also consistent with the literature.

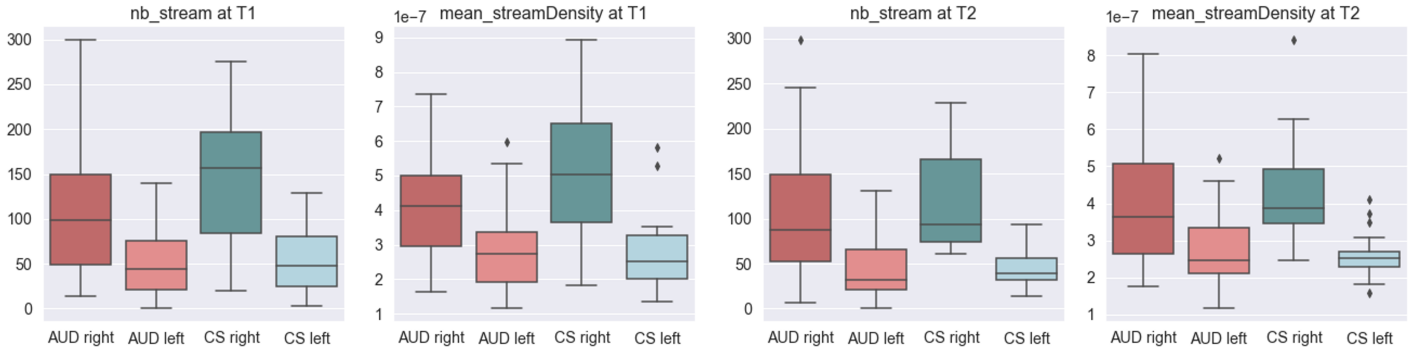


Figure H.1: Boxplots for the comparison of the UFs left and right using the number of fibres and de fibre density (normalised to the total fibre density of the total brain tractography) at T1 and T2.

Microstructural comparison

Comparisons can also be made on the basis of the microstructural metrics and their evolution over time. Tables H.2 (a, b and c) show the p-values of these analyses. In a nutshell, at T1, the DIAMOND, MF and NODDI models show significant differences between the left and right UFs for most of the metrics, generally in the three populations (except for `wFA`, `fvf_tot`, `odi` that are not significant for any of the populations). At T2, fewer metrics are significant. The significant metrics from MF at T1 are still significant at T2. The change is mostly noticeable for patients in the DIAMOND model. At T1, they had 9 significant metrics in all, but only 4 remain significant at T2. The controls, who also had 9 significant metrics at T1, lost only 2 at T2. Finally, the differences between the left and right UF in terms of variations in metrics between T1 and T2 were not very significant. Only the differences between the evolutions of `wMD` and `wRD` from DIAMOND are significant for the patients and for all subjects together.

Limitations

It is important to note that tractography, which has been used here as a basis for comparison in terms of volume and density, does not initially aim to achieve quantitative precision. Initially, tractography served more as a visual tool. General indications, supported by other arguments, can therefore be drawn from these analyses without taking them as accurate and quantitative conclusion. As mentioned in the future perspectives of this master's thesis, more accurate axonal density measurements can be obtained using, for instance, the SIFT2 method proposed by Smith et al. [85].

Asymmetry between the left and right UFs at T1

<0,05 Significantly different

	DTI				DIAMOND						MF			NODDI			
Population	FA	MD	AD	RD	wFA	wMD	wAD	wRD	frac csf	frac ftot	fvf tot	frac csf	frac ftot	wfvf	fiso	fintra	fextra	odi
Patients	0,393	0,532	0,532	0,616	0,423	1,7E-04	6,2E-03	8,8E-03	7,4E-03	7,5E-03	0,437	1,7E-04	1,8E-04	0,097	3,4E-05	0,362	0,047	0,174
Controls	0,158	0,657	0,217	0,770	0,518	0,015	8,9E-03	0,448	1,7E-03	1,8E-03	0,375	5,2E-04	5,2E-04	0,051	1,9E-04	0,010	0,010	0,078
All sujects	0,194	0,465	0,367	0,728	0,601	5,3E-06	1,6E-04	6,7E-03	6,4E-05	6,6E-05	0,300	4,7E-07	5,1E-07	0,022	3,7E-08	0,076	4,8E-03	0,084

(a) At T1.

Asymmetry between the left and right UFs at T2

<0,05 Significantly different

	DTI				DIAMOND						MF			NODDI			
Population	FA	MD	AD	RD	wFA	wMD	wAD	wRD	frac csf	frac ftot	fvf tot	frac csf	frac ftot	wfvf	fiso	fintra	fextra	odi
Patients	0,486	0,696	0,858	0,408	0,532	0,127	0,025	0,788	0,098	0,098	0,219	0,034	0,033	0,054	3,4E-04	0,508	0,157	0,317
Controls	0,824	0,171	0,319	0,331	0,330	0,075	0,010	0,932	4,6E-06	4,6E-06	0,877	2,6E-04	2,6E-04	0,263	1,6E-05	0,011	0,458	0,720
All sujects	0,627	0,813	0,533	0,800	0,274	0,029	1,0E-03	0,853	9,1E-04	9,0E-04	0,305	4,4E-04	4,3E-04	0,024	3,0E-07	0,676	0,109	0,285

(b) At T2.

Asymmetry between the left and right UFs in the evolution between T1 and T2

<0,05 Significantly different

	DTI				DIAMOND						MF			NODDI			
Population	FA	MD	AD	RD	wFA	wMD	wAD	wRD	frac csf	frac ftot	fvf tot	frac csf	frac ftot	wfvf	fiso	fintra	fextra	odi
Patients	0,689	0,915	0,909	0,947	0,358	1,0E-03	0,104	0,017	0,926	0,925	0,890	0,482	0,486	0,871	0,550	0,271	0,586	0,785
Controls	0,536	0,119	0,098	0,429	0,490	0,376	0,774	0,229	0,909	0,919	0,314	0,488	0,500	0,223	0,118	0,450	0,071	0,280
All sujects	0,483	0,335	0,305	0,576	0,243	3,4E-03	0,210	7,3E-03	0,997	0,995	0,631	0,315	0,324	0,387	0,130	0,518	0,118	0,785

(c) Evolution between T1 and T2.

Figure H.2: p-values of the comparison of the microstructural metrics between the UFs left and right at T1 **(a)**, at T2 **(b)** and for the evolution of these metrics between T1 and T2 **(c)**. The significant p-values are highlighted in red.

UNIVERSITÉ CATHOLIQUE DE LOUVAIN
École polytechnique de Louvain
Rue Archimède, 1 bte L6.11.01, 1348 Louvain-la-Neuve, Belgique | **www.uclouvain.be/epl**